UNIVERSITY OF CALIFORNIA, IRVINE

Atmospheric Aging of Monoterpene Secondary Organic Aerosol

DISSERTATION

submitted in partial satisfaction of the requirements for the degree of

DOCTOR OF PHILOSOPHY

In Chemistry

by

Stephen Anthony Mang

Dissertation Committee:

Professor Sergey Nizkorodov, Chair
Professor Craig Martens
Professor Reginald Penner

2008

The thesis of Stephen Anthony Mang is approved and is acceptable in quality and form for publication on microfilm.

_____

_____

_____
Committee Chair

University of California, Irvine
2008

TABLE OF CONTENTS

LIST OF FIGURES

LIST OF TABLES

ACKNOWLEDGEMENTS

Many people contributed in important ways to the completion of this thesis and my graduate career in general. Foremost I would like to thank my advisor, Dr. Sergey Nizkorodov, whose advice and guidance have made me a far better scientist and teacher. Serving as a teaching and research assistant for Dr. Nizkorodov has taught me many things that will serve me well in the future. I would also like to thank Dr. Reginald Penner, for whom I served as a teaching assistant in the fall of 2007, for teaching me so much about how to effectively teach a college class.

Several current and former graduate students in the Nizkorodov research group at UCI deserve my thanks. I am grateful to Dr. Maggie Walser for many discussions in the initial stages of the SOA photolysis project, and for her work in getting that research off the ground; Dr. Anthony Gomez, for his help with the photolysis project as well, and for training me to use the IR-CRDS system; and Xiang Pan and Adam Bateman for many fruitful discussions regarding the SOA photolysis project.

Dr. Jiho Park gave me a good deal of advice and assistance on the microwave torch project, particularly in the area of software programming. And the GC analysis of the SOA photolysis samples would not have been possible without the assistance of Dr. Mads Andersen and Dr. Donald Blake. Dr. Michael Gonsoir provided advice and instrument time for the fluorescence analysis of fresh and aged SOA, and his help is appreciated as well.

Of course, my family has been very important from the beginning of my education in keeping me encouraged and motivated. My parents, Robert Mang and Linda Owen, helped me more than I can say by teaching me from the beginning that learning is important and enjoyable, and that reading a good book is one of the greater pleasures in the world. My sister, Joanna Mang, has also been invaluable as a friendly ear and as a source of advice. Finally, I would like to thank Clare Peyrebrune for all of her support, especially as I finished the research and writing for this thesis, during which time I was often less than pleasant to be around.

CURRICULUM VITAE

Stephen A. Mang

Department of Chemistry 949-824-7473
University of California, Irvine smang@uci.edu
Irvine, CA 92697 http://aerosol.chem.uci.edu/

EDUCATION

University of California, Irvine
Ph.D. in Chemistry May 2008
Specialization in Chemical and Materials Physics
Thesis: "Atmospheric Aging of Monoterpene Secondary Organic Aerosol"

Master of Science in Chemistry April 2007
Thesis: "Development of a Microwave Plasma Torch for Single Particle Counting with Chemical Information"

University of San Diego
Bachelor of Arts in Chemistry, *Cum Laude* January 2003

PUBLICATIONS

Stephen A. Mang, Maggie L. Walser, John M. Laux and Sergey A. Nizkorodov. *Measurement of Ozone Emission and Particle Removal Rates from Portable Air Purifiers*. Submitted to the *Journal of Chemical Education*.

Stephen A. Mang, Maggie L. Walser, Xiang Pan, Jia-Hua Xing, Adam P. Bateman, Joelle S. Underwood, Anthony L. Gomez, Jiho Park, Sergey A. Nizkorodov. *Photochemistry of Secondary Organic Aerosol Formed From Oxidation of Monoterpenes*. Submitted to *ACS Symposium Series*.

Stephen A. Mang, Adam P. Bateman, Mads Andersen, Donald R. Blake, and Sergey A. Nizkorodov. *Contribution of Carbonyl Photochemistry to the Aging of Monoterpene Secondary Organic Aerosol*. Submitted to *Journal of Physical Chemistry A*.

PRESENTATIONS

Global Climate Change: How can we change the world? Stephen Mang. Invited Seminar, Environmental Science Department, Whittier College. September 2007.

Photochemistry of Model Organic Aerosol Systems. Stephen Mang, Adam Bateman, Mark Dialo, Thong Do, Xiang Pan, Joelle Underwood, Maggie Walser and Sergey Nizkorodov. Talk presented at the 2007 American Geophysical Union Joint Assembly, Acapulco, Guerrero, Mexico, May 2007.

Photochemistry of Oxidized Organic Aerosol Particles. Stephen A. Mang, Adam P. Bateman, Maggie L. Walser and Sergey A. Nizkorodov. Poster presented at the 24th Informal Symposium on Kinetics and Photochemical Processes in the Atmosphere, Los Angeles, CA, February 2007.

Single Particle Counting with Chemical Information Using Microwave Plasma Torch Atomic Emission Spectroscopy. Stephen A. Mang and Sergey A. Nizkorodov. Poster presented at the 2006 International Aerosol Conference, St. Paul, MN, September 2006.

Microwave Plasma Torch Atomic Emission Spectroscopy for Aerosol Particle Counting with Chemical Information. Stephen Mang, Jiho Park and Sergey Nizkorodov. Poster presented at the 23rd Informal Symposium on Kinetics and Photochemical Processes in the Atmosphere, Pasadena, CA, February 2006.

Single Particle Analysis using Microwave Plasma Torch Atomic Emission Spectroscopy. Stephen Mang, Jiho Park and Sergey Nizkorodov. Talk presented at the American Chemical Society 40th Annual Western Regional Meeting, Anaheim, CA, January 2006.

Microwave Plasma Torch Atomic Emission Spectroscopy for Aerosol Particle Counting with Chemical Information. Stephen Mang, Jiho Park and Sergey Nizkorodov. Poster presented at the American Association for Aerosol Research 2005 Annual Meeting, Austin, TX, October 2005.

Investigating the Effect of Microwave Heating and Vaporization on Atmospheric Aerosol Particles. Stephen Mang, Ao Lin and Sergey Nizkorodov. Poster presented at the 22nd Informal Symposium on Kinetics and Photochemical Processes in the Atmosphere, Irvine, CA, February 2005.

ABSTRACT OF THE THESIS

Atmospheric Aging of Monoterpene Secondary Organic Aerosol

Stephen Anthony Mang

Submitted in partial satisfaction of the requirements for the degree of Doctor of Philosophy in Chemistry

University of California, Irvine

2008

Sergey Nizkorodov, Doctoral Committee Chair

The behavior of monoterpene SOA with respect to tropospheric radiation is an important field of study because of the potential impacts on the chemical composition and energy balance of the Earth's atmosphere. Of concern is the lack of understanding of the absorption profiles of real atmospheric aerosol particles. Most models assume that the only aerosol absorbers of radiation are those particles that contain black carbon; all other particles are treated as scatterers and assigned negative radiative forcings. In Chapter 3 of this thesis, I have described a method of measuring the absorption spectra of films of aerosol particles, the results of which cast doubt on this assumption. The new procedure allows us to measure spectra of the particles directly, without worrying about solvent effects. The results show that SOA formed from the ozonolysis of monoterpenes have absorption profiles that overlap significantly with the tropospheric actinic window (radiation with $\lambda > 295$ nm). We have calculated the

lifetime of these SOA with respect to photolysis, and found that it is often an order of magnitude shorter than the most important competing aging process, attack by OH.

The lifetime of the particles with respect to photolysis depends on the kind of reactions that absorbed radiation will be able to initiate. In Chapter 2 we investigated this question by detecting the gas phase products of limonene SOA photolysis in order to draw conclusions about the mechanisms of monoterpene SOA photolysis. Based on the product distribution and on the known products of limonene ozonolysis, we proposed that the Norrish type I and II photolysis of carbonyl-containing molecules will be an important mechanism of photochemical aging for monoterpene aerosols in the troposphere.

In Chapter 3, I have presented results from experiments on particle aging in the absence of UV radiation. These results imply that particles can be aged by non-photochemical processes, meaning that particles will be modified during their time in the troposphere even when conditions are unfavorable to photochemistry. The mechanism of the changes that alter the absorption profile of monoterpene SOA in the absence of radiation is unknown at this time.

Chapter 1

Previous Literature on the Atmospheric Chemistry of Volatile Organic Compounds and Aerosols

1.1 The Role of Organics in the Atmosphere

Organic aerosol particles play an important role in the chemistry and energy balance of the Earth's atmosphere. The direct climatic effect of aerosols in general is due to their ability to scatter and absorb solar radiation, while an indirect effect is caused by their ability to act as cloud condensation nuclei [1]. Both effects depend on the chemical composition of the aerosol particles.

Atmospheric measurements have shown that nearly all atmospheric aerosol particles contain at least some organic material [2, 3], even if they have an inorganic core [2]. Organic aerosols can either be emitted directly into the atmosphere (primary organic aerosol, POA) or formed in the atmosphere from oxidation products of volatile organic compound precursors (secondary organic aerosol, SOA) [4]. Volatile and semivolatile organic compounds are emitted directly into the atmosphere either by anthropogenic or biogenic sources.

Organic aerosols and volatile organic compounds (VOCs) have many anthropogenic sources, including food cooking [5-7], vehicle emissions [6-11], home heating (wood burning or natural gas) [6, 7, 10, 12], industrial fuel oil

burning [7, 13] and cigarette smoke [6, 7, 14, 15]. Field measurements in urban areas have determined that organic particles can comprise as much as 15% of total particulates [16] and between 40% and 75% of particles with diameters smaller than 2.5 microns ($PM_{2.5}$) [11, 17, 18].

While emissions of VOCs from anthropogenic sources are important to the pollution budget in urban areas, emissions of biogenic VOCs (BVOCs) are far more significant globally. Guenther [19] estimated a total natural VOC flux of 1150 teragrams (Tg) carbon per year, of which more than 75% was produced by woodlands. Of the total flux, isoprene was by far the most important component (44% of the total), followed by monoterpenes (11%). In contrast, estimates for anthropogenic VOC emissions have been estimated at around 150 Tg/year [20].

Upon emission into the atmosphere, VOCs are exposed to oxidants and radiation. Studies on the oxidation of organic films have been important in determining the likely fates of organics in the atmosphere. For example, when films of 1-dodecene were reacted with ozone, oxidation products such as alkanes, carboxylic acids and aldehydes resulted. When the same alkene was reacted with OH radicals, a more complicated product distribution (including alcohols and ketones in addition to the functional groups formed by ozone) was observed [21]. Small gas phase products such as formaldehyde were observed from the reaction of ozone with surface-bound alkenes [22] in addition to the oxidized products that remained on the surface. Oxidation also red-shifted the UV absorption spectra of alkene films, making them photo-active in the actinic region of the solar spectrum ($\lambda > 295$ nm) [23, 24]. Ozone reaction rates are

significantly slower than those with OH, but it is likely that the overall rates in the atmosphere will be similar because of ozone's higher concentration. This only applies to unsaturated molecules, however, because ozone reacts with saturated organics much more slowly than with unsaturated molecules [25].

1.2 Secondary Organic Aerosol Production

The importance of secondary organic aerosols formed from the various VOC precursors has become clearer in recent years. Not only do SOA contribute heavily to the total budget of aerosols in the atmosphere, but they can also contribute significantly to air pollution on a local scale. Lim [18] concluded that SOA was responsible for almost half of urban total organic aerosol mass as a daily average, and that short-term contributions could be up to 88%. In some cases, the semivolatile component of primary organic aerosol can be oxidized by NO_3, O_3 or OH to form SOA, further contributing to aerosol burdens in polluted areas [26]. Globally, SOA production is predicted to amount to between 120 and 910 Tg/year [26, 27], with most of this coming from oxidation of VOCs by O_3 and OH. Up to 25 Tg of this budget may be the result of the oxidation of anthropogenic VOCs [4]. The significant uncertainty in the amount of SOA produced yearly comes from an incomplete understanding of aerosol yields from BVOC oxidation and the dependence of SOA formation on local parameters such as temperature and the presence or absence of seed particles.

1.2.1 Determining Secondary Organic Aerosol Yields

The yield of SOA produced by the oxidation of a given compound depends on various factors, not all of which are unique to that compound. Initial research into aerosol yield resulted in a parameter known as the Fractional Aerosol Coefficient (FAC), defined simply as the fraction of a given VOC converted into aerosol [28]. The shortcomings of this method are obvious, since in calculating FAC the effects of temperature and total aerosol mass on aerosol yield are not taken into account. To get a more accurate measure of aerosol yield from the oxidation of a given VOC, it is especially important to consider the aerosol mass.

The fractional yield of aerosol (Y) from the oxidation of a given reactive organic compound (ROG) can be defined as

$$Y = \Delta M_o / \Delta ROG \quad (1)$$

where ΔM_o is the change in the organic aerosol mass concentration and ΔROG is the mass of the organic compound that has reacted. In other words, the yield is a measure of how much of the reacted volatile compound ends up partitioned into the particle phase. Initially it was thought that the mass of aerosol particles would be made up of only compounds that were present in concentrations above their saturation vapor pressures. A model developed by Pankow [29] showed that this was not necessarily the case, and indeed any species present in the gas phase will be partitioned into the particle phase to some extent if the particle's surface is organic. Odum [30] extended the Pankow model to describe the partitioning coefficients for a variety of species between the particle and gas phases, and in so doing determined that the SOA yield was highly dependent on

the organic aerosol mass concentration. This model was not applied to the formation of SOA in the atmosphere, however, because the yield also depends on the mass of the organic compounds present in the gas phase, which varies to a largely unknown extent for atmospheric species. This variation was not addressed by Odum's model.

Donahue [31] further generalized the description of the partitioning of semi-volatile organics into the particle phase. Semi-volatile molecules can be grouped into two classes: truly semi-volatile organics (SVOCs), which are present in both the condensed and vapor phase somewhere in the atmosphere (i.e. not all in particles or all in the vapor phase), and intermediate volatility organics (IVOCs), which are volatile but are very likely to produce low vapor pressure oxidation products. Donahue developed a model using a set of possible volatility "bins" to describe any organic compound in the atmosphere, resulting in a far more general description of the gas/particle phase partitioning. The model was also able to address the change in aerosol yield caused by the multiple steps, or generations, of oxidation of the VOCs that had previously been proposed [32]. Over time, SVOCs and IVOCs are oxidized first into low volatility products (moving them into the particle phase), and then into smaller, higher volatility molecules (moving them back into the vapor phase). The competition between these two processes resulted in a peak in aerosol mass after about 4 generations of simulated oxidation.

Volatile organics can be oxidized to products which end up in the particle phase as a consequence of oxidation by several different oxidants: ozone, the

hydroxyl radical (OH), and the nitrate radical (NO_3). The relative importance of these reactants differs based on the organic molecule with which they will react, and also the ambient conditions. In general, the most important atmospheric fate for molecules without a double bond is reaction with OH. Reactions of OH with organics produce ketones and aldehydes, as well as carboxylic acids and alcohols in certain cases; these products will often have lower vapor pressures than the parent organic and are therefore likely to partition to the particle phase. Since OH is produced in the atmosphere by photochemical reactions, this process will only be important during the daytime. Organic molecules with double bonds will also react with OH during daylight hours, but at night reactions with NO_3 and ozone become important. NO_3 is destroyed photochemically, meaning that it is only an important oxidant at nighttime. Ozone can oxidize unsaturated molecules at any time. The major products from ozonolysis of unsaturated organics are carboxylic acids, and the major products from NO_3 oxidation are organic nitrates. Both of these functional groups have lower volatility than their parent molecules, making particle formation a likely consequence of these kinds of oxidation reactions.

1.2.2 SOA from Anthropogenic Precursors

SOA from anthropogenic precursors is important to the particulate budget of urban areas [33]. This fact was recognized as early as 1952, when researchers in the Los Angeles County Air Pollution Control District experimented with gasoline vapors and oxidants [34]. They found that when the

vapors were combined with the oxidants (ozone and/or nitrogen oxides) in the presence of sunlight, a dense haze of particles formed, and these particles had similar characteristics to those collected from Los Angeles smog.

Particles formed from the oxidation of anthropogenic hydrocarbon pollutants can be very complex. A study of SOA from oxidation of toluene by OH radicals identified 74 products [35], including organic acids, aromatics, and dicarbonyls, among other functional groups. The authors estimated that the identified species represented only 10% of the total mass present in the particles. Changes in relative humidity can alter the composition of these SOA particles. Tobias [36] analyzed SOA formed from the reaction of 1-tetradecene from ozone and found that particles formed at elevated relative humidity contained hydroperoxides as the major products, while particles formed in dry air contained mostly secondary ozonides. Changes in NO_x levels can impact the extent of particle formation as well as the composition. Song [37] oxidized *m*-xylene, a component of gasoline, in the absence and presence of NO_x. The experiments performed without NO_x resulted in higher aerosol mass without an appreciable change in ozone or nitrate radical concentrations. Particle composition was not measured in these experiments, but it is reasonable to think that condensable products formed from the reaction of NO_2 (for example) with a given alkyl radical will be distinctly different from those formed from the reaction of oxygen molecules with the same alkyl radical.

1.2.3 SOA from Biogenic Precursors

In less polluted areas, SOA formation can still be a significant contributor to the overall aerosol budget because of the abundance of BVOCs such as isoprene and various monoterpenes. The fact that volatiles emitted from plant leaves can be oxidized to form particles was first observed by Went in 1960 [38]. Upon crushing pine needles and putting them into a bell jar with ozone, Went noticed a "blue haze" from the formation of secondary organic aerosol particles. Went noted that there are mountain ranges on several continents with names such as "Blue Mountains" or "Blue Ridges", and suggested that the mountains take their names from the layer of SOA that forms over them on sunny days.

Research into the production of SOA from biogenic precursors has focused especially on isoprene (2-methyl-1,3-butadiene, C_5H_8) because of its dominance of the BVOC budget, although conclusions as to its SOA forming potential have varied. SOA formation from the reaction of ozone with isoprene is generally thought to be unimportant. OH radicals produced during the ozonolysis account for up to 50% of the particles produced [39]. Oxidation of isoprene in the presence of NO_x has been reported to produce particles with less than 1% yield [40]. For isoprene oxidation by OH in the presence of NO_x the yields are similarly small [41], but when NO_x is removed the initial particle yield increases to almost 10% before decreasing to around 4% due to photochemical aging [42]. Globally, the OH-initiated photooxidation of isoprene accounts for an estimated 2 Tg of SOA precursors per year [43]. In models which incorporate SOA, inclusion of

isoprene as a source of particles doubles the global SOA budget, and increases the production of SOA from other hydrocarbon precursors by 17% [44].

Although isoprene is by far the most common BVOC, it is not the only potential SOA precursor emitted from vegetation. Monoterpenes, a class of compounds made up of two isoprene subunits (chemical formula $C_{10}H_{16}$) are also emitted, and make up 11% of total NVOC emissions. The structures of isoprene and the most common monoterpenes are shown in Figure 1.1.

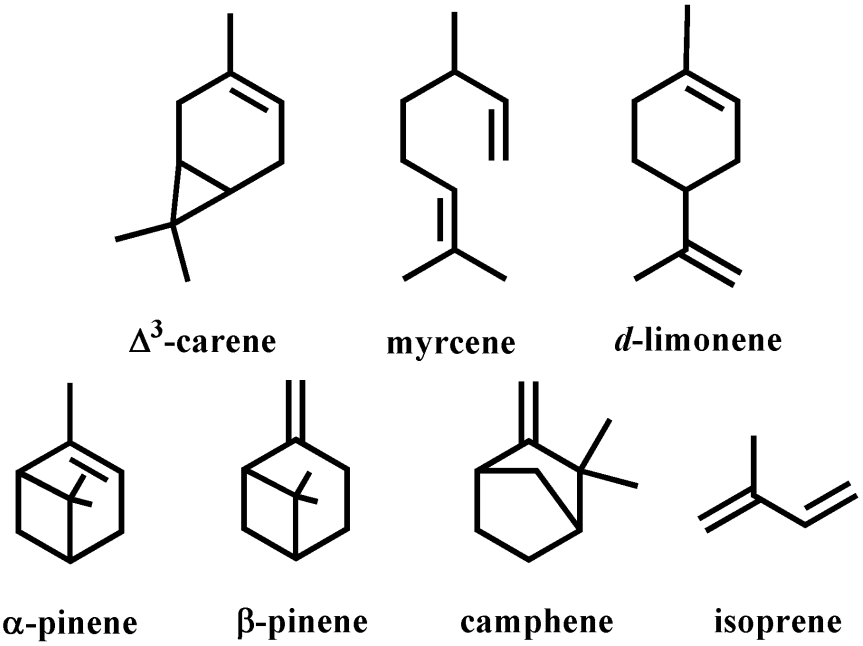

Figure 1.1. Structures of the most commonly occurring monoterpenes and of isoprene, the monoterpene building block.

Monoterpene oxidation products are more highly oxidized than those from isoprene, and so in general they have higher aerosol yields upon oxidation [40]. By far the most studied monoterpene is α-pinene, which is emitted from many

species of plants [45, 46], and from many forested areas in general [19, 47-51]. Oxidation of α-pinene results in a fractional aerosol yield (defined as the fraction of the terpene that is converted into aerosol, see Equation 1) between 1 and 25% [52], depending on temperature, the presence or absence of light, the nature of the oxidants present and the organic aerosol mass concentration. The chemistry of selected monoterpenes is discussed in more detail below.

1.3 Chemistry of SOA from Biogenic Precursors

1.3.1 α- and β-Pinene

The chemical composition of the aerosol formed from the oxidation of α-pinene is dependent on the identity of the oxidizer, among other factors. Monoterpenes can be oxidized by OH, O_3 or NO_3 as mentioned previously. The composition of the aerosol resulting from the three oxidation mechanisms has been studied by modeling and instrumental methods. The atmospheric lifetime of α-pinene with respect to ozone is between 0.5 and 4 hours, depending on the ambient ozone concentration [52, 53]; this is shorter than its lifetime with respect to either OH or NO_3. The aerosol yield from ozonolysis of α-pinene is on the order of 20% for dark experiments [52]. The first product of the ozonolysis of α-pinene is a primary ozonide formed by addition of the ozone molecule to the double bond. The primary ozonide is unstable and decomposes into a stable carbonyl and an unstable carbonyl oxide known as a Criegee intermediate. The Criegee intermediate can either recombine with the carbonyl to form a more

stable secondary ozonide, or it can be stabilized either thermally or via reactions with ambient species. The latter pathway leads to a wide distribution of products depending on the stabilization reaction. In the case of the α-pinene + O_3 reaction, many functional groups have been observed in the particle phase, including carboxylic acids [54, 55] and aldehydes [56-58], as well as secondary ozonides formed from the stabilized Criegee intermediates [59]. Mass spectrometry measurements [60] have also suggested a key role for oligomers as large as tetramers in the formation of SOA from oxidized α-pinene. Carbonyl products of the ozonolysis of α-pinene have been observed in ambient aerosol particles above forests [61].

The chemical composition of SOA formed from ozonolysis of α-pinene was modeled by Jenkin [62], who confirmed the importance of carboxylic acids and aldehydes, but also suggested a significant role for hydroperoxides, especially when the OH radicals produced in ozonolysis are removed by the inclusion of a scavenger. The role of peroxides was confirmed experimentally for ozonolysis of α-pinene and other monoterpenes in smog chamber studies [63] using cyclohexane, 1-propanol or formaldehyde as OH scavengers.

The oxidation of β-pinene proceeds in much the same way as that of α-pinene, and results in similar products. Oxidation of β-pinene results from addition of the oxidant (OH or ozone) to the carbon-carbon double bond and results in several carbonyl products [58]. When OH radical scavengers are added so that ozonolysis is the only oxidation mechanism, the number of

carbonyl products decreases, but carbonyls still make up the majority of product species [64].

1.3.2 d-Limonene

Compared to α-pinene, the global flux of *d*-limonene is relatively small. While it is present in lower amounts, the aerosol yield of *d*-limonene as a result of ozonolysis is much higher, as much as 40% [52] in daylight experiments conducted in the presence of NO_x (compared to a maximum 12% yield for α-pinene under similar conditions). In addition, *d*-limonene has a much shorter lifetime with respect to ozone oxidation (68 minutes, [52]) than does α-pinene.

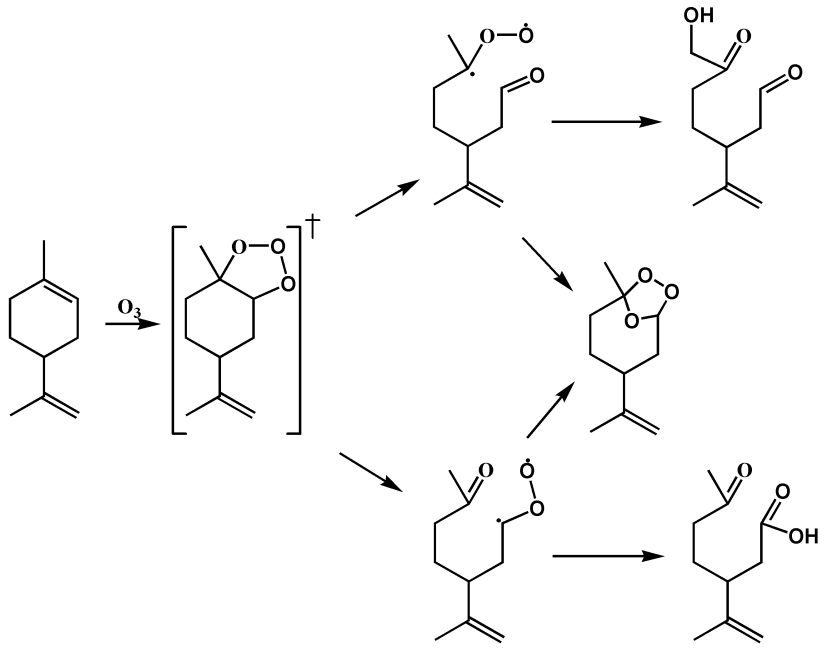

Figure 1.2. A simplified representation of the first steps of the oxidation of d-limonene. The product marked with a (†) is an unstable primary ozonide which decomposes quickly into biradicals. These biradicals can each form the same secondary ozonide or produce aldehyde, ketone and carboxylic acid products.

The ozonolysis of *d*-limonene proceeds in much the same way as the α-pinene oxidation discussed above, with the main difference being that *d*-limonene has two double bonds. These two are designated the endo-double bond (the double bond inside the ring) and the exo-double bond (the double bond outside the ring). The reaction of ozone with the endo-double bond is favored, with a branching ratio of 0.85 [65]. Ozone addition to the endo-double bond forms a primary ozonide (see Figure 1.2), which quickly decomposes into biradicals. These intermediate radicals can re-form into secondary ozonides (as discussed previously and as shown in Figure 1.2) or go on to form various carbonyl products. The secondary endo-ozonide formed from this rearrangement has been observed experimentally [66] as a major product of samples collected 16 seconds after the initiation of ozonolysis. Products consistent with ozone attack only on the exo-double bond have been detected in the gas phase [58, 64], indicating that this reaction channel should not be ignored as a potential source of particle-phase products.

The secondary ozonide is far from the only product formed from the ozonolysis of *d*-limonene. When the primary ozonide decomposes, biradical Criegee intermediates (CI) are formed that can have many fates. About half the time, the intermediate thermally stabilizes to a stable biradical; the stabilized CIs generally react with water to form carboxylic acids or aldehydes. Modeling results suggest that less than 1 % of the stabilized CIs form seed aerosol by reactions with larger molecules [65]. The stabilized CI can also react with various other atmospheric molecules to form a variety of functional groups, or re-

arrange to form secondary ozonides. Measurements have confirmed these findings; carboxylic acids, aldehydes and ketones were common particle phase products of *d*-limonene ozonolysis in smog chamber experiments [67].

The importance of *d*-limonene comes not only because it is emitted into the atmosphere by vegetation, but also because it is very common in orange-scented cleaning products intended for indoor use. Studies have shown that indoor reactions between monoterpenes and ozone can be a significant source of sub-micron particles [68] even if ozone is not present at concentrations higher than ordinary outdoor background levels.

1.4 Atmospheric Photochemistry

Interactions between molecules and oxidants are not the only initiator of chemistry in the atmosphere. Light-initiated reactions are also important contributors to the atmospheric chemistry of many areas. Perhaps the most infamous light-initiated reaction is the formation of photochemical smog when VOCs and NO_x react in the presence of light, catalytically producing ozone. Many nitrogen-containing pollutants are also produced [25]. Before strict emission controls were implemented, this photochemical process led to severe degradation of air quality in the Los Angeles area on sunny days, with results such as crop damage, decreased visibility, eye and respiratory irritation, and rubber cracking [34]. Many of the world's larger cities are affected by

photochemical smog, for which the sufficient conditions are high concentrations of VOCs and NO_x (for example, traffic emissions), and an abundance of sunlight.

Important radiation-initiated reactions occur throughout the atmosphere, but stratospheric reactions will be ignored for the remainder of this section. Tropospheric photochemistry is necessarily limited in scope because of the presence of stratospheric ozone. This protective layer of ozone prevents any solar radiation with wavelength shorter than approximately 295 nm from reaching the troposphere. In fact, because of scattering and absorptive processes, the solar spectrum that reaches the troposphere is severely attenuated compared to the actual solar spectrum. This attenuation limits the number of chemical processes that can be initiated by radiation in the troposphere, primarily by blocking the most energetic photons.

Despite this attenuation, a rich photochemistry does take place in the troposphere. Photochemical reactions can be responsible for the destruction of certain gas phase molecules, and also for the introduction of molecules into the gas phase. For example, organic films on urban surfaces may contain nitrate species, and photolysis of these films is likely to produce gas phase HONO and NO_2 [69].

The life cycle of tropospheric ozone is partially dictated by photochemistry. Ozone can be photolyzed to produce singlet oxygen at wavelengths up to 365 nm [25]; about 10% of the produced singlet oxygen reacts with water to form the important atmospheric oxidant OH. As the fate of tropospheric ozone is largely dictated by photochemistry, so too is its formation. The photolysis of nitrogen

dioxide to form nitrogen monoxide and an oxygen atom (which then recombines with molecular oxygen) is the only significant natural source of tropospheric ozone [25]. Ozone has also been shown to form during photooxidation of BVOCs in remote areas of the troposphere [70]; in some cases, up to 96% of the ozone concentration over forested areas can be attributed to this process. The loss and formation of many other gas phase molecules are largely controlled by solar radiation.

1.5 Photochemistry of Aerosols

1.5.1 Production of Aerosol Particles via Photooxidation

Ozone formation is not the only consequence of photochemical reactions of BVOCs. In many cases, photochemistry may initiate SOA formation or dictate the extent of particle production. Isoprene, the most common BVOC, has two double bonds and is therefore susceptible to attack by ozone, which can be produced photochemically in the presence of high levels (~200 ppb) of NO_x. Initial experiments by Pandis *et. al.* suggested that the first-generation products of photooxidation of isoprene were too volatile to partition to the particle phase [40], even in the presence of inorganic seed particles. These experiments showed that particle formation did not begin until about 250 ppb of isoprene had reacted, a concentration that is an order of magnitude higher than typical naturally occurring levels.

It is now well established that photooxidation of isoprene leads to particle formation [42-44, 70-72]. The confounding factor in Pandis's study was that the high NO_x levels suppressed alkoxy radical chemistry that was important to the creation of non-volatile products. The reduction of aerosol yields in the presence of high concentrations of NO_x is a well-known effect. Aerosol yields of 1% can be realized from the photooxidation of isoprene even at very low (tens of ppb) initial VOC concentrations, as long as no NO_x is present [42]. Photooxidation of monoterpenes also results in particle formation [40, 65, 73-76]. Samples of atmospheric aerosol collected over forests in Hungary contained polar oxygenated compounds, such as carboxylic acids, that were also produced in laboratory photooxidation of α-pinene in the presence of NO_x [76]. The existence of these compounds in the particle phase, in the words of the authors, "points to extensive photooxidation of α-pinene in the forest atmosphere". β-pinene was also photooxidized to form SOA precursors in experiments performed in the presence of NO_x, with initial monoterpenes concentrations of about 100 ppb [77]. A third monoterpene, *d*-limonene, has also been shown to form SOA after photooxidation [65]. For all of the work cited, particle formation did not begin until sufficient photochemical production of ozone had occurred. For this reason, the initial oxidation of the monoterpenes should not be considered substantially different for oxidation in the dark (with ozone as the only oxidant); differences arise due to the reactions of NO_x with first-generation oxidation products. In practice, this results in reduced aerosol production when NO_x is present, as mentioned previously.

Although in some cases light is necessary to initiate the reactions that lead to SOA, in other cases aerosol yield from the photooxidation of VOCs is reduced in the presence of UV radiation. When the ozonolysis of α-pinene is conducted in the presence of UV radiation, such as by Presto [78], the yield of SOA may be reduced by as much as 40% depending on the reactant concentrations used. Presto observed this reduction in yield only during particle nucleation, implying that photolysis of non-volatile SOA precursors in the gas phase, prior to nucleation, was responsible. Presto did not observe a reduction in particle mass when already-formed particles were exposed to light. Once the oxidation of α-pinene was complete, the resulting SOA did not appear susceptible to mass loss via direct photolysis. More recent experiments have suggested that mass loss is not a necessary consequence of photochemical particle aging.

1.5.2 Photolysis of Aerosol Particle Components

Photochemical processes are important contributors to the aging of atmospheric aerosol particles independent of the nature of their source. Robinson *et. al.* indirectly provided support for this theory with their study of the photochemistry of diesel exhaust [26]. They found that photochemical reactions not only transform semivolatile organics into non-volatile SOA precursors, but that some of these semivolatile molecules may enter the gas phase via evaporation from POA particles. Robinson's results imply that certain molecules found in organic aerosol may be photolyzed, but only once they have partitioned

to the gas phase. The possibility that these components may be photolyzed in the particle phase was not investigated because of the nature of the experiments.

Considering the prevalence of organic molecules on and in atmospheric aerosol particles [2-5, 11, 16-18, 79] and the importance of SOA [4, 18, 26, 27] (which may have no inorganic component at all) the photochemical processing of organic molecules in the particle phase is of interest. Photochemistry in the particle phase can occur by direct photolysis, where the organic molecule absorbs a photon, or indirect photolysis, where oxidizers are formed in the particle by other species absorbing photons, and then go on to oxidize the organic molecule.

Direct photolysis of organic particle components can cause particle aging via modification of compounds in the particle phase. Guzmán [80] demonstrated this fact by observing photoinduced oligomerization of a dicarboxylic acid, pyruvic acid, in the aqueous phase. Pyruvic acid, $CH_3C(O)C(O)OH$, and other α-dicarbonyls are commonly found in aerosol particles. When pyruvic acid is irradiated with 321 nm radiation, it can be directly photolyzed, resulting in loss of carbon dioxide and the formation of radical products. Self-association of these radicals in the aqueous phase leads to formation of multi-functional oligomers. Polycyclic aromatic hydrocarbons appear to photodegrade by a direct process as well, but only when they are present in natural waters [81]. The process is very complicated, involving intermediates and excited species, but does appear to be direct. In contrast, photolysis of PAHs in organic particles in the troposphere is

an indirect process [82], with PAH molecules acting as synthesizers to generate highly reactive singlet oxygen.

Direct photolytic processing has also been observed on proxies for organic aerosol particles. In a 2006 paper [24], Park *et. al.* investigated the UV photolysis of alkene-terminated self-assembled monolayers (SAMs) after processing them with ozone to create oxygenated functional groups. This reaction modeled a process that could lead to secondary organic aerosol formation, namely the ozonolysis of alkene VOCs in the atmosphere. Irradiation of the oxidized SAM surfaces with actinic radiation produced gas-phase formic acid and formaldehyde, which are produced from the photolysis of secondary ozonides, a class of organic peroxides produced during the ozonolysis of carbon-carbon double bonds. No attempt was made to analyze the SAM layer after photolysis, although it is safe to say that since the non-processed ends of the alkyl silanes were chemically bound to a silicon surface they would not act in the same way as organic molecules in an atmospheric aerosol particle.

Similar results from the photolysis of films of oxidized undecylenic acid [23] reinforced the importance of organic peroxides in photolysis of oxidized alkenes and further suggested that such photochemical processes might be important in the atmosphere. In this case the effect of the photolysis reaction on the molecules remaining in the film was investigated using electrospray ionization mass spectrometry. Before photolysis, the film was made up of a series of oligomers with very little remaining undecylenic acid, indicating a highly oxidized sample. After photolysis the oligomers were still present, although most peaks in

the mass spectrum had been significantly reduced in intensity. New product peaks also appeared in the mass spectrum. Because the ozonolysis of undecylenic acid resulted in significant polymerization before photolysis, these results can neither support nor refute the importance of particle-phase oligomerization as a result of photolysis. The results do suggest that photolysis does not always decrease the size of the organic molecules, implying that UV radiation can age particles without causing substantial mass loss to the gas phase.

Particle-phase photochemistry is not limited to direct photolysis. In a study of the effect of irradiation on fog droplets [83], Anastasio observed indirect photodestruction of several dissolved organic nitrate species. Molecules such as tryptophan and methionine were rapidly ($t_{1/2}$ ~1 hour) destroyed by mid-day sunlight, while other molecules were destroyed with half-lives on the order of a day. Direct photolysis was not responsible for the destruction; instead various oxidants, possibly including OH radical, singlet O_2, and peroxy radicals, were formed in the droplet water and reacted with the organic nitrogen compounds. In a review of photochemical reactions in fog and cloudwater, Vione [84] outlined the importance of indirect photolysis by enumerating the ways in which photochemical processes can form OH radical in the tropospheric aqueous phase. Nitrate, nitrite, iron (III) and hydrogen peroxide are all photolyzed in cloud droplets to form OH radical, which can then go on to oxidize organics present in the droplet. In this way, even molecules that are relatively impervious to photolysis can still be destroyed via photochemical processes. Vione noted that

indirect photochemistry in the aqueous phase can result in several classes of pollutants in addition to the destruction of organic molecules. Indirect photoprocesses are implicated as the cause of the enhanced photolysis rates in water droplets as compared to photolysis on the surface of particles.

Such indirect processes are not limited to the aqueous phase. They can also take place in carbonaceous aerosols such as those produced from wood or fossil fuel combustion. Such aerosols typically have a carbonaceous core surrounded by a liquid organic layer. Polycyclic aromatic hydrocarbon (PAH) molecules are products of incomplete combustion and (along with many other classes of organic molecules) are present in this organic layer. In organic solvents, organics such as ketones, phenols and quinones enhanced the photodegradation of a common PAH, benzo[a]anthracene [82]. Since the first step in the process involves absorption of a photon by benzo[a]anthracene, it is perhaps not strictly accurate to call the process indirect photolysis, but it is clear that other components of the organic fraction of the aerosol can substantially affect the rate of PAH destruction.

Field studies have emphasized the importance of photochemical aging for atmospheric particles. Volkamer *et. al.* [4] noticed that many of their measurements of SOA concentration did not agree with model predictions, and that the effect was more pronounced for air masses that had more exposure to sunlight. The difference was attributed to a missing SOA source, namely photochemical production of non-volatile products from VOCs after sunrise. Another field study [11] was able to attribute daily variation in aerosol chemical

composition near a Los Angeles freeway to photochemical processing. Specifically, particles collected in the morning contained more *n*-alkanes from traffic emissions, whereas aerosol particles collected in the afternoon contained more organic acids. This is evidence that photochemical reactions result in lower volatility, oxygenated products, which then partition to existing POA particles. In both of these cases, the photochemical processing of aerosol particles comes not from direct photolysis of particle components, but from photolysis of gas phase compounds which change the composition of the aerosol by partitioning into the particle phase.

As mentioned earlier, research aimed at detecting the products of photochemical reactions of aerosol components have largely been done on films and monolayers meant to model atmospheric particles. In a few cases, however, actual aerosol particles have been used for this purpose. For example, number and mass concentrations of SOA formed from isoprene photooxidation were monitored with and without UV irradiation [71]. The mass in the particle phase decreased when the light was on, but the number of particles did not. This suggested that particles were losing mass due to photolysis, and not being removed by chamber walls or other processes. Also, the concentration of peroxides in the particles decreased with time, providing further support for the existence of photochemical processes. However, the authors of that study did note the possibility that chemical reactions or transport to the gas phase could be responsible for the significant decrease in peroxide concentration.

A more explicit confirmation that photochemistry was responsible for particle aging came from monitoring the gas phase products of irradiation of SOA from limonene oxidation [85]. High resolution infrared spectroscopy revealed the photochemical production of formic acid and formaldehyde, indicating that organic peroxides were responsible for the photochemical aging of these particles. Organic peroxides had previously been identified in SOA produced from the oxidation of anthropogenic [36] and biogenic [62, 63] VOCs, and it was reasonable to expect that they would be photoactive when exposed to tropospheric UV. Particle phase aldehydes have also been identified as likely contributors to the photochemical aging of SOA from the reaction of *d*-limonene with ozone [65]. The gas phase products of this photochemical aging would include formaldehyde as well, although formic acid would not be produced.

1.6 Goals of this Thesis

Above, I have outlined the state of knowledge in the field of organic aerosol photochemistry. A specific area in which our knowledge is incomplete deals with the molecular constituents of aerosol particles that are susceptible to photochemical aging, and the results of that aging both in terms of gas phase products and the molecules that remain in the particle phase. Chapter 2 of this thesis deals with the gas phase products of the particle-phase photodegradation of carbonyl containing molecules, specifically the production of carbon monoxide. Photodissociation action spectroscopy was used to monitor the wavelength-

dependent production of CO from SOA formed from limonene ozonolysis, the goal being to determine whether tropospheric photochemistry could age the SOA via carbonyl photodecomposition. We also used gas chromatography to analyze larger oxygenated products of the SOA photolysis. Many products were detected, leading us to make conclusions about the mechanisms of photochemical aging that were in play for these particles. The implications of our findings for the atmospheric behavior of SOA are discussed in Chapter 2.

Photochemical aging is not the only possible mechanism by which the atmospheric behavior of limonene SOA can change. During their time in the troposphere, organic aerosols can absorb, scatter or reflect radiation; the balance between the three determines the aerosol's direct radiative forcing. It is desirable, therefore, to know the precise absorption profile of the particles. We have developed a simple, reproducible method for measuring UV-Visible and FTIR absorption spectra of relatively homogeneous thin films of SOA, which is discussed in Chapter 3; spectra collected via this method are also presented. Chapter 3 further describes experiments wherein we examined the absorption profiles of the SOA particles as a function of residence time in open air. This is a new research project, and the results in Section 3.3 especially should be considered preliminary. However, some conclusions can be drawn about the changes that the particles undergo during time spent in open air. The absorption spectra of fresh and aged particles were compared to see how a particle's absorption profile might change during its lifetime in the troposphere. The atmospheric implications of these changes are also discussed in Chapter 3.

1.7 References

1. Forster, P., et al., *Changes in Atmospheric Constituents and in Radiative Forcing.* Climate Change 2007: The Physical Science Basis. Contribution of Working Group I to the Fourth Assessment Report of the Intergovernmental Panel on Climate Change., ed. S. Solomon, et al. 2007, Cambridge, United Kingdom: Cambridge University Press.
2. Middlebrook, A., D.M. Murphy, and D.S. Thomson, *Observations of organic material in individual marine particles at Cape Grim during the First Aerosol Characterization Experiment (ACE-1).* Journal of Geophysical Research, 1998. 103(D13): p. 16,475-16,483.
3. Tervahattu, H., et al., *Fatty acids on continental sulfate aerosol particles.* Journal of Geophysical Research, 2005. 110(D6): p. D06207.
4. Volkamer, R., et al., *Secondary organic aerosol formation from anthropogenic air pollution: Rapid and higher than expected.* Geophysical Research Letters, 2006. 33: p. L17811.
5. Rogge, W.F., et al., *Sources of fine organic aerosol. 1. Charbroilers and meat cooking operations.* Environ. Sci. Technol., 1991. 25(6): p. 1112-1125.
6. Schauer, J.J., et al., *Source apportionment of airborne particulate matter using organic compounds as tracers.* Atmospheric Environment, 1996. 30(22): p. 3837-3855.
7. Hildemann, L.M., G.R. Markowski, and G.R. Cass, *Chemical Composition of Emissions from Urban Sources of Fine Organic Aerosol.* Environ. Sci. Technol., 1991. 25(4): p. 744-759.
8. Rogge, W.F., et al., *Sources of fine organic aerosol. 2. Noncatalyst and catalyst-equipped automobiles and heavy-duty diesel trucks.* Environ. Sci. Technol., 1993. 27(4): p. 636-651.
9. Rogge, W.F., et al., *Sources of fine organic aerosol. 3. Road dust, tire debris, and organometallic brake lining dust: roads as sources and sinks.* Environ. Sci. Technol., 1993. 27(9): p. 1892-1904.
10. Tsapakis, M., et al., *The composition and sources of $PM_{2.5}$ organic aerosol in two urban areas of Chile.* Atmospheric Environment, 2002. 36(23): p. 3851-3863.
11. Ning, Z., et al., *Daily Variation in Chemical Characteristics of Urban Ultrafine Aerosols and Inference of Their Sources.* Environ. Sci. Technol., 2007. 41(17): p. 6000-6006.
12. Rogge, W.F., et al., *Sources of Fine Organic Aerosol. 9. Pine, Oak, and Synthetic Log Combustion in Residential Fireplaces.* Environ. Sci. Technol., 1998. 32(1): p. 13-22.
13. Rogge, W.F., et al., *Sources of Fine Organic Aerosol. 8. Boilers Burning No. 2 Distillate Fuel Oil.* Environ. Sci. Technol., 1997. 31(10): p. 2731-2737.
14. Gogou, A., et al., *Organic aerosols in Eastern Mediterranean: components source reconciliation by using molecular markers and atmospheric back trajectories.* Organic Geochemistry, 1996. 25(1-2): p. 79-96.
15. Rogge, W.F., et al., *Sources of Fine Organic Aerosol. 6. Cigaret Smoke in the Urban Atmosphere.* Environ. Sci. Technol., 1994. 28(7): p. 1375-1388.
16. Kadowaki, S., *Characterization of carbonaceous aerosols in the Nagoya urban area. 1. Elemental and organic carbon concentrations and the origin of organic aerosols.* Environ. Sci. Technol., 1990. 24(5): p. 741-744.
17. Gray, H.A., et al., *Characteristics of atmospheric organic and elemental carbon particle concentrations in Los Angeles.* Environ. Sci. Technol., 1986. 20(6): p. 580-589.
18. Lim, H.J. and B.J. Turpin, *Origins of Primary and Secondary Organic Aerosol in Atlanta: Results of Time-Resolved Measurements during the Atlanta Supersite Experiment.* Environ. Sci. Technol., 2002. 36(21): p. 4489-4496.
19. Guenther, A., et al., *A global model of natural volatile organic compound emissions.* Journal of Geophysical Research, 1995. 100(D5): p. 8873-8892.

20. Goldstein, A.H. and I.E. Galbally, *Known and Unexplored Organic Constituents in the Earth's Atmosphere.* Environ. Sci. Technol., 2007. 41(5): p. 1514-1521.
21. Eliason, T.L., J.B. Gilman, and V. Vaida, *Oxidation of organic films relevant to atmospheric aerosols.* Atmospheric Environment, 2004. 38(9): p. 1367-1378.
22. Thomas, E.R., G.J. Frost, and Y. Rudich, *Reactive uptake of ozone by proxies for organic aerosols: Surface-bound and gas-phase products.* Journal of Geophysical Research, 2001. 106(D3): p. 3045-3056.
23. Gomez, A.L., et al., *UV Photodissociation Spectroscopy of Oxidized Undecylenic Acid Films.* J. Phys. Chem. A, 2006. 110(10): p. 3584-3592.
24. Park, J., et al., *Ozonolysis and photolysis of alkene-terminated self-assembled monolayers on quartz nanoparticles: implications for photochemical aging of organic aerosol particles.* Physical Chemistry Chemical Physics, 2006. 8: p. 2506-2512.
25. Finlayson-Pitts, B.J. and J.N. Pitts, *Chemistry of the Upper and Lower Atmosphere*. 2000, San Diego: Academic Press.
26. Robinson, A.L., et al., *Rethinking Organic Aerosols: Semivolatile Emissions and Photochemical Aging.* Science, 2007. 315(5816): p. 1259-1262.
27. Chung, S.H. and J.H. Seinfeld, *Global distribution and climate forcing of carbonaceous aerosols.* Journal of Geophysical Research, 2002. 107(D19): p. 4407.
28. Grosjean, D. and J.H. Seinfeld, *Parameterization of the formation potential of secondary organic aerosols.* Atmospheric Environment, 1989. 23(8): p. 1733-1747.
29. Pankow, J.F., *An absorption model of the gas/aerosol partitioning involved in the formation of secondary organic aerosol.* Atmospheric Environment, 1994. 28(2): p. 189-193.
30. Odum, J.R., et al., *Gas/Particle Partitioning and Secondary Organic Aerosol Yields.* Environ. Sci. Technol., 1996. 30(8): p. 2580-2585.
31. Donahue, N.M., et al., *Coupled Partitioning, Dilution, and Chemical Aging of Semivolatile Organics.* Environ. Sci. Technol., 2006. 40(8): p. 2635-2643.
32. Donahue, N.M., et al., *Critical factors determining the variation in SOA yields from terpene ozonolysis: A combined experimental and computational study.* Faraday Discuss., 2005. 130: p. 295-309.
33. Griffin, R.J., et al., *Secondary organic aerosol 3. Urban/regional scale model of size- and composition-resolved aerosols.* Journal of Geophysical Research, 2002. 107(D17): p. 4334.
34. Haagen-Smit, A.J., *Chemistry and Physiology of Los Angeles Smog.* Ind. Eng. Chem., 1952. 44(6): p. 1342-1346.
35. Hamilton, J.F., et al., *Quantifying small molecules in secondary organic aerosol formed during the photo-oxidation of toluene with hydroxyl radicals.* Atmospheric Environment, 2005. 39(38): p. 7263-7275.
36. Tobias, H.J., et al., *Effect of Relative Humidity on the Chemical Composition of Secondary Organic Aerosol Formed from Reactions of 1-Tetradecene and O3.* Environ. Sci. Technol., 2000. 34(11): p. 2116-2125.
37. Song, C., K. Na, and D.R. Cocker, *Impact of the Hydrocarbon to NO_x Ratio on Secondary Organic Aerosol Formation.* Environ. Sci. Technol., 2005. 39(9): p. 3143-3149.
38. Went, F.W., *Blue Hazes in the Atmosphere.* Nature, 1960. 187: p. 641-643.
39. Kleindienst, T.E., et al., *Ozone-isoprene reaction: Re-examination of the formation of secondary organic aerosol.* Geophysical Research Letters, 2007. 34: p. L01805.
40. Pandis, S.N., et al., *Aerosol formation in the photooxidation of isoprene and b-pinene.* Atmospheric Environment, 1991. 25A(5/6): p. 997-1008.
41. Kroll, J.H., et al., *Secondary organic aerosol formation from isoprene photooxidation under high-NO_x conditions.* Geophysical Research Letters, 2005. 32: p. L18898.
42. Kroll, J.H., et al., *Secondary Organic Aerosol Formation from Isoprene Photooxidation.* Environ. Sci. Technol., 2006. 40(6): p. 1869-1877.
43. Claeys, M., et al., *Formation of Secondary Organic Aerosols Through Photooxidation of Isoprene.* Science, 2004. 303(5661): p. 1173-1176.

44. Henze, D.K. and J.H. Seinfeld, *Global secondary organic aerosol from isoprene oxidation.* Geophysical Research Letters, 2006. 33: p. L09812.
45. Christensen, C.S., et al., *Determination of the terpene flux from orange species and Norway spruce by relaxed eddy accumulation.* Atmospheric Environment, 2000. 34(19): p. 3057-3067.
46. Rapparini, F., R. Baraldi, and O. Facini, *Seasonal variation of monoterpene emission from Malus domestica and Prunus avium.* Phytochemistry, 2001. 57(5): p. 681-687.
47. Janson, R., *Monoterpene concentrations in and above a forest of scots pine.* Journal of Atmospheric Chemistry, 1992. 14(1): p. 385-394.
48. Davis, K.J., D.H. Lenschow, and P.R. Zimmerman, *Biogenic nonmethane hydrocarbon emissions estimated from tethered balloon observations.* Journal of Geophysical Research, 1994. 99(D12): p. 25587-25598.
49. Pio, C.A. and A.A. Valente, *Atmospheric fluxes and concentrations of monoterpenes in resin-tapped pine forests.* Atmospheric Environment, 1998. 32(4): p. 683-691.
50. Geron, C., et al., *A review and synthesis of monoterpene speciation from forests in the United States.* Atmospheric Environment, 2000. 34(11): p. 1761-1781.
51. Hayward, S., et al., *Monoterpene emissions from soil in a Sitka spruce forest.* Atmospheric Environment, 2001. 35(24): p. 4081-4087.
52. Hoffmann, T., et al., *Formation of Organic Aerosols from the Oxidation of Biogenic Hydrocarbons.* Journal of Atmospheric Chemistry, 1997. 26(2): p. 189-222.
53. Khamaganov, V.G. and R.A. Hites, *Rate Constants for the Gas-Phase Reactions of Ozone with Isoprene, α- and β-Pinene, and Limonene as a Function of Temperature.* J. Phys. Chem. A, 2001. 105(5): p. 815-822.
54. Glasius, M., M. Duane, and B.R. Larsen, *Determination of polar terpene oxidation products in aerosols by liquid chromatography-ion trap mass spectrometry.* Journal of Chromatography A, 1999. 833(2): p. 121-135.
55. Koch, S., et al., *Formation of new particles in the gas-phase ozonolysis of monoterpenes.* Atmospheric Environment, 2000. 34(23): p. 4031-4042.
56. Librando, V. and G. Tringali, *Atmospheric fate of OH initiated oxidation of terpenes. Reaction mechanism of α-pinene degradation and secondary organic aerosol formation.* Journal of Environmental Management, 2005. 75(3): p. 275-282.
57. Yu, J., et al., *Gas-Phase Ozone Oxidation of Monoterpenes: Gaseous and Particulate Products.* Journal of Atmospheric Chemistry, 1999. 34(2): p. 207-258.
58. Grosjean, D., E.L. Williams, and J.H. Seinfeld, *Atmospheric oxidation of selected terpenes and related carbonyls: gas-phase carbonyl products.* Environ. Sci. Technol., 1992. 26(8): p. 1526-1533.
59. Tolocka, M.P., et al., *Chemistry of Particle Inception and Growth during α-Pinene Ozonolysis.* Environ. Sci. Technol., 2006. 40(6): p. 1843-1848.
60. Tolocka, M.P., et al., *Formation of Oligomers in Secondary Organic Aerosol.* Environ. Sci. Technol., 2004. 38(5): p. 1428-1434.
61. Yokouchi, Y. and Y. Ambe, *Aerosols formed from the chemical reaction of monoterpenes and ozone.* Atmospheric Environment (1967), 1985. 19(8): p. 1271-1276.
62. Jenkin, M.E., *Modelling the formation and composition of secondary organic aerosol from α- and β-pinene ozonolysis using MCM v3.* Atmos. Chem. Phys., 2004. 4: p. 1741-1757.
63. Docherty, K.S., et al., *Contributions of Organic Peroxides to Secondary Aerosol Formed from Reactions of Monoterpenes with O_3.* Environ. Sci. Technol., 2005. 39(11): p. 4049-4059.
64. Grosjean, D., et al., *Atmospheric oxidation of biogenic hydrocarbons: reaction of ozone with β-pinene, D-limonene and trans-caryophyllene.* Environ. Sci. Technol., 1993. 27(13): p. 2754-2758.
65. Leungsakul, S., M. Jaoui, and R.M. Kamens, *Kinetic Mechanism for Predicting Secondary Organic Aerosol Formation from the Reaction of d-Limonene with Ozone.* Environ. Sci. Technol., 2005. 39(24): p. 9583-9594.

66. Norgaard, A.W., et al., *Secondary limonene endo-ozonide: A major product from gas-phase ozonolysis of R-(+)-limonene at ambient temperature.* Atmospheric Environment, 2006. 40(19): p. 3460-3466.
67. Jaoui, M., et al., *Analysis of Secondary Organic Aerosol Compounds from the Photooxidation of d-Limonene in the Presence of NO_x and their Detection in Ambient $PM_{2.5}$.* Environ. Sci. Technol., 2006. 40(12): p. 3819-3828.
68. Weschler, C.J. and H.C. Shields, *Indoor ozone/terpene reactions as a source of indoor particles.* Atmospheric Environment, 1999. 33(15): p. 2301-2312.
69. Handley, S.R., D. Clifford, and D.J. Donaldson, *Photochemical Loss of Nitric Acid on Organic Films: a Possible Recycling Mechanism for NO_x.* Environ. Sci. Technol., 2007. 41(11): p. 3898-3903.
70. Tsigaridis, K. and M. Kanakidou, *Importance of volatile organic compounds photochemistry over a forested area in central Greece.* Atmospheric Environment, 2002. 36(19): p. 3137-3146.
71. Surratt, J.D., et al., *Chemical Composition of Secondary Organic Aerosol Formed from the Photooxidation of Isoprene.* J. Phys. Chem. A, 2006. 110(31): p. 9665-9690.
72. Ng, N.L., et al., *Contribution of First- versus Second-Generation Products to Secondary Organic Aerosols Formed in the Oxidation of Biogenic Hydrocarbons.* Environ. Sci. Technol., 2006. 40(7): p. 2283-2297.
73. Zhang, S.-H., et al., *Photochemical aerosol formation from a-pinene and b-pinene.* Journal of Geophysical Research, 1992. 97(D18): p. 20,717-20,729.
74. Griffin, R.J., et al., *Organic aerosol formation from the oxidation of biogenic hydrocarbons.* Journal of Geophysical Research, 1999. 104(D3): p. 3555-3567.
75. Lee, A., et al., *Gas-phase products and secondary aerosol yields from the photooxidation of 16 different terpenes.* Journal of Geophysical Research, 2006. 111: p. D17035.
76. Claeys, M., et al., *Hydroxydicarboxylic Acids: Markers for Secondary Organic Aerosol from the Photooxidation of β-Pinene.* Environ. Sci. Technol., 2007. 41(5): p. 1628-1634.
77. Hoffmann, T., et al., *Aerosol formation potential of biogenic hydrocarbons.* Journal of Aerosol Science, 1996. 27(Supplement 1): p. S233-S234.
78. Presto, A.A., K.E. HuffHartz, and N.M. Donahue, *Secondary Organic Aerosol Production from Terpene Ozonolysis. 1. Effect of UV Radiation.* Environ. Sci. Technol., 2005. 39(18): p. 7036-7045.
79. Murphy, D.M., D.S. Thomson, and M.J. Mahoney, *In Situ Measurements of Organics, Meteoritic Material, Mercury, and Other Elements in Aerosols at 5 to 19 Kilometers.* Science, 1998. 282(5394): p. 1664-1669.
80. Guzman, M.I., A.J. Colussi, and M.R. Hoffmann, *Photoinduced Oligomerization of Aqueous Pyruvic Acid.* J. Phys. Chem. A, 2006. 110(10): p. 3619-3626.
81. Mill, T., et al., *Photolysis of polycyclic aromatic hydrocarbons in water.* Chemosphere, 1981. 10(11-12): p. 1281-1290.
82. McDow, S.R., et al., *An approach to studying the effect of organic composition on atmospheric aerosol photochemistry.* Journal of Geophysical Research, 1996. 101(D14): p. 19593-19600.
83. Anastasio, C. and K.G. McGregor, *Photodestruction of Dissolved Organic Nitrogen Species in Fog Waters.* Aerosol Science and Technology, 2000. 32(2): p. 106 - 119
84. Vione, D., et al., *Photochemical reactions in the tropospheric aqueous phase and on particulate matter.* Chemical Society Reviews, 2006. 35: p. 441-453.
85. Walser, M.L., et al., *Photochemical Aging of Secondary Organic Aerosol Particles Generated from the Oxidation of d-Limonene.* J. Phys. Chem. A, 2007. 111(10): p. 1907-1913.

Chapter 2

Gas Phase Photolysis Products from Monoterpene Secondary Organic Aerosol

2.1 Introduction

As explained in the previous chapter, secondary organic aerosols (SOA) have the potential to be significantly aged by tropospheric actinic radiation. When one sets out to determine the nature of this aging, there are two routes that can be taken: either the products left behind in the particle phase can be analyzed before and after the photochemical aging, or the gas-phase byproducts of aging can be monitored in real time. Studying photochemical aging by monitoring the gas phase products of aging processes offers some obvious advantages. The most important of these advantages is that the experiments can be performed quickly and non-destructively, and the sample is available for detection in real time (and only when desired, that is, when the sample is irradiated). In the case of the CRDS experiment described in this chapter, this means that the number of data points that can be taken from one SOA sample before it degrades or is otherwise modified is greatly increased. This is a significant practical concern, because of the time limitations imposed by the non-photochemical aging processes that will be discussed in Chapter 3 of this work.

2.1.1 Gas phase products from ozonolysis

Previous studies on the oxidation of monoterpenes and other alkenes have identified gas phase products in addition to modification of the alkene molecules. For example, all SOA precursors from monoterpene oxidation start out in the gas phase; those with the lowest vapor pressures partition into the particle phase (or self-nucleate, in the absence of seed particles) to form the SOA. This partitioning depends on the aerosol mass present, the temperature, and the vapor pressure of the gas phase species [1, 2]. In the same way that the gas phase products of photolysis can give information on the mechanism of photochemical aging, so too can the gas phase products of oxidation reveal details about the mechanism of chemical aging.

One of the most straightforward ways to monitor the gas phase products of ozonolysis is to anchor the alkene to be oxidized on a surface. This can be accomplished using self assembled monolayers (SAMs) with a C=C bond at the end of the chain. When the SAM is exposed to ozone, the large products of ozonolysis will remain bound to the surface and the smaller gas phase products will be free to escape and be detected in the gas phase. Such a technique has been used by multiple research groups to investigate the oxidation of unsaturated hydrocarbons on surfaces [3, 4] and on quartz nanoparticles [5]. In both cases, ozonolysis of a terminal double bond produced gas phase formaldehyde but very little formic acid, providing an unambiguous indication of the mechanism of primary ozonide decomposition. Gas phase products have

also been monitored in chamber experiments performed to investigate the mechanism of biogenic volatile organic compound (BVOC) ozonolysis [6-9].

If the mechanism of ozonolysis (and by extension the expected product distribution) is known, gas phase molecules can be used as markers for whether or not ozonolysis reactions are ongoing in a particular area. This was first demonstrated by Calogirou [10], who measured the gas-phase concentrations of nopinone and pinonaldehyde, from the ozonolysis of β- and α-pinene respectively, over a forest atmosphere. Since then, many other researchers have detected the gas phase products of BVOC oxidation in the troposphere [8, 9, 11-13], emphasizing the atmospheric importance of these reactions.

2.1.2 Previous use of gas-phase products to analyze photolysis

There is actually a long history of research that indirectly (and in some cases unintentionally) addresses the nature of the gas phase products of SOA photochemistry. The earliest example is the body of literature on the mechanism of carbonyl photolysis in solution; this is relevant to our discussion because of the high prevalence of carbonyl products [6, 7, 9, 14-23] in SOA formed via oxidation of monoterpenes. The first explanation of the mechanism of aldehyde and ketone photolysis was a result of research by Norrish and coworkers; Bamford and Norrish summarized the results in a 1935 paper [24]. These photoprocesses are discussed more fully in section 2.3.3 of this chapter. More than three decades after the description of these processes, the Norrish type I and II photolysis of ketones was again an active research topic. This time, the research

was motivated by the implications for the aging of polymer films (specifically polypropylene). A pure film of saturated hydrocarbons absorbs light only at wavelengths shorter than 200 nm, meaning that sunlight ($\lambda > 295$ nm) would not degrade the pure polymer. Polypropylene at the time did degrade in sunlight, however, because of the presence of impurities that absorbed light at wavelengths longer than 295 nm. Research into the photodissociation of these impurities, which were largely carbonyl-containing, was undertaken in part to produce more effective stabilizers for polypropylene films [25].

Branched ketones that had structures similar to impurities found in polypropylene were observed to absorb UV radiation in solution with a maximum at around 285 nm and an extinction coefficient of around 30 L $mol^{-1}cm^{-1}$ [25], and collection of the gas-phase products of photolysis suggested that type I (evidenced by production of CO and CH_4) and type II (evidenced by production of acetone) photoprocesses were occurring. Other studies on the photolysis of these model impurities, usually branched ketones, showed that the quantum yields for the type I and II processes are dependent on the chain length of the carbonyl molecule [26]. The type II process generally has the higher quantum yield, being roughly an order of magnitude more likely than the type I process for a ten-carbon ketone. For larger systems such as ethylene-carbon monoxide copolymers [27], the quantum yield for all types of bond breaking in solution was found to be 0.04, intermediate between the large-molecule limits [26] for type I (quantum yield = 0.01) and type II (quantum yield = 0.06) photolysis.

Photolysis of the ethylene-carbon monoxide copolymers produced gas phase carbon monoxide in measurable quantities. The quantum yield for CO production (related to the quantum yield for the type I process) was found to be about 0.01, increasing with temperature [27]. The temperature dependence of type II photolysis of the ethylene-carbon monoxide copolymers (the related quantum yield of terminal double bond formation was actually measured) was studied as well, and was shown to be independent of temperature above about 240 K, at which point the polymer undergoes a phase shift to a glass-like state that presumably hinders the formation of the six-membered intermediate necessary for type II photolysis. Indeed, below 150 K (at which point formation of the intermediate is kinetically hindered), no type II photolysis is observed [27]. At temperatures around 298 K, type II photolysis was the dominant process for the ethylene-carbon monoxide copolymers.

2.2 Infrared Cavity Ring-Down Spectroscopy

2.2.1 Infrared Cavity Ring-Down Spectroscopy

Since Infrared Cavity Ring-Down Spectroscopy (IR-CRDS) is not a common spectroscopic technique, a short discussion of the method is appropriate. Briefly, CRDS uses a stable optical cavity defined by two highly reflective concave mirrors to increase the pathlength of an infrared laser through a gas-phase sample. A CRDS spectrometer has three important components: the optical cavity, where the absorption measurements take place; a laser to

pump the cavity; and the detector, positioned outside the cavity mirror farthest from the laser to measure light leaking from the cavity.

When there is no gas phase absorber in the cavity, each laser pulse gradually decreases in intensity over time due to light losses through the mirrors due to the reflectivity of the mirrors being less than 1. The term “ring-down” was coined because the photons from the laser pulse can be though of as *ringing* back and forth in the cavity, while the pulse’s intensity goes *down* exponentially with each successive interaction with the cavity mirrors [28]. The light loss over successive trips is described by the following relationship:

$$S(t) = S_0 \exp(-\beta t) \qquad (1)$$

in which S(t) is the signal observed by the detector at a given time after the injection of the pulse and S_0 is the initial signal. Performing an exponential fit on a plot of S(t) vs. t allows the real-time extraction of β as a function of wavelength. The signal at the detector is simply the intensity inside the cavity times the mirror reflectivity [29], so that the relationship between the two is constant in the regime where the mirrors are optimized to remain highly reflective. The decay constant β is a function of the number of reflections per round trip (two), the loss per reflection (or the mirror reflectivity), and the number of round trips made by the laser pulse [30]. Our CRDS system uses mirrors that are 99.98% reflective, meaning that 0.02% of the intensity is lost at each mirror.

This exponential decay of the intensity in the cavity is normally described by the ring down time τ, which is the inverse of the exponential decay constant β. The time constant τ for the decay of light intensity in the cavity is given by:

$$\tau = t_r \times (2(1-R))^{-1} \quad (2)$$

where R is the mirror reflectivity and t_r is the time required for the laser pulse to make one round trip across the cavity [30]. This can also be thought of as the ring-down time for an empty cavity with no gas phase absorber, or τ_0. For our instrument under typical experimental conditions, τ_0 is approximately 6 μs (the theoretical value for our cavity is approximately 6.5 μs).

When a gas phase absorber is introduced to the cavity, additional intensity is lost due to absorption by the gas molecules. This causes a reduction in the ring-down time that depends on the concentration of gas phase absorber. The additional loss from absorption depends on the loss per round trip and the number of round trips made by the light pulse [30]. The first of these quantities can be written as a Beer's Law-type relationship, where absorbance is equal to an absorption coefficient times twice the pathlength through the sample. The number of trips made by the laser pulse is just the distance that the pulse travels, divided by the length of one round trip. Therefore, the absorption is given by:

$$\text{loss} = (2\ \alpha\ L)(t\ c\ /\ 2\ L) \quad (3)$$

where α is the absorption coefficient, L is the length of one pass through the cavity, and the quantity (t c / 2 L) is the number of round trips that the laser pulse makes in a time t. The absorption coefficient is given by the product of the absorber's concentration and its absorption cross section, σC. The equation that describes τ for a cavity containing an absorber is very similar to the equation for the empty cavity (Equation 2), with an extra term that accounts for molecular absorption:

$$\tau = t_r \times (2[(1-R)+ \alpha L])^{-1} \quad (4)$$

Equations 2 and 4 can be combined and solved for α [30] to eliminate the dependence on the mirror reflectivity. The resulting expression for the absorption cross section is dependent only on change in the ring-down time for a sample-filled cavity compared to the empty cavity:

$$\alpha = (1/c)(1/\tau - 1/\tau_0) \quad (5)$$

Equation 5 is the most important equation used in interpreting data collected via cavity ring-down spectroscopy. As the pulsed laser wavelength is scanned, a new α(λ) is collected for each wavelength, and the vibrational absorption spectra of the molecules in the cell can be plotted as a graph of α(λ) vs. λ after two laser scans (one for the background values of τ and one to measure τ with an absorber in the cavity). The absorption cross section has a linear relationship to the concentration of the absorber:

$$\alpha(\lambda) = [X]\, \sigma(\lambda)_X \quad (6)$$

where $\sigma(\lambda)_X$ is the wavelength-dependent absorption cross section of the absorber X. In practice, this relationship is often non-linear, especially in cases when the laser bandwidth is larger than the linewidth of the transition being monitored; this is the case in our system. In such cases, absolute absorbances can only be measured by explicit calibration of the instrument with known concentrations of the absorber.

2.2.2. The History of CRDS

Cavity ring-down spectroscopy was first developed by O'Keefe and Deacon [31] in 1998, who used it to measure the very weak forbidden transitions of molecular oxygen in ambient laboratory air. They reported a detection limit for absorption of one part in 10^6 using a pulsed, visible (λ = 686-695 nm) light source. In the following decade, the CRDS technique was used for studies of kinetics, molecular beams, and various other systems. UV and visible light sources were used for these studies. In 1995, Scherer [32] and co-workers extended the CRDS technique into the infrared wavelength range. Specifically, they probed the 1.6 μm region to detect acetylene and the 3.3 μm region to detect methane. In the decades after Scherer's work was published, IR-CRDS found use in a variety of experiments; reviews of these were compiled by Berden [33] and Atkinson [28]. The CRDS technique gained extensive popularity in the last years of the 20th century, to the point where its use has become unremarkable; indeed, as Berden noted, many authors do not bother to include the phrase "cavity ring-down spectroscopy" in their paper titles even when the technique is central to their research.

2.2.3 Atmospheric Research With CRDS

In his review, Atkinson outlined the relative strengths and weaknesses of the CRDS technique with respect to spectroscopy of environmental samples. The main advantage of CRDS is that it provides a very long pathlength, and consequently high sensitivity, for a relatively low cost. The fact that the long

pathlength exists within a small (~1 meter) cavity that can be pumped by a fairly cheap diode laser means that portable CRDS systems are straightforward to assemble. On the negative side, though, CRDS systems can be easily saturated, and sensitivity at atmospheric pressure is reduced significantly because of pressure broadening. However, the results of O'Keefe [31] and (more significantly) Fawcett [34] showed that atmospheric pressure detection of species in air (molecular oxygen and methane, respectively) is possible with very low detection limits.

One aspect of environmental sampling to which CRDS would seem ideally suited is the detection and monitoring of trace contaminants and other species with low mixing ratios in the atmosphere. CRDS has been used in the laboratory to sensitively detect various oxides of nitrogen, and field-portable instruments have been constructed to detect aerosol particles and also NO_3, an important nighttime oxidant [28]. The vapor form of mercury has also been detected in ambient laboratory air using the same instrument [28]. Further, the detection of methane at atmospheric pressure at levels down to 52 ppb [34] implies that CRDS has utility for the monitoring of hydrocarbons in the atmosphere.

2.3 Measuring Gas Phase Photolysis Products from Monoterpene Secondary Organic Aerosol

2.3.1 Experimental Methods

Particle Production and Collection. Monoterpene SOA was produced from the reaction of *d*-limonene (1-methyl-4-prop-1-en-2-yl-cyclohexene) with ozone in a Teflon chamber. Reactions were conducted in the dark at 750 torr, 298K, and low relative humidity (<1%). Limonene was injected into the chamber using a microsyringe. In order to accelerate oxidation of the *d*-limonene molecules and improve SOA yield, a large excess of ozone was used in the initial experiments. Ozone was produced by flowing high-purity (99.994%) oxygen through a commercial ozone generator. Typical reagent concentrations were 300 ppm ozone and 10 ppm limonene (97%, Fisher Scientific), and a 300 L Teflon chamber was used for these high concentration experiments. Although these concentrations are very high in absolute terms compared to what would be found in the troposphere, the ratio of limonene to ozone concentration is within reasonable limits for terpene/ozone ratios measured at night [35]. Particles were also prepared at lower concentrations (1 ppm O_3, 500 ppb limonene) to ensure that the results of the photolysis experiments were not concentration-dependent. A depiction of the particle preparation and collection apparatus is shown in Figure 2.1.

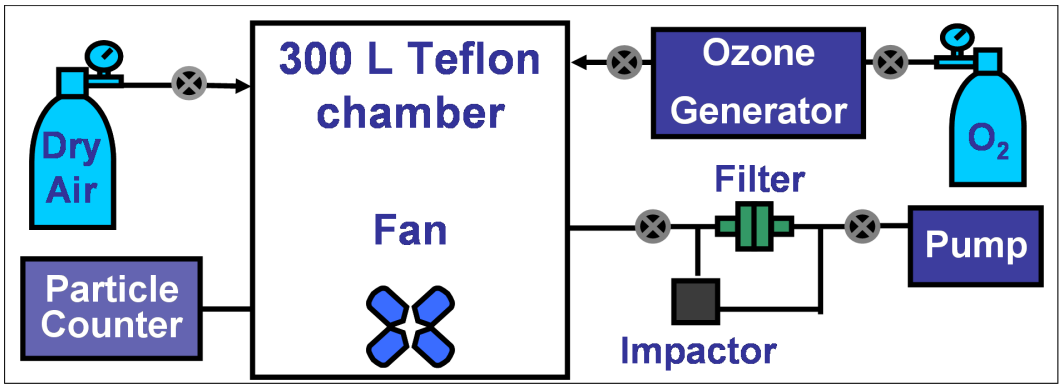

Figure 2.1. Particle production and collection setup. Replacing the particle counter with an ozone meter allows us to determine the ozone concentration in the bag for each experiment. Particles were collected onto filters for the experiments described in this chapter; the impactor was used for the experiments described in Chapter 3.

The low concentration particles were prepared in a larger chamber (~ 400 L), and collection proceeded for a longer time in order to increase the mass of SOA available for experiments. Particle collection commenced ten minutes after the injection of ozone into the chamber. For GC experiments, particles were collected onto 47 millimeter diameter glass fiber filters (Millipore) at 2 standard liters per minute (SLM) for 60 minutes. For IR-CRDS experiments, particles were collected onto six identical 10 mm glass fiber filters in parallel at 1 SLM for 30 min using a constant flow rotary pump (Hi-Q Environmental, 1023CV) with six calibrated flow meters. Prior to collection, the glass fiber filters were baked overnight to remove organic contamination. For UV/Vis absorption spectroscopy, particles were collected in parallel onto two, 1" diameter CaF_2 windows using single-jet impactors (PIXE Stage L2, 120 nm particle diameter cutoff) operated at 1 SLM for 60 min (longer in the case of low concentration experiments). All filters

and windows were weighed before and after particle collection using a microbalance (Sartorius ME 5-F).

SOA Photolysis Analyzed by IR-CRDS. The CRDS system used in this work is composed of an optical cavity and a tunable infrared laser system. A schematic representation of the IR-CRDS system is shown in Figure 2.2.

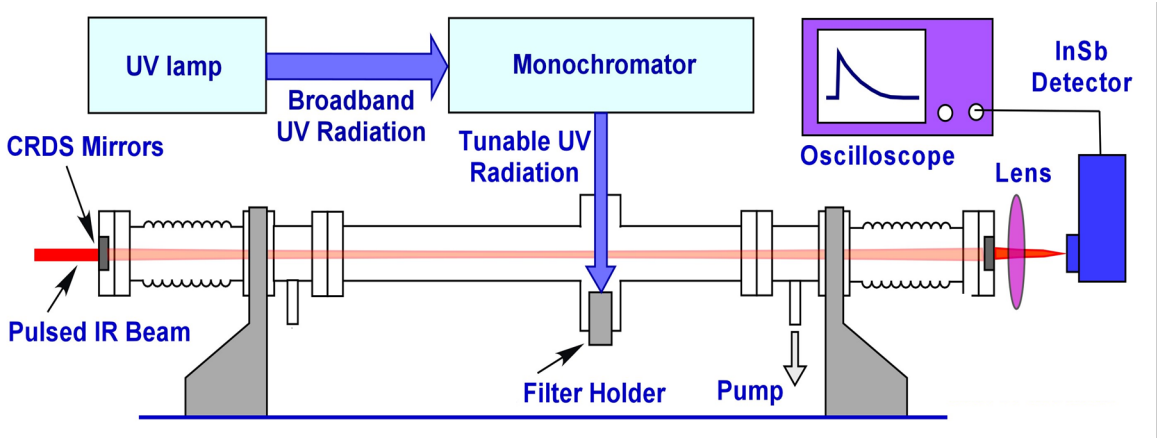

Figure 2.2. The IR-CRDS system used for the experiments described in this chapter.

The optical cavity is defined by two highly reflective (stated reflectivity: 99.98%, Los Gatos Research) mirrors with coatings optimized at 4.5 μm to enable detection of the C=O stretching vibration. The mirrors are spaced approximately 75 cm apart. Purging flows of UHP Helium are used to protect against deposition of photolysis products on the mirrors. The laser used to pump the cavity is an IR optical parametric oscillator with 0.1 cm^{-1} bandwidth, pulse duration of 8 ns, pulse energy of 11 mJ per pulse, and 20 Hz repetition rate. IR

radiation leaking through the back mirror of the optical cavity is detected with a liquid nitrogen cooled InSb detector, the signal from which is averaged for 20 laser pulses and digitized with an oscilloscope. A custom LabView program is used to collect and display the data from the oscilloscope. To ensure accurate wavelength calibration and facilitate line identification, an optoacoustic spectrum of CO was collected in parallel with the CRDS spectrum.

A sample holder containing the SOA sample is placed in the cavity just below the pulsed IR beam, and filtered UV radiation from a Xenon lamp (Oriel PhotoMax) is directed onto the sample. For wavelength dependence experiments, the light is first sent through a 1/4-m monochromator (Spectra Physics). The slits of the monochromator were wide open, resulting in 10 nm bandwidth and transmitted power of 3-20 mW. Photolysis experiments were conducted under conditions of ultrahigh purity (UHP, 99.999%) He flow at ~100 torr, with a residence time in the cavity of ~1 second. Heating of the filter by absorbed UV radiation was negligible (< 2°C).

Two kinds of spectroscopic data were collected using the IR-CRDS instrument. The first of these were simple product spectra, wherein the IR wavelength is scanned over a range that includes the vibrational transitions of the molecule to be detected while the UV radiation is incident on the sample. The second kind of spectra were *photolysis action spectra*, wherein the IR laser is parked on one of the peaks identified in the product scans. The UV irradiation wavelength was then changed in 10 nm increments, and changes in the amount of CO produced from photolysis were monitored. The signal from CO absorption

was normalized to the power incident on the sample to correct for the effect of the xenon lamp's spectral output. For the action spectrum experiments discussed in this chapter, the IR laser was parked on the R(6) carbon monoxide peak at 2169.2 cm^{-1}.

SOA Photolysis Analyzed by GC. Samples for GC analysis were collected onto glass fiber filters, which were then placed inside a quartz tube (I.D. = 15 mm). UHP helium was flowed over the sample for 10 minutes at reduced pressure to remove the most volatile species adsorbed to the filter. The sample was photolyzed for 30 minutes with a Xe-lamp illuminator at pressures near 1 atmosphere of UHP helium, with radiation output modified by a 330 nm dichroic mirror and a 295 nm high-pass filter. The total radiation power incident on the sample was ~50 mW, which mostly consisted of wavelengths between 300 and 350 nm. Sample heating was negligible over the course of the photolysis.

Gaseous photolysis products were collected into conditioned, evacuated 2-L stainless steel canisters each equipped with a bellows valve, and pressurized to 650 Torr with pure He diluent. The canisters were promptly analyzed upon collection. Samples were cryogenically trapped and injected into a multicolumn/detector gas chromatography system for NMHC and OVOC detection. The detectors included two flame ionization detectors (FID), two electron capture detectors (ECD), and a quadrupole mass spectrometer (MSD). Five different column/detector combinations were used: PLOT/FID, DB-1/FID, DB-5/ECD, RTX-1701/ECD, and DB-5ms/MSD. In addition, methane and carbon

monoxide were analyzed using separate GC/FID systems, while GC with thermal conductivity detection was utilized for analysis of CO_2. The calibration scheme, which is routinely cross-checked against absolute standards from other groups, employs a combination of primary standards, and secondary working standards of air collected from different environments and calibrated to certified standards. This analysis allows accurate quantification of a large variety of different gas species. For a detailed discussion of gas analysis using this system, see Ref. [36].

2.3.2 Results

Particle Production. SOA from limonene ozonolysis were produced at high and low reagent concentrations, and the efficiency of the particle production was clearly different in each case. To compare the two cases, it is instructive to look at particles collected onto the CaF_2 windows. The windows were much easier to weigh than the glass fiber filters, because of the degradation of the outer millimeter or so of the filter that we observed even at relatively low (800 sccm) pumping speeds. In a typical high concentration experiment, 13 μL of limonene was injected into the chamber with a large excess of ozone and the resulting particles were collected with two impactors onto two windows for one hour at 1 LPM each, so that a total of 120 L of air was collected from the bag. The average mass of aerosol particles collected by this method was 573 ± 109 μg (from an initial limonene mass of 1.09×10^4 μg), which corresponds to an aerosol yield of about 5%. This is lower than reported values for particle yields from

limonene ozonolysis (e.g. more than 50%, [22]). Our chamber has a much higher surface-to-volume ratio than those used in many studies, however, and no attempt to collect the total mass of aerosol in the chamber was made. The SOA mass collected in a 1 hour period was not dependent in an obvious way on the ozone concentration over the range 100-500 ppm.

CO Emission From SOA Photolysis. When SOA filter samples were placed in the CRDS sample holder and photolyzed, we expected to see CO production. To check whether or not this was actually the case, the laser was scanned over the wavelength range containing the strongest vibrational transitions in the CO molecule. The results of such a scan are shown in Figure 2.3.

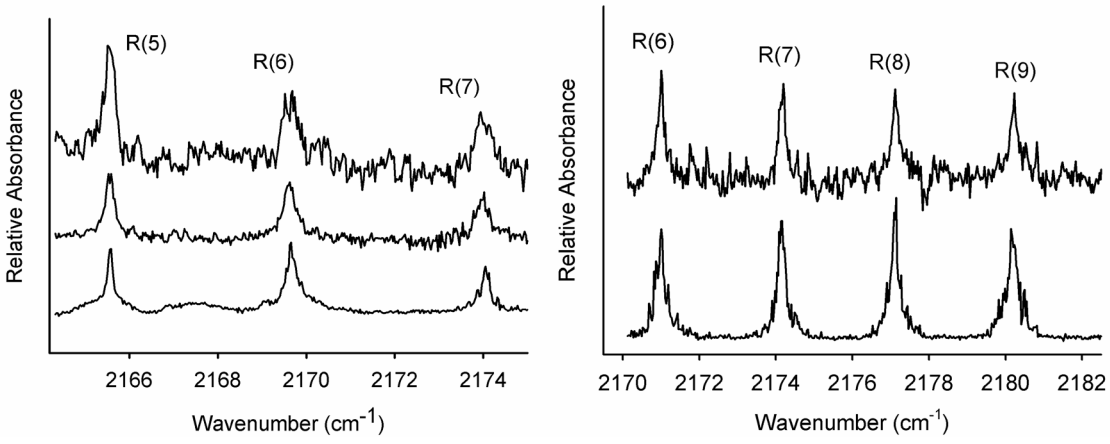

Figure 2.3. CO evolution during broadband photolysis of high concentration (left) and low concentration (right) SOA. In the left plot, the bottom trace is the optoacoustic spectrum, the middle trace is from photolysis with a 295 nm cutoff filter, and the top trace is from broadband photolysis. In the right plot, the bottom trace is the optoacoustic spectrum and the top trace is from broadband photolysis. Peak positions are shifted because the alignment of the OPO laser changed between these scans.

The three peaks in the left panel of Figure 2.3 correspond to the R(5), R(6) and R(7) transitions, moving from lowest to highest wavenumber; R(6) and R(7) are the strongest transitions that can be easily probed by our laser system. The four peaks in the right panel of Figure 2.3 are from the R(6), R(7), R(8) and R(9) transitions in CO. The y-axes are displayed in terms of relative absorbance because the units of the optoacoustic spectrum are detector voltage, not an actual measurement of absorption. The non-adjusted absorption coefficients α for the peaks in the SOA photolysis spectrum are approximately 2.5×10^{-6} cm^{-1}. The shift in absolute peak positions from scan to scan arises because the absolute alignment of the OPO laser varies with time; this is in fact one of the reasons that the optoacoustic spectrum is recorded in parallel.

Action Spectroscopy of CO Emission. As mentioned previously, action spectroscopy involves monitoring the amount of CO produced during irradiation of particles with different wavelengths of UV radiation. Action spectra can give more sensitive information about whether, for example, a particle that absorbs radiation in the tropospheric actinic window will be significantly aged by that radiation. Figure 2.4 shows the raw action spectroscopy data.

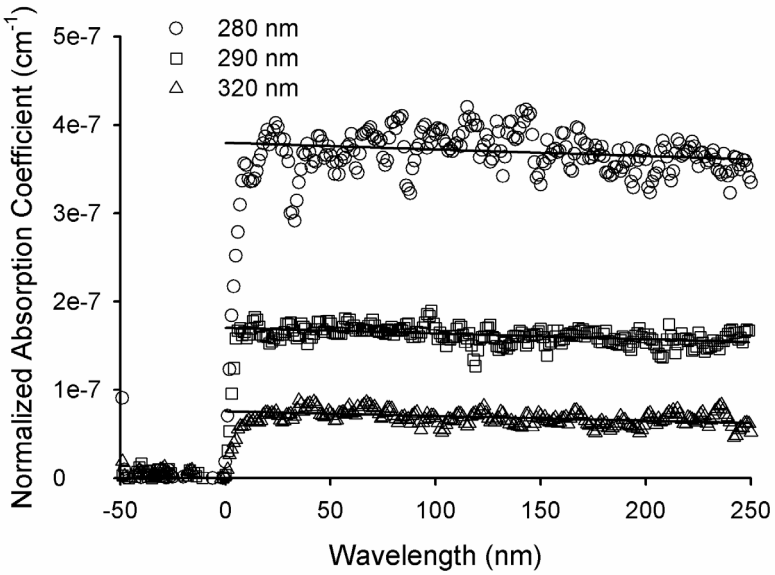

Figure 2.4. Carbon monoxide signal measured by IR-CRDS at different UV radiation wavelengths as a function of photolysis time. The measured absorption coefficient was scaled by the wavelength dependent photon flux at each photolysis wavelength to correct for different power output at different wavelengths. Lines represent a linear fit to the data. Photolysis begins at time = 0.

The data in Figure 2.4 are plotted in terms of the normalized absorption coefficient, which represents the absorption coefficient calculated using the ring-down time, normalized for the wavelength-dependent lamp power output. Photolysis begins at time = 0, with the 50 seconds before that used to establish a baseline ring-down time. The ring-down time over these 50 points is used as the background to calculate the non-normalized absorption coefficient, which is then normalized to the wavelength dependent photon flux from the lamp. So that the absolute absorption coefficient was changed as little as possible, the photon flux at 280 nm was set to 1 and all other values were expressed relative to this flux. The photon flux changed by about a factor of 2 over the wavelength range from 280 to 320 nm.

During photolysis experiments, there is a constant flow of UHP He through the cavity that serves to protect the mirrors from possible deposition of photolysis products. Because of this, the data must be fitted to a line that regresses back to time = 0 in order to find the initial yield from photolysis; that is, the amount of CO produced before any aging of the particles, when they still have their full complement of photo-active functional groups. The black lines in Figure 2.4 show the regression back to these intercepts. In terms of absolute amounts of CO produced, we see the largest signal from 290 nm photolysis, because at this wavelength a large power output is combined with a relatively large extinction coefficient for the particles. Once the data is corrected for lamp output, however, the expected trend emerges, namely an increase in photochemical production of CO with increasing photon energy.

The data points of CO production at the beginning of photolysis are plotted on a graph of photolysis wavelength versus the absorption coefficient (normalized as previously discussed) to give the photolysis action spectrum:

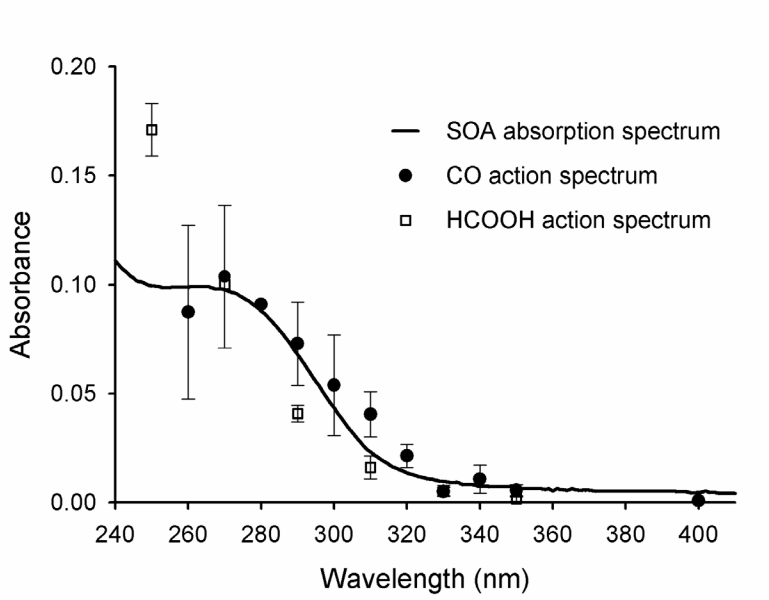

Figure 2.5. A photolysis action spectrum from irradiation of monoterpene SOA. The formic acid data points are taken from Ref [37]. The discussion of the SOA absorption profile and its relationship to the action spectrum is left until Chapter 3.

Figure 2.5 compares the photolysis action spectrum for the production of CO to the absorption spectrum of the SOA (see Chapter 3) and to a similar action spectrum for formic acid production (taken from Ref. [37]). The action spectrum data points have been arbitrarily scaled to facilitate comparison with the absorption profile. Of note is the fact that the CO and HCOOH action spectra have different shapes and that both are different from the absorption profile, indicating that not all components of the aerosol are important for aging at all UV wavelengths. These implications will be discussed in detail in the Discussion section.

Gas Chromatography Analysis of Photolysis Products. Gas chromatography was carried out on the products of SOA photolysis with an eye toward clarifying the

mechanism of photolysis, rather than constructing action spectra. Since a 295 nm cutoff filter was used to modify the lamp's spectral output, the GC results contain information about the photochemical aging mechanisms that are likely to be important for particles in the troposphere. Unfortunately, the GC system used to analyze the photolysis products was designed for trace gas monitoring and not product identification. This meant that many of the larger oxygenated gas phase products of photolysis were not identifiable because they eluted close together at long times. In addition, calibration standards were unavailable for most of these larger photolysis products. Still, the GC system gave us valuable information about the identities and, in some cases, relative amounts of the gas phase products of SOA photochemical aging. A sample chromatogram is shown in Figure 2.6.

Panel A shows the results of running a "blank" sample through the GC system. To collect the blank samples, UHP Helium was flowed over the SOA sample (which was on a glass fiber filter) and for ten minutes, after which time the photolysis cell was filled to near 1 atmosphere with UHP Helium and held at that pressure for 30 minutes. The valve to the sample can was then opened and the products were allowed to expand into the stainless steel sample can, which was then filled to near atmospheric pressure with UHP Helium. Any peaks seen in this chromatogram, then, represent molecules that are volatile but are adsorbed to the filter after particle collection. In any case, they are not photolysis products (the tube holding the filter was wrapped in aluminum foil during this step

to prevent accidental photolysis by the very small UV component of room lights), and they were ignored in the analysis of the sample chromatograms.

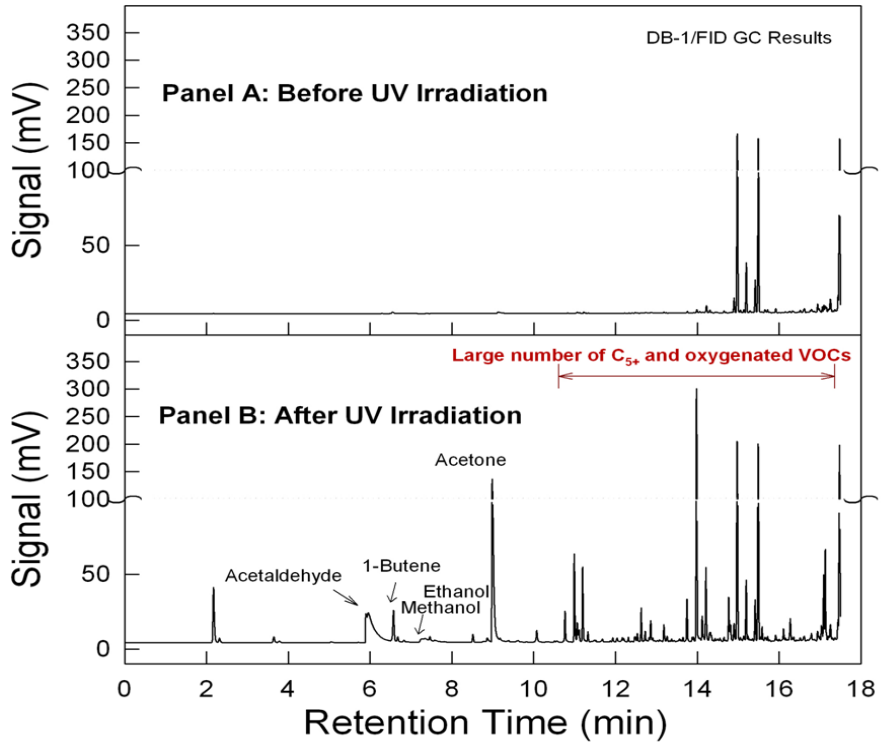

Figure 2.6. Gas Chromatography analysis of photolysis products.

Panel B of Figure 2.6 is a chromatogram from analysis of one of the SOA photolysis sample cans. In this sample, we see the small volatile products released into the gas phase during photolysis. Acetaldehyde and acetone are the two most prominent peaks, with 1-butene, methanol and ethanol also positively identified. There are also a large number of longer-chained, oxidized molecules that were not identified because standards were unavailable. Carbon monoxide and methane were seen in larger amounts than any of the oxygenated

VOCs, but were analyzed with different columns and detectors. It is clear that there are a number of different photolysis pathways available to the molecules in the SOA sample. Table 2.1 shows a complete listing of the expected and observed photolysis products for the most common components of SOA formed from the ozonolysis of limonene.

2.3.3 Discussion

The absorption profile of the *d*-limonene SOA is red-shifted significantly from that of pure limonene. Weak absorption of light in the region between 270 and 330 nm is consistent with $n \rightarrow \pi^*$ transitions in non-conjugated aldehydes and ketones, which are expected products of ozonolysis of monoterpenes. Molecules with these functional groups have frequently been detected in monoterpene SOA [15, 18, 22, 38-40]. The portion of the absorption spectrum smoothly decaying with wavelength between 250 and 350 nm is indicative of $n \rightarrow \sigma^*$ transitions in organic peroxides, which account for a significant fraction of SOA material produced by ozonolysis of monoterpenes [20, 41-43]. The implications that the shape of the absorption profile holds for the atmospheric lifetimes of these particles will be discussed in Chapter 3.

Experiments of longer duration than those plotted in Figure 2.4 show that CO production persists for a long time (> 20 minutes) before the SOA samples are photobleached. In contrast, the production of formic acid from photolysis of organic peroxides in the SOA ceased in less than 10 minutes under similar experimental conditions [37]. This suggests that effective photolysis rates of

peroxides in SOA are larger than those for carbonyls, which serve as CO photochemical precursors.

A number of other small molecules that were produced during photolysis and identified by GC methods (Table 2.1) can also be accounted for by photochemistry of carbonyls. Carbonyls are well known to experience Norrish type I and II photocleavage [24]. In the type I process, the carbonyl dissociates into two radicals via breaking of the C-C bond between the carbonyl and one of the α carbons:

$$RC(O)R' + h\nu \longrightarrow R\bullet + \bullet C(O)R' \qquad (7)$$

The fragment with the C=O bond can then decarbonylate, resulting in an alkyl radical and carbon monoxide, or abstract a hydrogen from another molecule to give an aldehyde. The Norrish type II reaction is an intermolecular reaction that proceeds through a six-membered cyclic intermediate [44]

$$RR'CHCH_2CH_2C(O)R'' + h\nu \longrightarrow RR'C{=}CH_2 + CH_3C(O)R'' \qquad (8)$$

resulting in the formation of a smaller ketone and an alkene [45]; the cleavage point is between the α and β carbons. For the type II photocleavage to occur, a γ hydrogen atom must be present [46, 47] because this atom is abstracted during

the reaction. The two Norrish processes can account for several of the observed products.

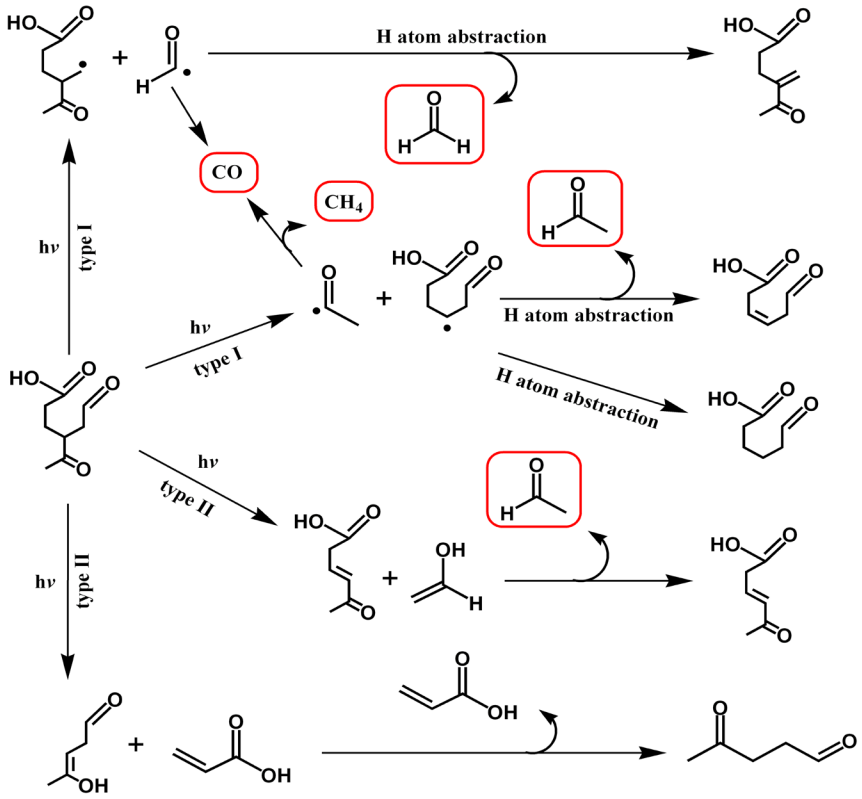

Figure 2.7. Likely pathways for the photolysis of keto-limonalic acid, a representative component of SOA from limonene ozonolysis. The pathways shown here represent only Norrish type I and II (designated by I and II under reaction arrows) photocleavage and should not be considered exhaustive. Molecules in boxes are volatile and have been observed in the GC analysis.

Examples are shown in boxes in Figure 2.7, which includes type I and II processes undergone by keto-limonalic acid, a representative component of SOA from limonene ozonolysis [15]. Carbon monoxide is only a marker for the type I photocleavage of carbonyls; type II photolysis tends to produce larger (2-3 carbons) oxygenated VOCs. Table 2.1 shows a complete listing of the expected small VOC products from type I and II photolysis of 13 of the most common

particle phase limonene ozonolysis products; each of them undergoes photolysis *via* processes similar to those shown in Figure 2.7.

Carbon monoxide is an expected product from type I photolysis of each of these molecules, because any molecule with a carbonyl radical can decarbonylate to give CO. Formaldehyde is produced from the type I photolysis of aldehydes as well as from the photolysis of organic peroxides, and was detected in previous experiments from our group [37]. Other peaks in the chromatogram (Figure 2.6) correspond to expected photolysis products acetaldehyde (produced from type I photolysis of ketones and type II photolysis of aldehydes), methanol (a result of hydrogen abstraction by a radical from type I photolysis of molecules with a 7-OH group), acetone (a marker for type II photolysis of molecules with a 7-methyl group). Methane, CO and CO_2 were also detected via GC using a different column. Very little CO_2 was observed, while CO and CH_4 were the most abundant gas phase photolysis products. Methane is a marker for type I photolysis of compounds with a 7-methyl group and for hydrogen and is also produced when the methyl radical from the decarbonylation of a CH_3CO radical abstracts a hydrogen atom.

Carbonyl-containing product from limonene + O_3	Expected photolysis products – small VOCs	
	Observed with GC or CRDS	**Not observed**
Limona ketone	CO, acetaldehyde, methane	---
Limononaldehyde	CO, formaldehyde, methane, acetaldehyde, acetone	---
Keto-limononaldehyde	CO, formaldehyde, methane, acetaldehyde, acetone	3-buten-2-one
7-hydroxy-limononaldehyde	CO, formaldehyde, methanol, acetaldehyde	hydroxyacetaldehyde, 4-hydroxy-2-butanone
7-hydroxy-keto-limononaldehyde	CO, formaldehyde, methanol, methane, acetaldehyde	hydroxyacetone, hydroxyacetaldehyde, 1-hydroxy-2-butanone,
Limononic acid	CO, acetaldehyde, methane, acetone	---
Keto-limononic acid	CO, methane, acetaldehyde, acetone	3-buten-2-one
Nor-limononic acid	CO, methane, acetaldehyde, acetone	---
7-hydroxy-limononic acid	CO, methanol	hydroxyacetaldehyde, hydroxyacetone
7-hydroxy-keto-limononic acid	CO, acetaldehyde, methane, methanol,	hydroxyacetaldehyde, hydroxyacetone, 1-hydroxy-3-buten-2-one
Limonalic acid	CO, formaldehyde, acetaldehyde	---
Keto-limonalic acid	CO, formaldehyde, acetaldehyde, methane	acrylic acid
Keto-limonic acid	CO, acetaldehyde, methane	acrylic acid, acetic acid

Table 2.1. Expected and observed small (< 4 carbons) gas-phase products from the photolysis of 13 molecules produced from the ozonolysis of limonene. CO and formaldehyde were observed with both gas chromatography and IR-CRDS, while other observed products were only detected by GC. No oxygen or other atmospheric species were present during photolysis. Products of limonene + O_3 are named according to [48].

Several of the other peaks in the sample chromatogram cannot be accounted for by the type I and II photolysis mechanisms of the primary products of limonene oxidation. In particular, the presence of short-chain alkenes such as ethene is puzzling. Secondary photolysis of the predicted photolysis products 3-buten-2-one or acrylic acid via the type I pathway could account for the presence of ethene, and since the sample stays in the photolysis cell for 30 minutes before being collected this secondary photolysis has ample time to occur. The Norrish mechanisms do not predict the production of ethene from photolysis of any of the most common products of limonene ozonolysis (see Table 2.1).

A final feature of the sample chromatogram (Figure 2.6) is the numerous peaks at long retention times. These peaks represent large (more than 5 carbons), oxygenated products. A lack of standards for these molecules precluded their identification, but it is likely that some of them are larger photolysis products like those shown in Figure 2.7. In particular, 5 carbon dicarbonyls such as 4-oxopentanal (a product of the type II photocleavage of keto-limonalic acid, 7-hydroxy-keto-limonalic acid, keto-limonaldehyde, and 7-hydroxy-keto-limonaldehyde) are likely to make their way into the gas phase. 4-oxopentanal is produced from reactions of ozone on the surfaces of foliage [49] and has been measured over forests in both the gas and particle phases [11, 50]. Molecules with these structures could also be chromophores, and if they stay in the particle phase they may influence the absorption profile of the SOA.

The results reported in Table 2.1 are from the GC analysis of the products of photolysis of SOA produced under high ozone concentrations (300 ppm

ozone, 10 ppm limonene). The experiment was repeated with SOA produced at lower concentrations (1 ppm ozone, 0.5 ppm limonene) to examine the effect of reactant concentrations on the photolysis products. In a typical experiment, up to 140 μg of SOA were collected from the low concentration particle generation, compared to 450 μg or more from the high concentration particle generation. Photolysis of the low concentration SOA produced the same compounds as the high concentration SOA, but in lesser amounts as expected. The low concentration SOA was also photolyzed with actinic UV radiation in the IR-CRDS system, and CO production was observed in small amounts. This demonstrates that carbonyl functional groups are present in the SOA independent of the oxidant concentrations, and that type I and II photoprocesses occur in both cases.

Thus far we have only discussed the gas-phase products from photolysis of SOA in our oxygen-free system. It is instructive to also consider the molecules left behind in the particle phase. As we have said, photochemical aging of monoterpene SOA is likely to be due to photolysis of organic peroxides and molecules with carbonyl functional groups. Particle-phase carbonyls and peroxides are toxic [51-53], and the destruction of these groups may decrease the overall toxicity of the particles. Some of the gas phase products of type II photolysis shown in Figure 2.7 (such as acrylic acid and acetaldehyde) have been classified as Toxic Air Contaminants by the California Air Resources Board [54]. Since the overall amount of these compounds produced from photolysis of SOA will be small, the toxicity of the molecules left in the particle phase will be

more important because of the ability of particles to deposit in the lungs [55-57] and, in the case of ultrafine particles, in the bloodstream [58] and brain [59].

Further complicating the question of photochemistry's influence on particle composition and toxicity is the effect of other atmospheric species. The nature of the molecules left behind in the particle phase will be different from those shown in Figure 2.7 in the case where photolysis occurs in the presence of oxygen. The products of the type II photolysis will be largely the same, but the products of the type I process will be altered. This is because the type II process results in alkyl radicals, which react quickly with molecular oxygen in the atmosphere [54] to form alkylperoxy radicals. This process will only be important at the surface of the particles. Alkylperoxy radicals formed on the particle surface can then go on to form alkoxy radicals, alcohols and aldehydes via self-reaction, or alkyl nitrates and alkoxy radicals via reaction with NO. The alkoxy radicals may be converted to carbonyl compounds via reaction with molecular oxygen, break via C-C bond scission to give an aldehyde and a smaller alkyl radical, or (for larger molecules) isomerize into an alkyl radical via intramolecular hydrogen abstraction [54]. Alkyl radicals formed in the bulk of the particles may recombine with other radicals to form polymeric species. It is possible that photolysis in the presence of oxygen may actually *increase* the toxicity and CCN activity of the SOA by forming more carbonyl functional groups. Further study of these potential health effects is warranted.

2.4 Conclusions

The results discussed in this chapter have shown conclusively that monoterpene SOA can be aged significantly by ultraviolet radiation in the tropospheric actinic window. The mechanism of this aging is the photodegradation of carbonyl-containing molecules; the aging proceeds via one of the well-defined Norrish mechanisms. Ketone groups are most susceptible to this photoprocessing, and larger ketones will have higher quantum yields. The presence of oligomers in the SOA makes it likely that the quantum yield will be large enough to make photolysis an efficient aging mechanism for monoterpene SOA in the troposphere.

Photochemical aging of monoterpene SOA will result in a small flux of low molecular weight oxygenated species back into the gas phase, and will also lead to the modification of the particles themselves. Our results imply that the oxygen content of photochemically aged aerosol will decrease. However, our SOA were photolyzed in the absence of oxygen and other atmospheric species. If we extrapolate from our results and consider especially the chemistry of oxygen addition to alkyl radicals, it is possible that the oxygen content of the SOA may actually increase or that the molecules in the aged SOA may be more polymerized than those in the fresh SOA. This result has implications for particle toxicity and for the ability of the aged particles to act as cloud condensation nuclei. It is clear that organic aerosol particles should not be thought of as unchanging during their time in the atmosphere. Whether via chemical or

photochemical means, particles are likely to be significantly altered even after a day in the troposphere; we have shown that any particle with carbonyl functional groups is susceptible to aging by tropospheric actinic radiation as well as by tropospheric oxidants.

2.5 References

1. Hoffmann, T., et al., *Formation of Organic Aerosols from the Oxidation of Biogenic Hydrocarbons.* Journal of Atmospheric Chemistry, 1997. 26(2): p. 189-222.
2. Odum, J.R., et al., *Gas/Particle Partitioning and Secondary Organic Aerosol Yields.* Environ. Sci. Technol., 1996. 30(8): p. 2580-2585.
3. Dubowski, Y., et al., *Interaction of Gas-Phase Ozone at 296 K with Unsaturated Self-Assembled Monolayers: A New Look at an Old System.* J. Phys. Chem. A, 2004. 108(47): p. 10473-10485.
4. Thomas, E.R., G.J. Frost, and Y. Rudich, *Reactive uptake of ozone by proxies for organic aerosols: Surface-bound and gas-phase products.* Journal of Geophysical Research, 2001. 106(D3): p. 3045-3056.
5. Park, J., et al., *Ozonolysis and photolysis of alkene-terminated self-assembled monolayers on quartz nanoparticles: implications for photochemical aging of organic aerosol particles.* Physical Chemistry Chemical Physics, 2006. 8: p. 2506-2512.
6. Grosjean, D., et al., *Atmospheric oxidation of biogenic hydrocarbons: reaction of ozone with β-pinene, D-limonene and trans-caryophyllene.* Environ. Sci. Technol., 1993. 27(13): p. 2754-2758.
7. Grosjean, D., E.L. Williams, and J.H. Seinfeld, *Atmospheric oxidation of selected terpenes and related carbonyls: gas-phase carbonyl products.* Environ. Sci. Technol., 1992. 26(8): p. 1526-1533.
8. Lee, A., et al., *Gas-phase products and secondary aerosol yields from the ozonolysis of ten different terpenes.* Journal of Geophysical Research, 2006. 111: p. D07302.
9. Lee, A., et al., *Gas-phase products and secondary aerosol yields from the photooxidation of 16 different terpenes.* Journal of Geophysical Research, 2006. 111: p. D17035.
10. Calogirou, A., et al., *Polyphenylenesulfide, noxon® an ozone scavenger for the analysis of oxygenated terpenes in air.* Atmospheric Environment, 1997. 31(17): p. 2741-2751.
11. Matsunaga, S., M. Mochida, and K. Kawamura, *High abundance of gaseous and particulate 4-oxopentanal in the forestal atmosphere.* Chemosphere, 2004. 55(8): p. 1143-1147.
12. Yu, J., et al., *Observation of gaseous and particulate products of monoterpene oxidation in forest atmospheres.* Geophysical Research Letters, 1999. 26(8): p. 1145-1148.
13. Kavouras, I.G., N. Mihalopoulos, and E.G. Stephanou, *Formation of atmospheric particles from organic acids produced by forests.* Nature, 1998. 395(6703): p. 683-686.
14. Glasius, M., M. Duane, and B.R. Larsen, *Determination of polar terpene oxidation products in aerosols by liquid chromatography-ion trap mass spectrometry.* Journal of Chromatography A, 1999. 833(2): p. 121-135.
15. Glasius, M., et al., *Carboxylic Acids in Secondary Aerosols from Oxidation of Cyclic Monoterpenes by Ozone.* Environ. Sci. Technol., 2000. 34(6): p. 1001-1010.
16. Koch, S., et al., *Formation of new particles in the gas-phase ozonolysis of monoterpenes.* Atmospheric Environment, 2000. 34(23): p. 4031-4042.
17. Librando, V. and G. Tringali, *Atmospheric fate of OH initiated oxidation of terpenes. Reaction mechanism of α-pinene degradation and secondary organic aerosol formation.* Journal of Environmental Management, 2005. 75(3): p. 275-282.
18. Yu, J., et al., *Gas-Phase Ozone Oxidation of Monoterpenes: Gaseous and Particulate Products.* Journal of Atmospheric Chemistry, 1999. 34(2): p. 207-258.
19. Jaoui, M., et al., *Analysis of Secondary Organic Aerosol Compounds from the Photooxidation of d-Limonene in the Presence of NO_x and their Detection in Ambient $PM_{2.5}$.* Environ. Sci. Technol., 2006. 40(12): p. 3819-3828.
20. Jenkin, M.E., *Modelling the formation and composition of secondary organic aerosol from a- and b-pinene ozonolysis using MCM v3.* Atmos. Chem. Phys., 2004. 4: p. 1741-1757.
21. Claeys, M., et al., *Hydroxydicarboxylic Acids: Markers for Secondary Organic Aerosol from the Photooxidation of b-Pinene.* Environ. Sci. Technol., 2007. 41(5): p. 1628-1634.

22. Leungsakul, S., M. Jaoui, and R.M. Kamens, *Kinetic Mechanism for Predicting Secondary Organic Aerosol Formation from the Reaction of d-Limonene with Ozone.* Environ. Sci. Technol., 2005. 39(24): p. 9583-9594.
23. Presto, A.A., K.E. HuffHartz, and N.M. Donahue, *Secondary Organic Aerosol Production from Terpene Ozonolysis. 1. Effect of UV Radiation.* Environ. Sci. Technol., 2005. 39(18): p. 7036-7045.
24. Bamford, C.H. and R.G.W. Norrish, *359. Primary photochemical reactions. Part VII. Photochemical decomposition of isovaleraldehyde and di-n-propyl ketone.* J. Chem. Soc., 1935. DOI: 10.1039/JR9350001504: p. 1504-1511.
25. Carlsson, D.J. and D.M. Wiles, *The Photodegradation of Polypropylene Films. II. Photolysis of Ketonic Oxidation Products.* Macromolecules, 1969. 2(6): p. 587-597.
26. Hartley, G.H. and J.E. Guillet, *Photochemistry of Ketone Polymers. II. Studies of Model Compounds.* Macromolecules, 1968. 1(5): p. 413-417.
27. Hartley, G.H. and J.E. Guillet, *Photochemistry of Ketone Polymers. I. Studies of Ethylene-Carbon Monoxide Copolymers.* Macromolecules, 1968. 1(2): p. 165-170.
28. Atkinson, D.B., *Solving chemical problems of environmental importance using cavity ring-down spectroscopy.* The Analyst, 2003. 128(2): p. 117-125.
29. Zalicki, P. and R.N. Zare, *Cavity ring-down spectroscopy for quantitative absorption measurements.* The Journal of Chemical Physics, 1995. 102(7): p. 2708-2717.
30. Busch, K.W. and M.A. Busch, *2. Introduction to Cavity-Ringdown Spectroscopy*. ACS Symposium Series, ed. K.W. Busch and M.A. Busch. 1999: Oxford University Press.
31. O'Keefe, A. and D.A.G. Deacon, *Cavity ring-down optical spectrometer for absorption measurements using pulsed laser sources.* Review of Scientific Instruments, 1988. 59(12): p. 2544-2551.
32. Scherer, J.J., et al., *Infrared cavity ringdown laser absorption spectroscopy (IR-CRLAS).* Chemical Physics Letters, 1995. 245(2-3): p. 273-280.
33. Berden, G., R. Peeters, and G. Meijer, *Cavity ring-down spectroscopy: Experimental schemes and applications.* International Reviews in Physical Chemistry, 2000. 19(4): p. 565 - 607.
34. Fawcett, B.L., et al., *Trace detection of methane using continuous wave cavity ring-down spectroscopy at 1.65 [micro sign]m.* Physical Chemistry Chemical Physics, 2002. 4(24): p. 5960-5965.
35. Roberts, J.M., et al., *Monoterpene hydrocarbons in the nighttime troposphere.* Environ. Sci. Technol., 1985. 19(4): p. 364-369.
36. Colman, J.J., et al., *Description of the Analysis of a Wide Range of Volatile Organic Compounds in Whole Air Samples Collected during PEM-Tropics A and B.* Anal. Chem., 2001. 73(15): p. 3723-3731.
37. Walser, M.L., et al., *Photochemical Aging of Secondary Organic Aerosol Particles Generated from the Oxidation of d-Limonene.* J. Phys. Chem. A, 2007. 111(10): p. 1907-1913.
38. Jang, M. and R.M. Kamens, *Newly characterized products and composition of secondary aerosols from the reaction of α-pinene with ozone.* Atmospheric Environment, 1999. 33(3): p. 459-474.
39. Kamens, R., et al., *Aerosol Formation from the Reaction of α-Pinene and Ozone Using a Gas-Phase Kinetics-Aerosol Partitioning Model.* Environ. Sci. Technol., 1999. 33(9): p. 1430-1438.
40. Yokouchi, Y. and Y. Ambe, *Aerosols formed from the chemical reaction of monoterpenes and ozone.* Atmospheric Environment (1967), 1985. 19(8): p. 1271-1276.
41. Bonn, B., R. von Kuhlmann, and M.G. Lawrence, *High contribution of biogenic hydroperoxides to secondary organic aerosol formation.* Geophysical Research Letters, 2004. 31(10): p. L10108.
42. Docherty, K.S., et al., *Contributions of Organic Peroxides to Secondary Aerosol Formed from Reactions of Monoterpenes with O_3.* Environ. Sci. Technol., 2005. 39(11): p. 4049-4059.

43. Tolocka, M.P., et al., *Chemistry of Particle Inception and Growth during α-Pinene Ozonolysis.* Environ. Sci. Technol., 2006. 40(6): p. 1843-1848.
44. Rice, F.O. and E. Teller, *The Role of Free Radicals in Elementary Organic Reactions.* The Journal of Chemical Physics, 1938. 6(8): p. 489-496.
45. Davis, W. and W.A. Noyes, *Photochemical Studies. XXXVIII. A Further Study of the Photochemistry of Methyl n-Butyl Ketone.* J. Am. Chem. Soc., 1947. 69(9): p. 2153-2158.
46. McMillan, G.R., J.G. Calvert, and J.N. Pitts, *Detection and Lifetime of Enol-Acetone in the Photolysis of 2-Pentanone Vapor.* J. Am. Chem. Soc., 1964. 86(18): p. 3602-3605.
47. Srinivasan, R., *The Photochemical Type II Process in 2-Hexanone-5,5-d2 and 2-Hexanone.* J. Am. Chem. Soc., 1959. 81(19): p. 5061-5065.
48. Larsen, B.R., et al., *Atmospheric oxidation products of terpenes: A new nomenclature.* Chemosphere, 1998. 37(6): p. 1207-1220.
49. Fruekilde, P., et al., *Ozonolysis at vegetation surfaces: a source of acetone, 4-oxopentanal, 6-methyl-5-hepten-2-one, and geranyl acetone in the troposphere.* Atmospheric Environment, 1998. 32(11): p. 1893-1902.
50. Matsunaga, S., M. Mochida, and K. Kawamura, *Variation on the atmospheric concentrations of biogenic carbonyl compounds and their removal processes in the northern forest at Moshiri, Hokkaido Island in Japan.* Journal of Geophysical Research, 2004. 109: p. D04302.
51. Andreoli, S.P., J.A. McAteer, and C. Mallett, *Reactive oxygen molecule-mediated injury in endothelial and renal tubular epithelial cells in vitro.* Kidney Int, 1990. 38(5): p. 785-794.
52. Eder, E., et al., *The possible role of [alpha],[beta]-unsaturated carbonyl compounds in mutagenesis and carcinogenesis.* Toxicology Letters, 1993. 67(1-3): p. 87-103.
53. Witz, G., *Biological interactions of α,β-unsaturated aldehydes.* Free Radical Biology and Medicine, 1989. 7(3): p. 333-349.
54. Finlayson-Pitts, B.J. and J.N. Pitts, *Chemistry of the Upper and Lower Atmosphere*. 2000, San Diego: Academic Press.
55. Cohen, B.S., R.G. Sussman, and M. Lippmann, *Ultrafine Particle Deposition in a Human Tracheobronchial Cast.* Aerosol Science and Technology, 1990. 12(4): p. 1082 - 1091.
56. Lippmann, M., D.B. Yeates, and R.E. Albert, *Deposition, retention, and clearance of inhaled particles.* British Journal of Industrial Medicine, 1980. 37(4): p. 337-362.
57. Löndahl, J., et al., *Size-Resolved Respiratory-Tract Deposition of Fine and Ultrafine Hydrophobic and Hygroscopic Aerosol Particles During Rest and Exercise.* Inhalation Toxicology, 2007. 19(2): p. 109 - 116.
58. Nemmar, A., et al., *Passage of Inhaled Particles Into the Blood Circulation in Humans.* Circulation, 2002. 105(4): p. 411-414.
59. Oberdörster, G., et al., *Translocation of Inhaled Ultrafine Particles to the Brain.* Inhalation Toxicology, 2004. 16(6): p. 437 - 445.

Chapter 3

Aging of Particle Phase Components of Monoterpene Secondary Organic Aerosol

3.1 Introduction

In the previous chapter, we discussed the products of monoterpene SOA photolysis that were released into the gas phase. Investigating the gas phase products is one way to learn about the aging processes that are important to these particles. Information about changes in particle composition can be inferred, but not observed, based on the gas phase product distribution. Another way to study particle aging is to look at the changes in the particles themselves upon exposure to light or various atmospheric species. This chapter will focus on experiments wherein various spectroscopic techniques were used to study the aging of particle phase components of monoterpene SOA.

3.1.1 Composition and Aging of Monoterpene SOA

The initial composition of monoterpene SOA has been frequently studied and is reasonably well characterized for many systems. Chapter 1 contains a more extensive summary of research on the composition of monoterpene SOA. For SOA formed from the ozonolysis of monoterpenes (*d*-limonene, α- and β-

pinene in particular), modeling and particle analysis have identified many different functional groups in the particle phase. These include carbonyl functional groups (carboxylic acids, ketones and aldehydes) [1, 2], as well as secondary ozonides formed from the stabilized Criegee intermediates [3] and also hydroperoxides formed in reactions where OH scavengers are present [4, 5]. Mass spectrometry measurements [6] have also suggested a key role for oligomers as large as tetramers in the formation of SOA from oxidized α-pinene. Carbonyl products of the ozonolysis of α-pinene have been observed in ambient aerosol particles above forests [7].

Organic aerosols can be aged via two main processes: chemical attack and photochemical reactions. The former takes place largely through oxidative processing, such as when the organic surface layer of a particle is attacked by ozone or hydroxyl radicals. The results of chemical aging and photochemical aging are similar; both photochemistry [8, 9] and chemical aging [10, 11] result in modification of the particle's organic fraction and also in the release of small molecules into the gas phase. Oxidative aging can leave an organic particle with a modified index of refraction due to production of chromophores on the surface [10]. Aging via surface oxidation will also alter the hydrophilicity of a particle, meaning that even a strongly hydrophobic particle can become an active cloud condensation nucleus (CCN) [12].

Photochemical aging can be broken down into two main regimes, those being direct and indirect photochemistry. Direct photochemistry implies that the molecule undergoing the aging absorbs a photon, and the excess energy causes

dissociation or some other modification of the molecule. Indirect photochemistry, then, implies that some other species absorbs a photon, starting a reaction that causes the molecule of interest to be modified. For a discussion of direct and indirect photoprocessing of organic and mixed organic/inorganic particles, see Section 1.5.2.

3.1.2 Color Change in Atmospheric Aerosol

The 2007 report of the Intergovernmental Panel on Climate Change (IPCC) [13] estimated that aerosol particles in the atmosphere are responsible for a climate forcing of -0.50 +/- 0.40 W m^{-2}. The assignment of a negative forcing to the total burden of aerosol particles in the atmosphere means that they are collectively responsible for scattering and reflecting more solar radiation than they absorb, and that they lead to a net cooling of the atmosphere. The IPCC report does note, however, that most of the uncertainty in this figure comes from an incomplete knowledge of the extent of aerosol absorption. Most models assume that all absorption is due to black carbon aerosols, meaning that if other organic aerosols (such as monoterpene SOA) do absorb radiation in the tropospheric actinic window, climate models will under-predict the total aerosol climate forcing. This will be especially true in areas of low relative humidity, where the aerosol indirect effect (the ability of aerosol to act as cloud condensation nuclei, causing a large negative forcing) will not be significant. In fact, there is evidence for brown aerosol amplifying warming over Asia [14]. This

effect is thought to be a consequence of pollution (fuel and biomass burning), and should primarily be important over urban areas.

There is some evidence that non-black-carbon aerosol particles can become absorbers of solar radiation over the course of their atmospheric lifetime. Most of the research in this area has focused on sulfuric acid aerosols, which are found mainly in the stratosphere and have long lifetimes (at least 1-2 years). Aldol condensation of aliphatic aldehydes in concentrated sulfuric acid was shown to produce a large increase in the absorption index in the near UV and visible range [15-17] on a timescale that is short compared to this lifetime, although aldehyde concentrations much higher than those found in the stratosphere were used. Based on a two year residence time, reactions involving acetaldehyde only, and an absence of reactions that remove colored organic molecules from the aerosol, Nozière [16] estimated that acid-catalyzed reactions might increase the absorption index (between 200 and 500 nm) of a particle by four orders of magnitude. Uptake of gas-phase isoprene by acidic tropospheric particles has also been shown to form humic-like substances (HULIS) [18]. HULIS is also known as brown carbon and plays an unknown but possibly important role in the radiation balance of the troposphere [19].

3.1.3 Experimental Goals

The purpose of the experiments described in this chapter was twofold. The initial goal was to measure the absorption profile of monoterpene SOA in a sensitive, reproducible way that was free of confounding effects such as

scattering or solvent influences. This goal was motivated by the previously reported fact that the spectrum of limonene SOA in various solvents, while easy to measure, was difficult to reproduce and depended on the solvent used [9]. To facilitate comparison with the particles' action spectrum, it was necessary to develop a new method for collecting these absorption spectra. Section 3.2 of this Chapter presents the UV-Visible absorption spectra collected using this method.

The second goal of this work arose from observations of the behavior of the SOA samples after they had been collected. In the beginning of our experiments on limonene SOA, we noticed that SOA samples collected on filters and not discarded immediately after the experiment gradually acquired a red-brown color. This was true whether or not the particles had been exposed to UV light already. Initial spectroscopic study of the aged SOA showed an absorption spectrum qualitatively similar to that of HULIS, with significant absorption features at visible wavelengths. We realized the potential significance of this color change for the atmospheric behavior of the SOA, and began a line of inquiry aimed at finding the mechanism of the color change. The results described in Section 3.3 of this Chapter represent the preliminary investigations of color change processes in monoterpene SOA. Chapter 5 of this thesis contains future directions that I suggest for this project.

3.2 Spectroscopic Study of Monoterpene SOA Particles

3.2.1 Experimental Methods: Particle Production

Monoterpene SOA was produced from the reaction of *d*-limonene (1-methyl-4-prop-1-en-2-yl-cyclohexene) with ozone in a 300 L Teflon chamber as described previously [9]. Reactions were conducted in the dark at 750 torr, 298K, and low relative humidity (<1%). In order to accelerate oxidation of the *d*-limonene molecules and improve SOA yield, a large excess of ozone was used for the initial experiments. Ozone was produced by flowing high-purity (99.994%) oxygen through a commercial ozone generator. Typical reagent concentrations were 300 ppm ozone and 10 ppm limonene (97%, Fisher Scientific). Although these concentrations are very high in absolute terms compared to what would be found in the troposphere, the ratio of limonene to ozone concentration is within reasonable limits for terpene/ozone ratios measured at night [20]. Particles were also prepared at lower concentrations (1 ppm O_3, 500 ppb limonene) to ensure that the results of the photolysis experiments were not concentration-dependent. The setup for particle preparation and collection is shown in Figure 3.1.

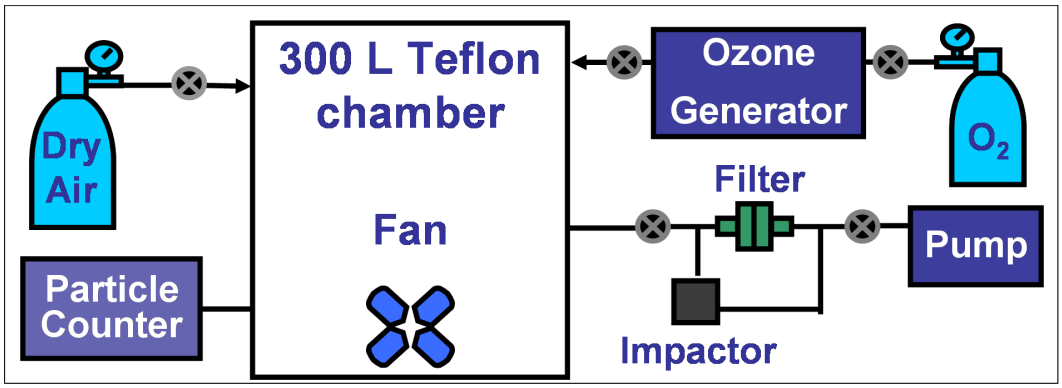

Figure 3.1. Particle production and collection setup. Replacing the particle counter with an ozone meter allows us to determine the ozone concentration in the bag for each experiment. Particles were collected using the impactor for the experiments described in this chapter; the filter holder was used for the experiments described in Chapter 2.

Particle collection commenced ten minutes after the injection of limonene into the chamber. Particles were collected in parallel onto two, 1" diameter CaF_2 windows using single-jet impactors (PIXE Stage L2, 120 nm particle diameter cutoff) operated at 1 SLM for 60 min (longer in the case of low concentration experiments). The windows were weighed before and after particle collection using a microbalance (Sartorius ME 5-F).

3.2.2 Experimental Methods: UV/Vis Absorption Spectroscopy

SOA material collected on CaF_2 windows was analyzed in a dual-beam UV spectrometer (Shimadzu). UV spectra were recorded immediately after collection, and periodically for up to 72 hours afterward to monitor changes in absorption with time. The collected particles were deposited in the center of the window during impaction. To create a more uniform film of organic aerosol material, the CaF_2 windows were pressed together and rotated several times.

This resulted in the aerosol material being spread over about 0.5 cm^2. Spectra were measured relative to clean CaF_2 windows and corrected for the expected reflection losses at the film-window and film-air interfaces assuming a refractive index of 1.43 for the SOA material [21] using the well-known Fresnel equation:

$$R = \frac{(n_1 - n_2)^2}{(n_1 + n_2)^2} \quad (1)$$

where n_1 and n_2 are the indices of refraction for the two materials that are in contact with one another, and R is the reflection loss at the interface. The refractive index losses from two clean CaF_2 windows amount to 10 percent of the incoming light; the initial intensity interacting with the SOA sample (I_o) is then 0.9 of the initial spectrometer source intensity. The addition of two films of SOA material leads to overall losses of approximately 13%, which makes the intensity at the detector equal to 0.87 of the initial spectrometer source intensity. Since the spectrometer used in these experiments measures base 10 absorbance, the baseline correction for reflection losses is:

$$A_{correction} = -\log (0.87/0.9) = 0.013 \quad (2)$$

This correction was subtracted from the baseline of all spectra. It is a very small absorbance; indeed, there was almost no change in the high concentration spectrum from this correction. The low concentration absorption spectra were more noticeably altered, owing to their much lower overall absorbance.

3.2.3 Results

Figure 3.2 shows the absorption profile of the SOA from limonene ozonolysis as compared to the spectrum of pure limonene. SOA absorption is red-shifted compared to pure limonene, which does not absorb in the tropospheric actinic window. This red-shift is due to the carbonyl–containing molecules in the SOA, which have a characteristic absorption centered near 300 nm. The SOA absorption spectrum in Figure 3.2 was collected using particles that were prepared at high reagent concentrations (10 ppm limonene, 300 ppm ozone).

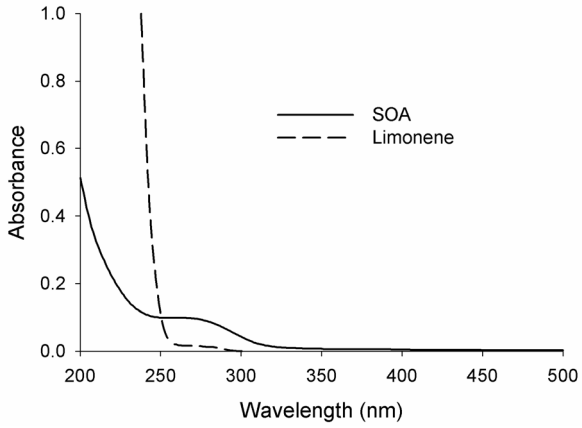

Figure 3.2. Absorption profiles of d-limonene and SOA from limonene ozonolysis. The *d*-limonene spectrum was collected from a sample of 97% purity liquid limonene pressed between two CaF_2 windows.

Figure 3.2 is somewhat misleading, because the limonene concentration is much higher than the SOA concentration for these spectra. The purpose of

Figure 3.2 is only to illustrate the red shift in the absorption spectrum before and after ozonolysis, and it should not be considered quantitative.

Figure 3.3 is a comparison of the absorption profiles of two different SOA samples between 200 and 500 nm, prepared using different concentrations of ozone and limonene. "Low concentration" here indicates that 500 ppb limonene and 1 ppm ozone were present in the Teflon reaction chamber, while "high concentration" refers to 300 ppm ozone and 10 ppm limonene.

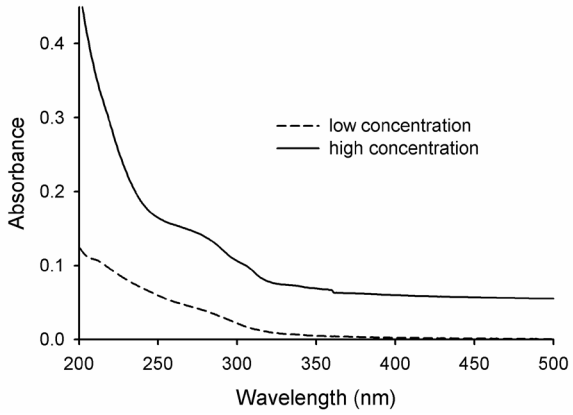

Figure 3.3. Absorption profiles of SOA produced at low and high reagent concentrations.

Because of the greater mass of SOA collected from the high concentration particle chamber, the absolute absorbance of the high concentration particles is much greater. The baseline of the high concentration spectrum is offset from zero for the same reason; the greater mass of particles makes it harder to create a homogeneous film of SOA material, and thus leads to scattering losses in addition to the expected reflection losses.

At wavelengths longer than about 350 nm, the spectra in Figure 3.3 are both featureless. Below 350 nm, however, there are reproducible differences between the two spectra in two specific areas: between 350 and 250 nm, and from 200 to 350 nm. There is a weak absorption hump in the region between 350 and 250 nm as in both spectra, although it is more pronounced in the particles prepared at higher oxidant concentrations.

Between 250 and 200 nm, the difference in the spectra is more pronounced. Specifically, the high concentration particles show an exponential rise to 200 nm that starts around 350 nm. The absorption profile of the particles prepared at lower reagent concentrations displays a much more gradual rise.

It is possible to prepare the sample in such a way as to avoid scattering losses. To do this, the particles are collected and spread over a 0.5 cm^2 area as before. Further spreading and homogenization of the film is accomplished by sintering it; that is, heating the windows gently with the particles pressed between them. The effect of the different sample preparation methods is shown in Figure 3.4.

The spectrum designated “no spreading” in Figure 3.4 was collected from SOA that had been impacted onto two CaF_2 windows with no additional sample preparation. The SOA in this case is localized in an area of approximately 5 mm^2 in the center of the window. This spectrum has a large baseline offset that makes up most of the spectrum. A small amount of absorption is visible around 300 nm. Spreading the particles over an area of 0.5 cm^2 (as discussed previously) reduces the scattering baseline by approximately half. In this

spectrum there are definite absorption features, caused by the improved transmission of UV radiation through the sample.

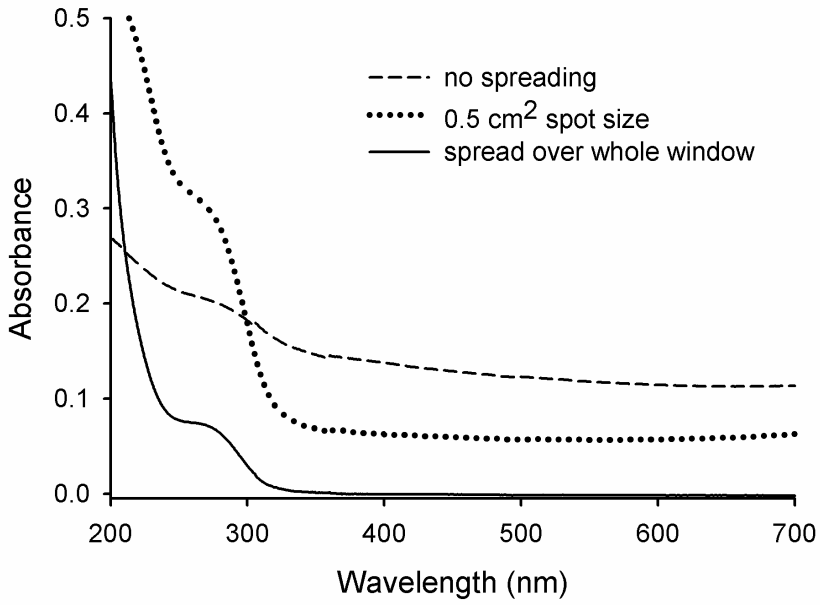

Figure 3.4. Effect of sintering on particle UV-Visible absorption spectrum.

The final spectrum in Figure 3.4 is that of the sintered particles that have been spread so that they cover the entire window area (~ 5 cm^2). The scattering losses are completely eliminated in this spectrum, and the shape of the absorption profile below 400 nm is conserved (although the intensity decreases as expected because of the shorter sample pathlength). Extinction coefficients and atmospheric lifetimes were not calculated using this sintering method because we have yet to explore the effect of heating the sample on its chemical composition. Instead, scattering losses have been assumed to be the sole cause

of any baseline offsets in the spectra of high concentration particles, and have been subtracted out when calculating these values.

3.2.4 Discussion

As mentioned briefly in Chapter 2 and demonstrated in Figure 3.2, the absorption profile of the *d*-limonene SOA is red-shifted significantly from that of pure limonene. Weak absorption between 270 and 330 nm is consistent with $n \rightarrow \pi^*$ transitions in non-conjugated aldehydes and ketones, which are expected products of ozonolysis of monoterpenes. Molecules with these functional groups have frequently been detected in monoterpene SOA [7, 22-26]. The portion of the absorption spectrum smoothly decaying with wavelength between 250 and 350 nm is indicative of $n \rightarrow \sigma^*$ transitions in organic peroxides, which account for a significant fraction of SOA material produced by ozonolysis of monoterpenes [3-5, 27].

The concentration-dependence of the spectra in Figure 3.3 indicates that, in general, the particles prepared at 300 ppm ozone are more highly oxidized (that is, contain a larger absolute amount of peroxide and carbonyl groups) than the particles prepared at 1 ppm ozone. This is demonstrated in the two regions discussed in the previous paragraph. The carbonyl absorption is far more pronounced in the more highly oxidized sample. Standard ozonolysis mechanisms (discussed in Chapter 2) predict that more ozone attack on limonene's double bonds will result in more carbonyl functional groups. The

increased absorption with a shape characteristic of peroxides also follows from the higher oxidant concentration.

Importantly, the particles prepared at the lower, more tropospherically-relevant oxidant concentration still display a significant overlap between their absorption profile and the tropospheric actinic window, indicating that monoterpene SOA formed in the actual atmosphere are likely to be aged by actinic radiation. As we will see below, the low concentration particles contain enough carbonyl groups that they should behave the same as the more oxidized particles with respect to tropospheric actinic radiation.

The absorption spectra of a known mass of SOA material can be used to estimate the effective (average) extinction coefficient of the SOA molecular constituents. The extinction should be dominated by absorption because individual particles in the collected SOA samples are agglomerated when the samples are prepared properly, and the reflection losses in the SOA film are explicitly subtracted. The baseline absorption (the value at 700 nm) was also subtracted from the high concentration spectra because it is dominated by scattering (as demonstrated in Figure 3.4). The extinction coefficient ε (in L mol^{-1} cm^{-1}) is calculated from measured base 10 absorbance (A) using Beer's Law, $A = \varepsilon C x$. The average concentration C (mol L^{-1}) is calculated from the assumptions that the SOA material has an average density of 1.5 g/cm^3 [28] and consists of molecules with an average molecular weight of 200 g/mol. This translates into a constant concentration of 7.5 M for all samples collected.

The effective pathlength (x, in cm) is estimated from measurements of the area over which the particles are spread and from the volume of the SOA (calculated from the assumed density and the gravimetrically-determined mass of the particles). A typical high concentration particle sample covers roughly half of the area of a 1" diameter CaF_2 window, meaning that the particles are spread over an area of 0.5 cm^2. Calculating the volume of the SOA sample from the density and the mass gives, for example, a volume of 3.06 x 10^{-4} cm^3 for a 450 µg SOA sample; this results in an effective pathlength of 6.12 x 10^{-4} cm through the particles. The pathlength is slightly less (2.1 x 10^{-4} cm for an 80 µg sample spread over a 0.25 cm^2 area) in the case of the SOA prepared at low reagent concentrations.

Using these approximations, an extinction coefficient at 295 nm of ε = 13.5 +/- 1.4 L mol^{-1} cm^{-1} is obtained for fresh SOA material, whether prepared at high or low concentrations. The values for high concentration particles were corrected for scattering influences. This value is within the typical range for $n \rightarrow \pi^*$ transitions of carbonyl-containing molecules [29], suggesting that a large fraction of the functional groups in the SOA are carbonyls independent of the oxidation conditions. Figure 3.5 shows the extinction coefficients and absorbances for two typical samples, one prepared at high concentrations and one at low concentrations.

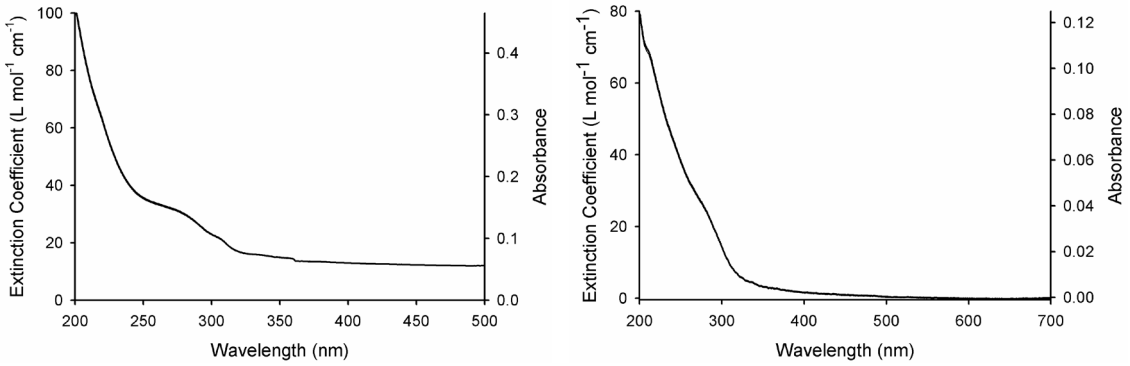

Figure 3.5. A comparison of the extinction coefficients and absorbances for SOA prepared at high (left panel) and low (right panel) concentrations. The baseline value of ε for the high concentration particles is approximately 11 L mol^{-1} cm^{-1}.

Based on the results presented in Chapter 2 of this thesis, we can now consider the implications of the measured absorption spectra for the atmospheric lifetime of the particles. The photolysis lifetime of any SOA constituent is the inverse of its photolysis rate constant, $k_p = \int_\lambda \sigma(\lambda)\Phi(\lambda)F(\lambda)d\lambda$, where σ(λ) is the absorption cross section, Φ(λ) is the photolysis quantum yield, and F(λ) is the actinic flux. The overall lifetime of the SOA particles can be estimated with the same equation. The lower limit for the photolysis lifetime can be estimated from the extinction coefficients assuming that every absorbed photon results in a photochemical reaction, so that Φ(λ)=1. The absorption cross section is calculated from the extinction coefficient at each wavelength via a transformation from base 10 to base *e*, and also via a unit conversion. For example, an extinction coefficient at 300 nm of 13.5 L mol^{-1} cm^{-1}, which converts to an absorption cross section of σ(300 nm) = 5.16 x 10^{-20} cm^2 $molecule^{-1}$. This is a small absolute cross section, but molecules with similar absorption cross

sections are photolyzed to a significant extent in the troposphere (c.f. acetone, $\sigma(300\ nm) = 2.77 \times 10^{-20}\ cm^2\ molecule^{-1}$).

For the high concentration particles, there is some offset in the baseline extinction coefficient values. Working from the assumption that the particles should have essentially zero absorption cross section at 700 nm, the extinction coefficient at 700 nm was subtracted from the coefficients at lower wavelengths; the absorption cross section was then calculated from these adjusted extinction coefficients. Convolution of these values of the absorption cross section with the actinic flux between 290 and 490 nm results in a photolysis lifetime of about 32 minutes for SZA (solar zenith angle) = 10°, which is characteristic of Southern California on July 1 at noon local time. Similar calculations for Midwestern US in summer (e.g. St. Louis, Missouri; SZA = 20°) result in a similar lifetime (33 minutes) The lifetime increases to 51 minutes in the case of 60° SZA, as would exist in Atlanta, Georgia at 6 PM on July 1st or during the day in other continental US locations in the winter months. In the extreme case of 86° SZA, when no radiation at wavelengths shorter than 315 nm penetrates to the troposphere, the lifetime increases to just under 10 hours because of the much smaller overlap between the absorption profile and the actinic window.

For the low concentration particles, convolution of the absorption profile with the actinic flux gives atmospheric photolysis lifetimes for small solar zenith angles of approximately 47 minutes. In the high solar zenith angle limit of 86°, the lifetime increases to over 15 hours. The atmospheric lifetime of the particles with respect to photolysis in the tropospheric actinic window are not dependent

on the reagent concentrations at which the particles are formed. This is reasonable because the ozonolysis mechanism is the same at both concentrations, meaning that a large proportion of carbonyls will be produced in both cases.

The lifetimes calculated using reasonable solar zenith angles are more than an order of magnitude less than the expected lifetime of aging due to surface oxidation of organic particles by OH (~30 hours for a surface reaction probability of 0.1 [30] and a typical atmospheric concentration of [OH] = 10^6 molecules cm^{-3}). Additionally, OH attack will primarily affect the molecules on the surface of the SOA, while photolysis has the potential to age molecules throughout the particles.

It is possible that this upper limit on the photolysis rate will not hold for *d*-limonene SOA in the troposphere. Studies on the photochemistry of large, carbonyl-containing molecules [31] have shown that the quantum yield for photolysis is always less than unity, substantially less in the case of Type I reactions of ketones. Research into polymeric ketone aging revealed that the quantum yield for photolysis decreases with chain length down to limiting values of 0.01 and 0.06 for the type I and II processes, respectively [32]. Primary products of limonene ozonolysis have ten carbons, and ketones of this chain length had quantum yields of 0.01 for the type I reaction and 0.1 for the type II reaction. This should be considered a lower bound on the quantum yield because of the presence of oligomers in the SOA. It is therefore possible that our estimate of the photolysis lifetime will be incorrect by as much as an order of

magnitude, considering the likely importance of ketone functional groups to the particle photochemistry. Using a quantum yield of 0.1 for type II processes results in a lower limit of 5.5 hours on the atmospheric lifetime of limonene SOA with respect to photolysis, assuming that the type II process dominates. The photolysis lifetime in these cases is still four times shorter than the lifetime with respect to OH oxidation, as mentioned previously. This further supports the implication that photochemical aging will be an important aging mechanism for monoterpene SOA in the troposphere.

3.3 Color Change in SOA Particles from Limonene Ozonolysis

3.3.1 Experimental Procedure

Color change experiments were performed using the aerosol samples that were collected for UV-Visible absorption spectroscopy (see section 3.2.2 for the procedure). Samples were not sintered and spread over the entire window, because we have yet to investigate whether heating has any effect on the chemical composition of the SOA. Instead, the baseline offset (which is shown to be from scattering only, c.f. Figure 3.4) was explicitly subtracted out when calculating extinction coefficients for these spectra.

For these experiments, the UV-Vis spectrometer was set to record a spectrum every 30 minutes for the duration of the experiment. When this kind of measurement method was used, the windows were placed in a custom-built sample holder flow cell with the SOA material facing in. The cell has inlet and

outlet valves, so that the SOA can be exposed to a flow of gases while the UV-Vis measurements were being taken. Gases such as nitrogen, oxygen, CO_2, NO_2 (0.1% in He) and purified air were flowed through the cell to investigate their effect (if any) on the rate or extent of change in the SOA absorption profile. A humidifier (Haake) was also used to investigate the effect of water vapor on the SOA. Between scans, the windows were stored either in the cell (approximate cell volume = 25 mL) under a 25 sccm flow of the purging gas, or in a stainless steel chamber (approximate chamber volume = 1000 mL) under a 1 LPM flow. Storage in the sample cell subjected the particles to irradiation with 700 nm light between samples (the default position for the spectrometer), which is unlikely to alter the particles because they have no absorption features in the red region of the visible spectrum (see Figure 3.2). Spectra were again measured relative to two clean CaF_2 windows, and were corrected for the expected film-window and film-air reflection losses as discussed previously.

Fourier Transform Infrared (FTIR) spectroscopy was used to monitor changes in the types and amounts of different functional groups in the particles during aging. Samples were collected onto zinc selenide (ZnSe) windows (Cradley Crystals), used because they afford a greater spectral range than the CaF_2 windows. The collection was performed in the same way as discussed in section 3.2. Samples were placed in the spectrometer (Perkin-Elmer) and FTIR spectra were recorded immediately after collection and after a period of aging, analogous to the procedure for UV-Vis analysis described above. Spectra were collected relative to a background of ambient air since the spectrometer's sample

compartment was not equipped with a purging flow. A spectrum of two clean ZnSe windows was subtracted from the SOA sample spectrum to compensate for absorption by coatings on the windows.

Mass spectra were also collected before and after aging using an electrospray ionization mass spectrometer (Waters). Since the particles had to be dissolved into methanol to be analyzed, the same particles were not used for the “fresh” and “aged” samples. Particles were dissolved in 10 mL of HPLC grade methanol and then diluted by a factor of 10 in more methanol before injection into the mass spectrometer. Mass spectra were collected in both positive and negative ion mode to ensure successful detection of as many particle components as possible.

Similar samples were prepared for analysis with fluorescence spectroscopy, with the exception that acetonitrile was used as the solvent instead of methanol. Three-dimensional fluorescence spectroscopy was used to analyze the fluorescence behavior of the particles before and after aging. In 3-D fluorescence spectroscopy, a complete fluorescence spectrum is collected while exciting the sample with an initial wavelength of UV radiation. The excitation wavelength is then increased by 5 nm and a complete emission spectrum is again collected.

3.3.2 Results

The color change phenomenon was initially observed in samples that had been collected on glass fiber filters and left in the dark in open air. To replicate

these conditions, the samples in the first color change experiments were simply allowed to age in the dark in the UV-Vis spectrometer's sample compartment. While in the sample compartment they were exposed to un-filtered laboratory air, which contains trace contaminants (such as organic solvents or dust) in addition to the standard trace pollutants in tropospheric air (such as ozone and oxides of nitrogen). Particles were also aged in a residential apartment (free of organic solvents) for several days, after which time the same color change was observed (although with different intensities, perhaps reflecting different levels of humidity and light in the apartment vs. the spectrometer's sample compartment).

Figure 3.6 shows the results of the first color change experiment, for which each sample of particles aged in the sample compartment of the UV-Vis spectrometer for two days, with spectra collected every 30 minutes. Initially, the absorption spectrum of the particles is what one would expect from a mixture of molecules with carbonyl and peroxide functional groups: an exponential decrease of absorption with increasing wavelength beginning at 200 nm (peroxides), and a peak in the region around 300 nm (carbonyls) as previously shown in Figure 3.3. These details are less pronounced in the low concentration aerosol, in keeping with the much lower ozone and limonene concentrations in the Teflon chamber and resulting lesser degree of oxidation.

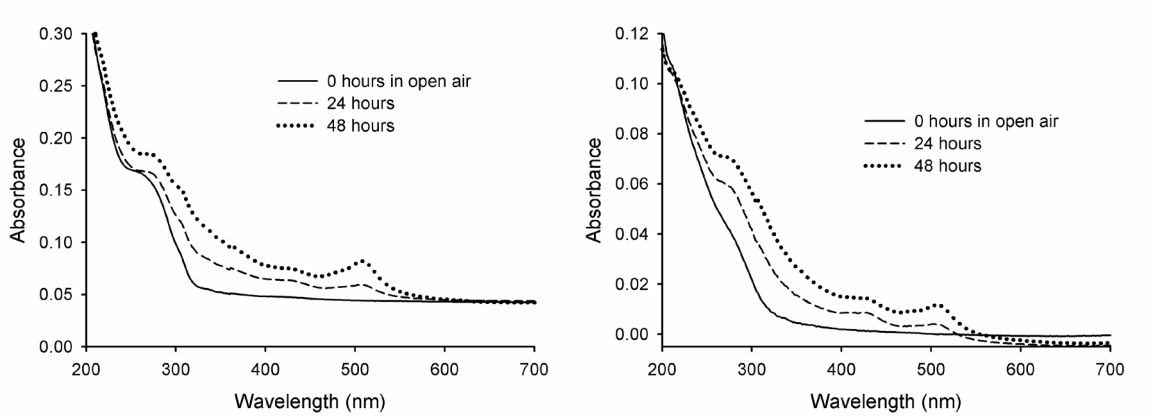

Figure 3.6. UV-Vis absorption spectra of limonene SOA collected on a CaF_2 window as a function of time stored in open air in the dark. The left plot shows spectra from particles made under high reactant concentrations; the spectra in the right plot are from low concentration SOA. The changes in the absorption profile are accompanied by a visible transition of the particles from colorless to red-brown in both cases.

Within the first 24 hours of aging, both sets of particles and their absorption spectra had changed considerably. The particles themselves had acquired a deep red-brown color and were also visibly wet, indicating that water uptake had occurred (relative humidity in our lab is generally between 30 and 50 % and research has ascribed excellent CCN activity to monoterpene SOA [33, 34]) or that condensation reactions were occurring inside the particles, producing water that did not evaporate from the particles' surface.

Mass spectra of the fresh and aged particles were also collected in an effort to more fully understand the chemical basis of the color change. The results are shown in Figure 3.7 for two sets of particles that were produced under the same reagent conditions. The aged particles were kept for 8 days in a stainless steel chamber under a 2 LPM flow of room air pumped through a HEPA filter. The particles were in the dark for the entire 8 days prior to the mass spectrometry analysis. UV-Visible absorption spectra of the particles were

collected before dissolving them for mass spectrometric analysis; the aged sample had a significantly modified spectrum analogous to those in Figure 3.6.

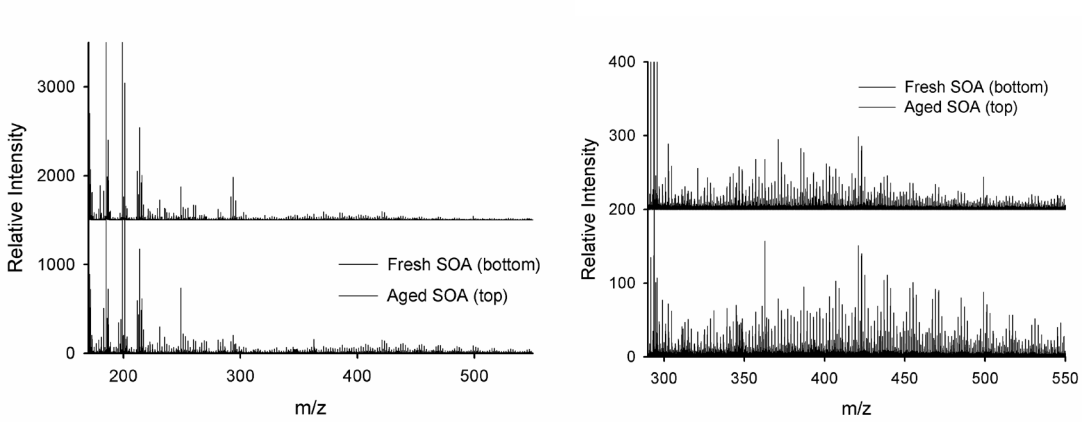

Figure 3.7. Negative-ion electrospray ionization mass spectra of fresh (bottom) and aged (top) SOA produced under the same conditions. The right panel is a detail view of the mass region between 290 and 550 m/z; peaks above 300 m/z are assumed to represent oligomers.

The mass spectra are remarkable for their similarity. Given the extent of the color change and the change in the absorption spectrum after 8 days, we expected the mass spectrum to change much more between the fresh and aged samples. The one notable change occurs in the region between 300 and 600 m/z, which is the region that is usually assigned to dimers and oligomers in fresh monoterpene SOA [6, 35]. After 8 days of aging, the distribution of these oligomers has very slightly shifted to lower mass values. The peaks in the monomer region of the mass spectrum (m/z < 300) are unchanged for the most part.

After observing the color changes and noting that the UV-Visible absorption spectra changed significantly, the obvious next step was to

qualitatively determine whether any atmospheric species were indirectly responsible for the change (e.g. via catalysis). This involved using the flow cell to expose the SOA to only certain components of laboratory air in order to find the combination that contributes to the changes in the absorption profile. We chose to first explore the role of nitrogen in the color change because of its atmospheric abundance; the role of water vapor was investigated at the same time because of the wet appearance of the aged particles. The left plot of Figure 3.8 shows the results of these investigations for particles prepared at high reagent concentrations. This SOA sample was exposed to dry nitrogen and then immediately switched to humid nitrogen after 18 hours.

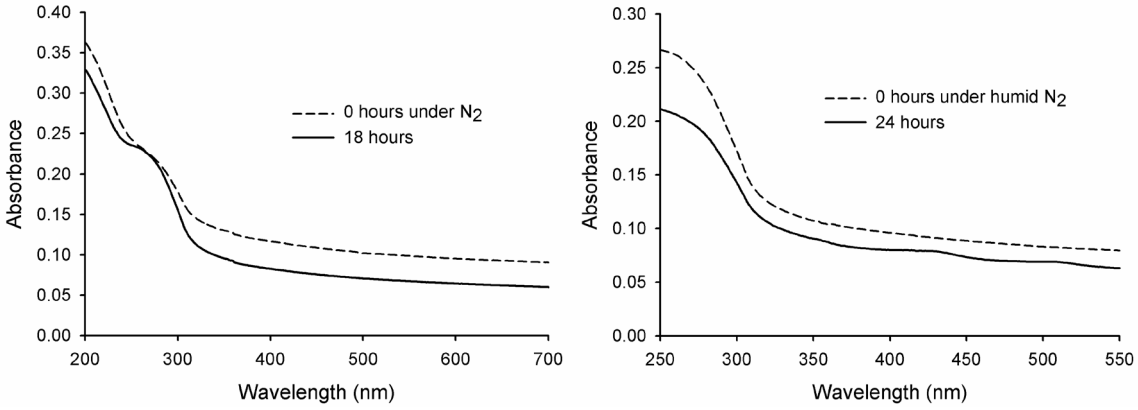

Figure 3.8. SOA aging under nitrogen (left) and humidified nitrogen (right, RH > 90%). These SOA were prepared at high reagent concentrations (10 ppm limonene, 300 ppm ozone).

The left panel of Figure 3.8 shows that there was very little change in the shape of the absorption profile during the period where dry nitrogen gas was flowing over the sample. A general reduction in the background absorbance did

occur, which we ascribe to evaporation of SOA components causing a reduction in scattering losses. The baseline reduction was observed in all samples where gas was continuously flowing over the sample, but generally not when the samples were in open air.

When a large amount of water vapor was added to the nitrogen flow, the absorption profile did begin to change, though much more slowly than when the particles were in the laboratory air. After 24 hours under the humid (RH > 90%) nitrogen, the particles began to show the same absorption features that were present in Figure 3.6, although their intensities were smaller.

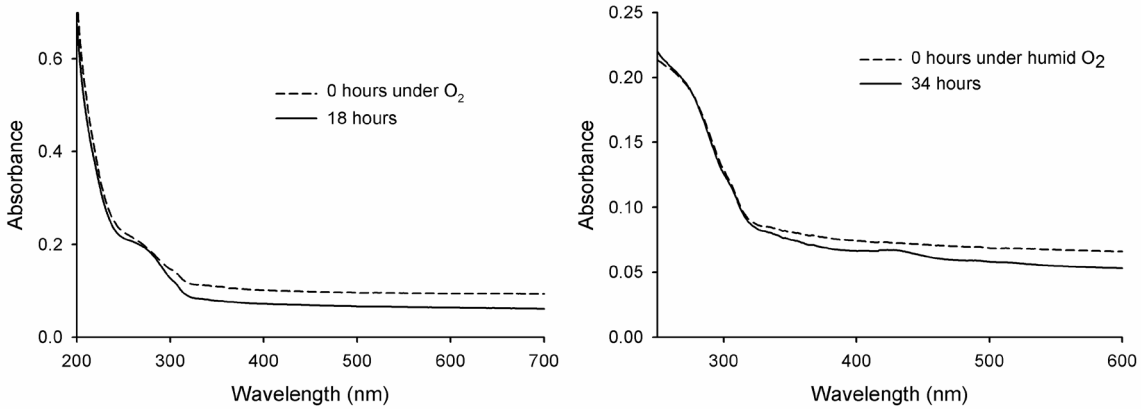

Figure 3.9. SOA aging under oxygen (left) and humidified oxygen (right, RH > 90%). The spectra have not been corrected for reflection losses. These SOA were prepared at high reagent concentrations.

Similar spectra were collected with the particles exposed to oxygen and humid oxygen (Figure 3.9). The same trend was observed: oxygen alone did not produce any absorption peaks in the visible region, but when the oxygen was

humidified the same absorption features (near 430 nm and, to a much lesser extent, 510 nm) were observed.

The influences of NO_2 and CO_2 on the color change were also investigated. Two days under CO_2 failed to change the particles' absorption profile, but the NO_2 flow (0.1% in He) had an effect, which is shown in Figure 3.10.

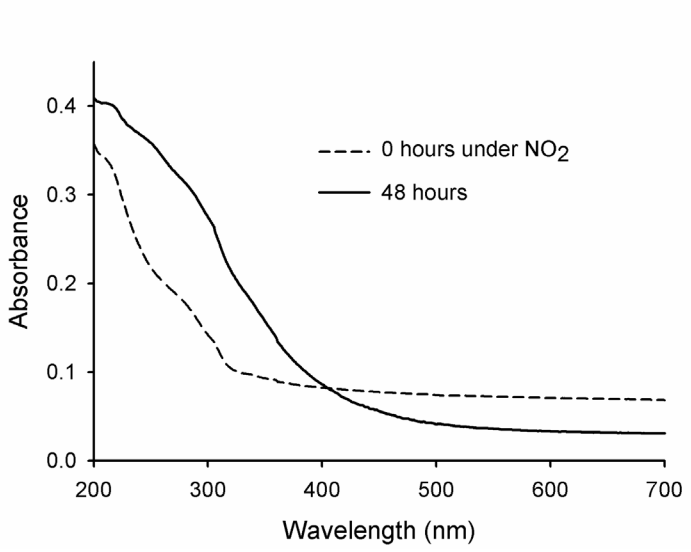

Figure 3.10. SOA before and after 48 hours under a flow of 0.1% NO_2.

Since NO_2 absorbs strongly in the visible region, spectra could only be taken after the flow was turned off and the sample holder had been briefly purged with zero-air. After two days under NO_2, the particles' absorption spectrum was significantly altered, although not in the same way as when the particles are aged in open air. As in other spectra, the baseline absorbance has been reduced by evaporation. Unlike in other spectra, however, the absorption is red-shifted by

time spent under NO_2. Also of interest is the fact that when the particles were removed from the sample holder and allowed to age in open air, no further modification of the absorption spectrum took place.

Three-dimensional fluorescence spectra collected before and after particle aging are shown in Figure 3.11. Initially the particles do not fluoresce when excited with any wavelengths between 250 and 500 nm. After two weeks of aging, however, the particles display significant fluorescence that matches up well with the changes in the absorption profile. Of particular note are the two fluorescence peaks that appear when the sample is excited with ~400 nm and ~500 nm radiation; the analogy to the aged UV spectra in Figure 3.6 is clear. The dramatic increase in the fluorescence activity of the particles implies that they are increasing in either conjugation or aromaticity.

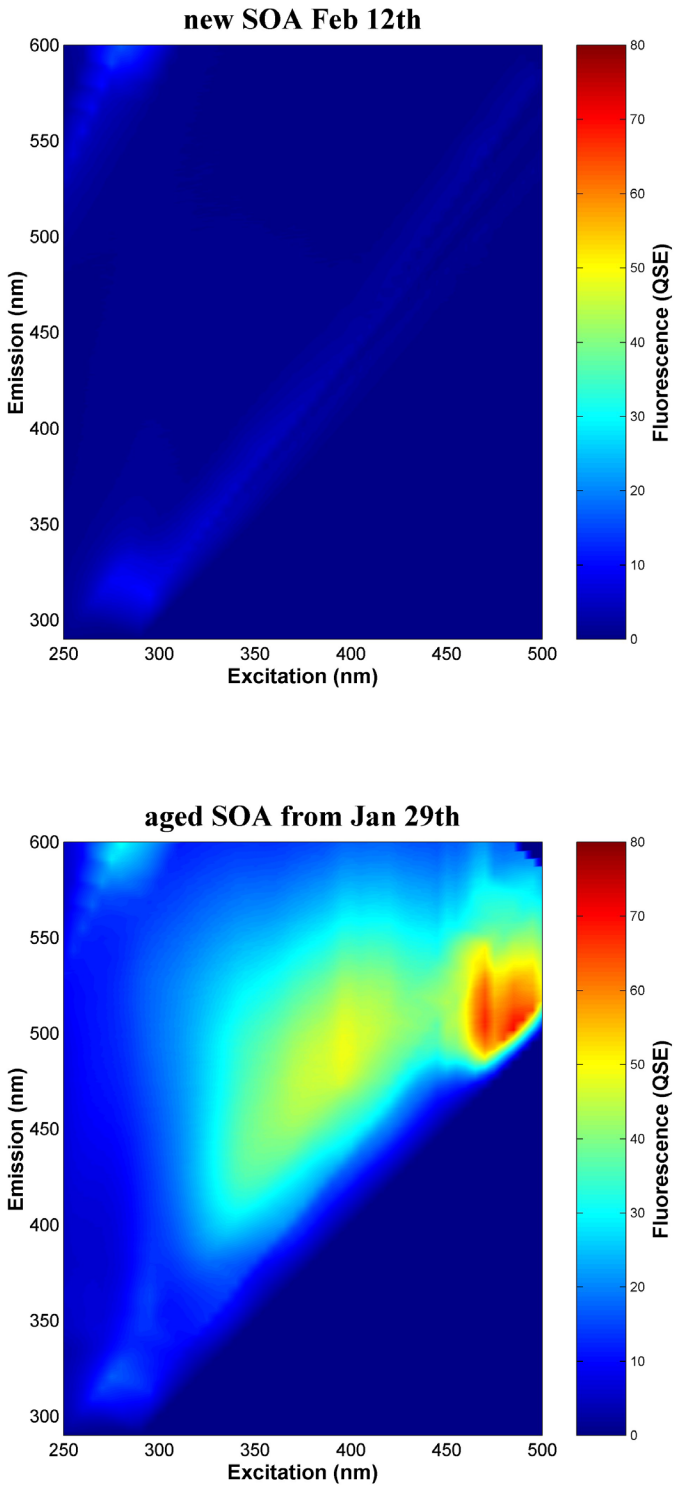

Figure 3.11. 3-D fluorescence spectra of SOA before and after aging in open air in the dark.

3.3.3 Discussion

The most striking change in the absorption profiles are the peaks located in the visible region, as seen to various extents in Figures 3.6, 3.8 and 3.9. Experiments similar to those plotted in Figure 3.5 (particles aging in open laboratory air in the dark) resulted in the most obvious changes. These spectra of the particles display a new peak centered at 508 nm, which implies greatly increased conjugation or the appearance of aromatic functionalities in the particles. Also evident is a general decrease in the amount of incident radiation transmitted through the sample, the effect being greater at lower wavelengths. This is consistent with increased scattering losses, an explanation that is supported by a visual inspection of the particles. The increase in scattering is smaller in the low concentration particles (the right panel of Figure 3.5), allowing a second visible peak near 430 nm to be seen. We also ascribe this peak to increased conjugation in the particles.

Further support for the presence of increased conjugation or aromaticity in the particles is that they become fluorescent as they age in the dark in open laboratory air, as shown in Figure 3.11. Previous researchers have noted that dissolved organic matter and humic-like substances (HULIS) in rainwater display fluorescence [36, 37]. In fact, the regions in which the SOA samples become fluorescent are well-correlated to the expected behavior of fulvic-like substances. Fulvic-like substances fluoresce when excited between 330 and 350 nm, emitting fluorescence between 420 and 480 nm; this roughly corresponds to the shortest-wavelength excitation seen in Figure 3.11. Most of

the fluorescence intensity of the SOA is shifted to higher wavelengths, indicating that while some fulvic-like substances may be present in the aged aerosol, the main fluorescent species are more highly conjugated and have higher average molecular weights than either humic- or fulvic-like substances.

Spectra were collected with the sample isolated from the laboratory air and exposed to selected gases one or two at a time. As Figure 3.8 shows, there was very little change in the shape of the absorption profile during the period where dry nitrogen gas was flowing over the sample. A general reduction in the background absorbance did occur, which we ascribe to evaporation of SOA components leading to a reduction in scattering losses.

Water vapor appears to catalyze a process that causes color change in the visible region of the spectrum. When the humidity of the nitrogen flow was increased above 90%, the familiar peaks at 430 and 508 nm began to appear. These peaks, seen in the right panel of Figure 3.8, are less intense than those observed as the particles aged in open air for 24 hours, suggesting that water alone is not responsible for the change in the sample or that an environment containing an excessive amount of water vapor might actually be less favorable to the reaction. The same behavior was observed when the particles were exposed to dry oxygen followed by humid oxygen (Figure 3.9).

Carbon dioxide had no effect on the absorption spectra of the particles (besides a baseline reduction due to evaporation), while NO_2 altered the visible region of the spectrum in a way that was distinct from the other atmospheric species that were studied. The mechanism of this alteration is different from that

leading to the distinct absorption features at ~430 and ~510 nm; the passivation of the sample (making it insensitive to time spent in open air) suggests that a chemical reaction between NO_2 and the SOA has taken place that prevents further changes in the absorption spectrum. The mechanism of this reaction, like the mechanism leading to the other color changes, is unknown at this time.

There was also a reduction in absolute absorbance in the region where carbonyls and peroxides absorb that was not observed when only dry nitrogen or oxygen was flowing over the particles. There are two possible reasons for this: either the chemical reaction that causes the color change consumes those functional groups, or they are evaporating. We have not ascribed the change in the spectrum to either possibility, although from examining the region around 700 nm it seems clear that some evaporation is occurring.

The extinction coefficient ε increases by almost an order of magnitude (depending on the wavelength) as the particles age in the dark in open laboratory air over the course of two days. Changes in the particles' extinction coefficient were calculated assuming that the refractive index of the particles did not change with aging; a constant value of 1.43 was used. In general, estimates of the refractive index of real organic aerosols are within 5% of this value [21, 38, 39] and are roughly independent of wavelength in the visible region [40]. Over the course of two and a half days spent on a CaF_2 window (in laboratory air and in the dark), the absorption profile of both the high and low concentration particles changes dramatically (Figure 3.12). The particles' extinction coefficient increases to some extent at all wavelengths below 550 nm, and well-defined

absorption peaks grow in at 508 nm and 430 nm. For the particles produced at high reagent concentrations, the peak at 508 nm grows to an extinction coefficient of ε ~7 L mol^{-1} cm^{-1} above the baseline value after two days (the same is true for low concentration SOA), while the extinction coefficient at 295 nm increases to as much as ε ~ 38 L mol^{-1} cm^{-1} (for the low concentration particles; the high concentration gain approximately 25 L mol^{-1} cm^{-1} above the baseline value). Figure 3.12 shows the change in absorbance and extinction coefficient for particles produced at high and low reagent concentrations.

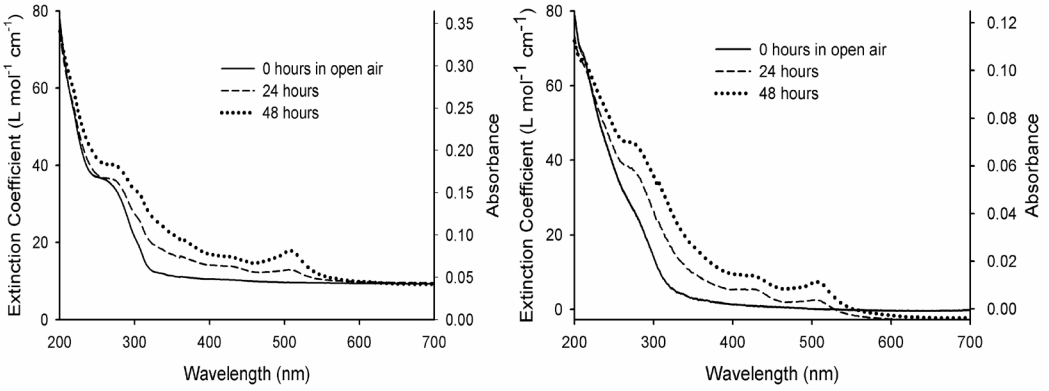

Figure 3.12. Changes in absorbance and extinction coefficient as a function of time spent in open air for aerosol produced at high (left) and low (right) reagent concentrations. The baseline corresponds to an "extinction coefficient" for the high concentration particles of approximately 11 L mol^{-1} cm^{-1}.

The new values of the extinction coefficient move the SOA into the realm of weak absorbers in the visible wavelength range, and increase their absorbance in the UV region of the tropospheric actinic window. This behavior implies that various reactions are resulting in increased conjugation, suggesting that polymerization is occurring in the particles as a result of reactions with

species in the ambient laboratory air. The importance of reactions that result in increased absorption indices has been suggested for acidic [16, 17] and water-soluble [10, 41] aerosol particles.

If particles over rural areas do indeed have a non-negligible extinction coefficient for light absorption, the consequences for the radiative forcing are profound. The cases where absorption by particles is greater than scattering (that is, when particles have a positive radiative forcing) are thought to be limited to particle masses with high concentrations of black carbon. If monoterpene SOA can acquire a non-zero absorption extinction coefficient over the course of their atmospheric lifetimes, it implies that particles may have positive radiative forcings even over rural areas where black carbon concentrations are low.

3.4 Summary and Conclusions

In Section 3.2 of this chapter, a procedure for measuring the absorption profiles of films of SOA particles has been described. The method involves creating a thin, homogeneous film from a collection of SOA particles impacted onto a UV-transparent window, followed by analysis in a dual-beam UV-Visible spectrometer. Spectra collected using this method were found to be reproducible and were interpreted in light of the known distribution of products of limonene ozonolysis. Extinction coefficients were calculated based on the measured base-10 absorbance, and these coefficients were used to calculate absorption cross sections for these SOA particles with respect to tropospheric radiation. Based on

the conclusions presented in Chapter 2 of this thesis, atmospheric lifetimes with respect to photolysis were estimated for the SOA particles. The estimated lifetimes were an order of magnitude shorter than the expected lifetime of organic aerosols with respect to OH radical attack, indicating that photochemical aging will be important for monoterpene SOA in the troposphere.

In Section 3.3 of this chapter, results have been presented from initial experiments on particle aging in the absence of UV radiation. Techniques such as mass spectrometry and UV-Visible spectroscopy were used to inspect the particles before and after a period of aging in open air or under various gases. The results of these experiments imply that monoterpene SOA particles can be aged by non-photochemical processes, meaning that the aerosols will be modified during their time in the atmosphere even when conditions are not favorable to photochemistry. The changes occurring in the particles lead to a substantial modification of their absorption profile, causing an increase in the particles' total extinction coefficient and an increased absorption profile in the visible region of the spectrum.

We have not calculated the effect of this non-photochemical aging on the particles' lifetime with respect to photolysis because the mechanism of the changes that alter the particles' absorption profile is unknown at this time. We have speculated that acid catalyzed reactions analogous to aldol condensation reactions may be occurring, but the matter is far from settled. Mass spectrometry experiments aimed at more fully understanding the changes taking place in the particles are ongoing.

3.5 References

1. Glasius, M., M. Duane, and B.R. Larsen, *Determination of polar terpene oxidation products in aerosols by liquid chromatography-ion trap mass spectrometry.* Journal of Chromatography A, 1999. **833**(2): p. 121-135.
2. Koch, S., et al., *Formation of new particles in the gas-phase ozonolysis of monoterpenes.* Atmospheric Environment, 2000. **34**(23): p. 4031-4042.
3. Tolocka, M.P., et al., *Chemistry of Particle Inception and Growth during α-Pinene Ozonolysis.* Environ. Sci. Technol., 2006. **40**(6): p. 1843-1848.
4. Jenkin, M.E., *Modelling the formation and composition of secondary organic aerosol from α- and β-pinene ozonolysis using MCM v3.* Atmos. Chem. Phys., 2004. **4**: p. 1741-1757.
5. Docherty, K.S., et al., *Contributions of Organic Peroxides to Secondary Aerosol Formed from Reactions of Monoterpenes with O_3.* Environ. Sci. Technol., 2005. **39**(11): p. 4049-4059.
6. Tolocka, M.P., et al., *Formation of Oligomers in Secondary Organic Aerosol.* Environ. Sci. Technol., 2004. **38**(5): p. 1428-1434.
7. Yokouchi, Y. and Y. Ambe, *Aerosols formed from the chemical reaction of monoterpenes and ozone.* Atmospheric Environment (1967), 1985. **19**(8): p. 1271-1276.
8. Robinson, A.L., et al., *Rethinking Organic Aerosols: Semivolatile Emissions and Photochemical Aging.* Science, 2007. **315**(5816): p. 1259-1262.
9. Walser, M.L., et al., *Photochemical Aging of Secondary Organic Aerosol Particles Generated from the Oxidation of d-Limonene.* J. Phys. Chem. A, 2007. **111**(10): p. 1907-1913.
10. Ellison, G.B., A.F. Tuck, and V. Vaida, *Atmospheric processing of organic aerosols.* Journal of Geophysical Research, 1999. **104**(D9): p. 11633-11641.
11. Park, J., et al., *Ozonolysis and photolysis of alkene-terminated self-assembled monolayers on quartz nanoparticles: implications for photochemical aging of organic aerosol particles.* Physical Chemistry Chemical Physics, 2006. **8**: p. 2506-2512.
12. Broekhuizen, K.E., et al., *Formation of cloud condensation nuclei by oxidative processing: Unsaturated fatty acids.* J. Geophys. Res., 2004. **109**(D24206): p. doi: 10.1029/2004JD005298.
13. Forster, P., et al., *Changes in Atmospheric Constituents and in Radiative Forcing.* Climate Change 2007: The Physical Science Basis. Contribution of Working Group I to the Fourth Assessment Report of the Intergovernmental Panel on Climate Change., ed. S. Solomon, et al. 2007, Cambridge, United Kingdom: Cambridge University Press.
14. Ramanathan, V., et al., *Warming trends in Asia amplified by brown cloud solar absorption.* Nature, 2007. **448**(7153): p. 575-578.
15. Casale, M.T., et al., *Kinetics of acid-catalyzed aldol condensation reactions of aliphatic aldehydes.* Atmospheric Environment, 2007. **41**(29): p. 6212-6224.
16. Nozière, B. and W. Esteve, *Organic reactions increasing the absorption index of atmospheric sulfuric acid aerosols.* Geophysical Research Letters, 2005. **32**: p. L03812.
17. Nozière, B. and W. Esteve, *Light-absorbing aldol condensation products in acidic aerosols: Spectra, kinetics, and contribution to the absorption index.* Atmospheric Environment, 2007. **41**(6): p. 1150-1163.
18. Limbeck, A., M. Kulmala, and H. Puxbaum, *Secondary organic aerosol formation in the atmosphere via heterogeneous reaction of gaseous isoprene on acidic particles.* Geophysical Research Letters, 2003. **30**(19): p. doi: 10.1029/2003GL017738.
19. Hoffer, A., et al., *Optical properties of humic-like substances (HULIS) in biomass-burning aerosols.* Atmospheric Chemistry and Physics, 2006. **6**: p. 3563-3570.
20. Roberts, J.M., et al., *Monoterpene hydrocarbons in the nighttime troposphere.* Environ. Sci. Technol., 1985. **19**(4): p. 364-369.

21. Fraser, R.S. and Y.K. Kaufman, *Relative importance of aerosol scattering and absorption in remote sensing.* IEEE Trans. Geosci. Remote Sens., 1985. **23**(5): p. 625-633.
22. Glasius, M., et al., *Carboxylic Acids in Secondary Aerosols from Oxidation of Cyclic Monoterpenes by Ozone.* Environ. Sci. Technol., 2000. **34**(6): p. 1001-1010.
23. Jang, M. and R.M. Kamens, *Newly characterized products and composition of secondary aerosols from the reaction of α-pinene with ozone.* Atmospheric Environment, 1999. **33**(3): p. 459-474.
24. Kamens, R., et al., *Aerosol Formation from the Reaction of α-Pinene and Ozone Using a Gas-Phase Kinetics-Aerosol Partitioning Model.* Environ. Sci. Technol., 1999. **33**(9): p. 1430-1438.
25. Leungsakul, S., M. Jaoui, and R.M. Kamens, *Kinetic Mechanism for Predicting Secondary Organic Aerosol Formation from the Reaction of d-Limonene with Ozone.* Environ. Sci. Technol., 2005. **39**(24): p. 9583-9594.
26. Yu, J., et al., *Gas-Phase Ozone Oxidation of Monoterpenes: Gaseous and Particulate Products.* Journal of Atmospheric Chemistry, 1999. **34**(2): p. 207-258.
27. Bonn, B., R. von Kuhlmann, and M.G. Lawrence, *High contribution of biogenic hydroperoxides to secondary organic aerosol formation.* Geophysical Research Letters, 2004. **31**(10): p. L10108.
28. Engelhart, G.J., et al., *CCN activity and droplet growth kinetics of fresh and aged monoterpene secondary organic aerosol.* Atmos. Chem. Phys. Discuss., 2008. **8**(1): p. 95-135.
29. Coxon, J.M. and B. Halton, *Organic Photochemistry, 2nd Ed.* 1987, Cambridge: Cambridge University Press.
30. Bertram, A.K. et. al., *The Reaction Probability of OH on Organic Surfaces of Tropospheric Interest*. J. Phys. Chem. A., 2001. **105**: p. 9415.
31. Robbins, W.K. and R.H. Eastman, *Photodecarbonylation in solution. I. Quantum yields and quenching results with dibenzyl ketones.* J. Am. Chem. Soc., 1970. **92**(20): p. 6076-6077.
32. Hartley, G.H. and J.E. Guillet, *Photochemistry of Ketone Polymers. II. Studies of Model Compounds.* Macromolecules, 1968. **1**(5): p. 413-417.
33. Huff Hartz, K.E., et al., *Cloud condensation nuclei activation of monoterpene and sesquiterpene secondary organic aerosol.* Journal of Geophysical Research, 2005. **110**: p. D14208.
34. Prenni, A.J., et al., *Cloud droplet activation of secondary organic aerosol.* Journal of Geophysical Research, 2007. **112**: p. D10223.
35. Heaton, K.J., et al., *Oligomers in the Early Stage of Biogenic Secondary Organic Aerosol Formation and Growth.* Environ. Sci. Technol., 2007. **41**: p. 6129-6136.
36. Kieber, R.J., et al., *Photobleaching of chromophoric dissolved organic matter (CDOM) in rainwater.* J Atmos Chem, 2007. **58**: p. 219-235.
37. Duarte, R.M.B.O., C.A. Pio, and A.C. Duarte, *Synchronous Scan and Excitation-Emission Matrix Fluorescence Spectroscopy of Water-Soluble Organic Compounds in Atmospheric Aerosols.* Journal of Atmospheric Chemistry, 2004. **48**: p. 157-171.
38. Dickerson, R.R., et al., *The Impact of Aerosols on Solar Ultraviolet Radiation and Photochemical Smog.* Science, 1997. **278**(5339): p. 827-830.
39. Finlayson-Pitts, B.J. and J.N. Pitts, *Chemistry of the Upper and Lower Atmosphere*. 2000, San Diego: Academic Press.
40. Nilsson, B., *Meteorological influence on aerosol extinction in the 0.2-40-μm wavelength range.* Appl. Opt., 1979. **18**(20): p. 3457.
41. Gelencsér, A., et al., *In-situ Formation of Light-Absorbing Organic Matter in Cloud Water.* Journal of Atmospheric Chemistry, 2003. **45**(1): p. 25-33.

Chapter 4

Development of an Atmospheric Pressure Microwave Plasma Torch for Single Particle Counting with Chemical Information

4.1 Introduction and Literature Survey

Aerosol particles have important effects on human health [1-3] because their size allows them to penetrate deep into the lungs. Metals from industrial pollution and carcinogenic organic compounds from biomass burning or automobile exhaust can be delivered into various organs of the body by aerosol particles. Fine particulate matter is linked to lung cancer and heart disease [4], and cumulative exposure to ambient levels of particulates increases the risk of respiratory disease [5]. Despite their importance, the chemical composition of metal-containing atmospheric aerosols and the reactions in which particle components can take part are still poorly understood.

Particles produced by industrial use of fossil fuels are particularly problematic [6,7]. Recent legislation in the United States aims to clean up emissions from factories and power plants; monitoring the emissions from such factories will ensure that required limits are being followed. Detection of metals in particulate emissions is especially important, since many metals emitted from industrial sources have adverse effects on human health [8]. Pressing

environmental concerns necessitate sensitive, field portable instrumentation for the detection of metallic elements in particle samples from ambient air.

In order to simultaneously measure aerosol particle concentration and extract information about their chemical composition, it has traditionally been necessary to use mass spectrometric techniques [9-11]. Aerosol mass spectrometry is a large and growing field, with many powerful capabilities and widespread applications. Mass spectrometry provides a sensitive, chemically specific detection method for the molecular and atomic components of aerosol particles. Portable aerosol mass spectrometers have been developed [9], mostly for installation on sampling aircraft. The major drawbacks of aerosol mass spectrometers are their high power requirements and high cost. Also, they are relatively large, making their field operation suited to placement on sampling airplanes or some similarly large platforms. The availability of a smaller, less energy and cost intensive alternative for field aerosol sampling is desirable so that more source-specific sampling can be done.

An obvious detection strategy for the detection of airborne metals is atomic emission spectroscopy (AES). In laboratory situations, where power and working gas requirements are not an issue, the inductively coupled plasma (ICP) has found widespread use as an excitation source. ICP instruments use a radio frequency coil to produce an electrodeless plasma in a stream of argon gas at atmospheric pressure [12]. A solution of the analyte of interest is nebulized and a small fraction is sent into the plasma, where it is electronically excited. Detection is commonly accomplished using a monochromator and photomultiplier

tube (or similar detector such as a CCD array), so that a spectrum of the plasma and emission from any introduced analytes is obtained. The main drawback of the ICP is that it is inefficient at exciting nonmetals, especially halogens, due to its inability to use helium as the plasma gas [13]. Also, several studies on solvent loading in the ICP have concluded that desolvation of the sample (i.e. removing excess solvent from the sample aerosol) is necessary for optimal excitation of the analyte species [14], although contradictory results have also been reported. Most studies in which ICP-AES is used in a laboratory involve a desolvation system; this would limit the usefulness of the ICP to real-time field sampling applications, especially to the sampling of aerosols with a high water content (such as those found in coastal areas or in areas of elevated relative humidity). For such applications, an alternative atmospheric pressure plasma source better suited to analysis of "wet" aerosols is necessary.

One such atmospheric pressure plasma source is the microwave plasma torch (MPT). When coupled with atomic emission spectroscopy and an ultrasonic nebulizer, the MPT has been used for the analysis of aqueous metal-containing solutions in the laboratory [13]. In most cases, a solution of one or more metals is nebulized and desolvation is used to remove much of the water. The resulting dried metal aerosol is sent through the plasma, analogous to ICP-AES, and detection limits in the range of 10 ppb can be realized for many elements, although when desolvation is not used the detection limits can be much higher [13]. Even when desolvation is not used, the number of elements

that can be detected by MPT-AES is still large and detection limits as low as 100 ppb (e.g. for cadmium) can be achieved [15].

The following sections will describe the development and preliminary tests of an MPT instrument for atomic emission spectroscopy of both model and actual atmospheric aerosol particles. After the initial construction of the instrument, studies were carried out to characterize the performance of the torch, and also to investigate the size-dependent emission from several kinds of aerosol particles. Aerosol properties and composition were studied using an apparatus consisting of a scanning mobility particle sizer (SMPS), an argon-based MPT, and a monochromator with a photomultiplier tube for detection. The operational principles of the SMPS and MPT will be discussed briefly in the following sections.

The major goal of this research was the qualitative detection and characterization of single aerosol particles passing through the torch plasma. Such detection has been demonstrated for sea-salt particles using a nitrogen/oxygen/hydrogen flame [16,17], but it was expected that the MPT would be a better excitation source for such measurements. The high excitation temperature for the atmospheric pressure argon plasma relative to a conventional flame will permit more specific and sensitive detection of the elements in the particles that pass through the plasma. Also, the simplicity of the working gas (argon versus the nitrogen/oxygen/hydrogen flame) will result in a simpler background spectrum and less interference with a wider variety of analytes. Additionally, the demonstrated linearity of emission intensity as a

function of concentration [18] at low solution concentrations means that MPT-AES has the potential to be used as a quantitative method for detection of many elements as a function of individual particle size.

4.2 Instrumentation

4.2.1 Microwave Plasma Torch

The MPT was used as the excitation source for detecting atomic emission from metal-containing aerosol particles. Our design is based on the torch developed by Jin and coworkers [15] and is shown in Figure 4.1. Jin's design was adapted from the surfatron [19], which was an early atmospheric pressure microwave- induced plasma source that used surface electromagnetic waves to produce a plasma contained within a quartz tube. The microwave torch is made up of three concentric tubes of varying widths and materials. The outer tube, which serves as the body of the torch, is 1/2" diameter stainless steel; it has a sliding 50 ohm connector with a cylindrical copper antenna to couple the output from a commercial microwave generator (Sairem GMP 03KE/D, 2.45 GHz, 300 W) to the torch. This outer tube is also connected to the common ground via the connector of the waveguide and can be used to introduce a sheath gas into the area around the plasma when necessary.

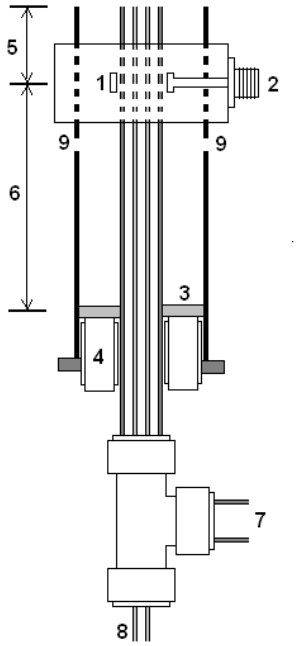

Figure 4.1. Diagram of the microwave plasma torch: 1) Cylindrical copper antenna, 2) microwave waveguide connector, 3) brass short-circuit plate, 4) adjustment for short-circuit plate height, 5) L_A, the height from the antenna to the top of the torch, typically around 25 mm, 6) L_S, the distance from the antenna to the short circuit plate, typically around 75 mm, 7) Argon flow inlet (1/4" tube), 8) Aerosol inlet (1/8" tube), 9) Nitrogen sheath gas inlets. Solid black lines indicate the main body of the torch.

The torch's central tube is made of 1/4" outer diameter copper, and conducts the microwave radiation; this tube also carries the plasma support gas. The copper antenna encircles this tube, and it is at this point that the microwave radiation is coupled to the torch. The innermost tube is 1/8" outer diameter stainless steel. It runs through the central tube and delivers the analyte aerosol to the plasma. In total the MPT is less than seven inches tall and requires very little space. Even smaller torches of similar construction have been described in the literature [20,21].

At the bottom of the torch body is a brass plate, which creates a short circuit with the central (copper) tube. When the microwaves are coupled to the

copper tube via the antenna, they can either propagate up over L_A, the distance from the antenna to the top of the torch, or down over the length L_S, in which case they are reflected by the short circuit plate. This results in a standing wave in the body of the torch. It is important that the antenna height be such that the phase of the standing wave below the antenna is identical to the phase of the traveling wave above the antenna; this means that the impedance of the torch is matched to the impedance of the waveguide and ensures resonant operation. It also ensures that very little microwave power is reflected back to the magnetron (less than 10% at forward powers up to 250 W), protecting the microwave generator from damage.

Careful tuning of the antenna height results in a maximum in the electric field a few millimeters above the top of the torch, and this is where the plasma is generated in the argon working gas [13], which flows through the outer copper tube. With correct lengths L_A and L_S (approximately 25 mm and 75 mm, respectively) and with plasma being generated, microwave leakage from the torch is very low. As a precaution, the torch is enclosed in a copper and aluminum Faraday cage to contain any stray microwave radiation; the cage also helps to keep air currents and ambient light out of the system. The plasma is ignited by touching the tip of the copper tube with a screwdriver or other metal object while the working gas is flowing, and microwave power in excess of 50 W is being applied. This provides a sufficient electron density in the maximum electric field region to stimulate the breakdown in the argon carrier gas. The plasma will stay ignited until the working gas supply is cut off or until the

microwave power is reduced below 50 W, as long as a large percentage of gas in the plasma volume is easily ionizable (i.e. argon or helium).

The plasma is supported in a candle-shaped “flame” due to the argon gas flow, as seen in Figure 4.2.

Figure 4.2. Argon MPT plasma with no nitrogen sheath flow. The candle shaped flame is caused by the flow of argon from the 1/4" tube. When a sheath flow is added, the plasma loses much of the tail flame and becomes thinner and more transparent.

Because of the relative positions of the concentric tubes in the torch, the plasma has a central channel containing no plasma gas. In other words, the plasma density is at a minimum around the rotational axis of symmetry of the plasma. Introducing an analyte through this central channel causes very little perturbation of the plasma [22] compared to that experienced by a plasma lacking this hollow structure (e.g. a low-pressure cavity plasma or an inductively coupled plasma), especially in the case of aqueous aerosols [23]. Traditional plasma sources, especially those held at low pressures, are easily extinguished

by the introduction of aqueous or solvent-rich aerosols. The MPT represents a significant step forward in this regard. Particles are delivered directly through the hollow core and into the hottest part of the plasma, and are excited by the plasma as the flow spreads out after leaving the 1/8" tube. This aerosol delivery process also ensures more complete ionization and excitation of the sample as compared to other atomic emission excitation sources.

4.2.2 Particle Size Separation and Counting

During characterization of the MPT as a particle sizing instrument, particle sizes and concentrations are measured using a scanning mobility particle sizer (SMPS). The SMPS has two stages: one element for separating aerosol particles according to their diameters, and a second element for counting the particles. The particle sizing system separates particles by size based on their mobility in zero-air in an electric field, and is known as a Differential Mobility Analyzer (DMA, TSI model 3081). The DMA is used to select a monodisperse component from a polydisperse aerosol.

Structurally, the DMA consists of a hollow tube containing a charged rod inside. A sheath gas flows from top to bottom in this tube, and the polydisperse, singly charged aerosol particles are injected from the top. An opening at the bottom of the rod allows particles of the desired size to escape the hollow tube and be directed to the outlet of the DMA. When a potential is applied to the central rod, only certain sizes of particles will be able to flow through the opening and into the output flow. Larger particles will not be affected enough by the

potential, and will be carried by the sheath gas to the bottom of the hollow tube. Smaller particles will be affected strongly by the potential, and will be pulled into the charged rod. In this way, a monodisperse flow of aerosols is sent to the output of the DMA.

The resulting flow, flowing at a rate of about 300 standard cubic centimeters per minute (sccm), is sent to the next stage of the SMPS, which is the condensation particle counter (CPC, TSI model 3025A). The CPC counts particles by passing the aerosol through a supersaturated butanol vapor. The butanol condenses on the particles until they are large enough to scatter laser light, and the amount of light scattered is proportional to the number of particles present. The CPC by itself cannot give information on how many particles of a given size are present in a system. Only by knowing what potential was applied to the DMA when a given aerosol particle count was recorded can the instrument to create a graph of number concentration versus particle size.

Alternatively, the CPC can be bypassed and the monodisperse flow of particles can be sent directly to the torch plasma. In this way, emission from particles passing through the plasma can be correlated with the size of particles that produced the emission. A complete diagram of the experimental setup is shown in Figure 4.3.

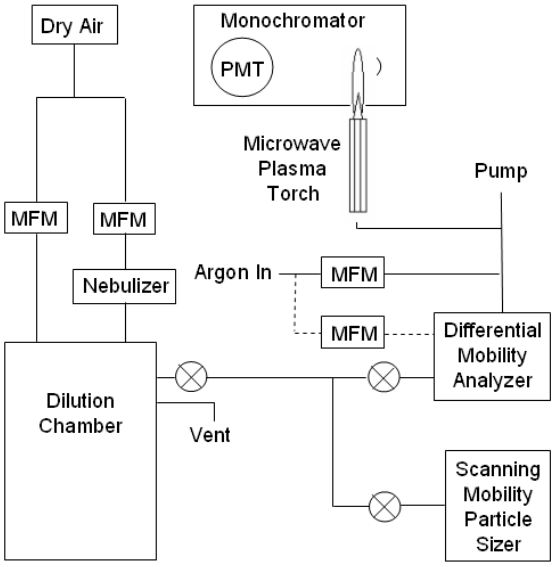

Figure 4.3. The experimental setup. MFM = mass flow meter, PMT = photomultiplier tube. The scanning mobility particle sizer and differential mobility analyzer can not be used at the same time. Not shown: computer and data acquisition card for collection and analysis of the PMT signal.

4.2.3 Signal Detection and Data Acquisition

Atomic emission was chosen as the detection method for the different elements in the aerosol particles under study and for detecting the presence of particles in the plasma. Every atom, when appropriately excited, emits light at a wavelength or set of wavelengths that are characteristic of that element. This makes it possible to determine with certainty which elements exist in the aerosol particles that pass through the MPT plasma. Atomic emission spectroscopy of aerosols using a flame as the excitation source has been practiced for some time, and it has been shown that single large aerosol particles containing sodium can be detected, and their size determined, after excitation by a flame source [16,17].

The plasma flame in our studies was imaged by a single lens onto the entrance slit of a home-built monochromator. The monochromator was operated in two different modes: either it was scanned over a range of wavelengths to produce a full spectrum, or it was set to a single wavelength (589 nm for sodium) to detect the characteristic emission of the element under study for single particle applications. Emission was monitored by a photomultiplier tube (PMT, Electron Tubes 9558B), and the signal was sent to an analog-to-digital converter (National Instruments PCI-6125) and read by a computer program.

The homebuilt LabView computer program could be operated in two data acquisition modes and was also used to control the monochromator. In the spectrum mode, the monochromator grating was scanned through the selected wavelength range and signal was collected continuously at some constant interval. In the single particle mode, the monochromator grating was set to a single position and the signal was collected in 20 microsecond time windows. Each time interval was processed internally to determine if it contained a signal peak, defined as a certain number of consecutive points with intensity above a pre-determined threshold. Single particle signals were analyzed using a separate *Mathematica* program, which was able to count and integrate the peaks collected by the LabView program, and also to calculate statistics pertaining to the collected set of peaks.

4.3 Experimental Methods

4.3.1 Particle Generation and Size Selection

The aerosol particles in this study were produced from aqueous NaCl solution using an ultrasonic nebulizer (Meinhard TR-30-A3). Dry air from an FTIR purge gas generator (Parker 75-52), flowing at 1 standard liter per minute (SLM), was used as the carrier gas. The particle distribution produced by the nebulizer (Figure 4.4) depends only slightly on the flow through the nebulizer.

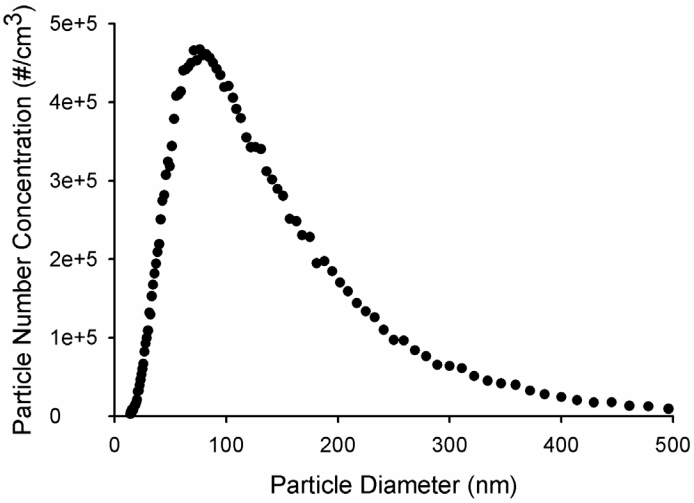

Figure 4.4. A typical number distribution of particles produced by the ultrasonic nebulizer.

In order to observe the emissions from single particles, it is necessary that as few particles as possible are in the plasma at any given time and that they consist of mostly sodium chloride (i.e. they should contain little water). The 120 L dilution and drying chamber in Figure 4.3 was built for this purpose. The

chamber is constructed of polycarbonate; losses to the walls of the chamber caused by the lack of electrical conductivity were not considered to be a problem because a low number concentration of particles was desired. The aerosol from the nebulizer is sent to this chamber and mixed with dry air at various flow rates. Once the aerosol in the chamber is sufficiently dilute, the tank valve is opened and the aerosol particles are allowed to flow to the Differential Mobility Analyzer (DMA), the Scanning Mobility Particle Sizer (SMPS), or directly to the torch, depending on the nature of the experiment. A continuous flow of aerosol into the chamber is maintained during the experiment to ensure a constant particle number density and relative humidity in the chamber.

It was noted experimentally that the torch plasma was perturbed less by a flow of argon in the central channel than by a flow of air. To take advantage of this behavior, in some cases the aerosol was mixed with a flow of argon before being sent to the 1/8" torch tube. In these cases, the aerosol flow was sent through a Swagelok T-joint, in which the mixing with argon took place. The resulting flow contained particles suspended in a combination of argon and dry air; this mixture was observed to perturb the plasma less than when dry air only was used. Nonetheless, dry air alone was still used in some cases with the goal of making the MPT apparatus as simple as possible.

4.3.2 Spectroscopic Analysis

The MPT was set up in a vertical orientation and the flame was imaged by a single lens onto the entrance slit of the monochromator. In an attempt to

improve the stability of the plasma and minimize intrusion of ambient air, a nitrogen sheath flow was added through slits in the sides of the torch body. The effect of these additions on plasma temperature and optical density was investigated.

Plasma parameters such as temperature and background spectra were studied with the torch in several configurations, but the vertical orientation was found to be optimal and will be the only orientation discussed. A spectrum of the plasma over the wavelength range of interest is reproduced in Figure 4.5.

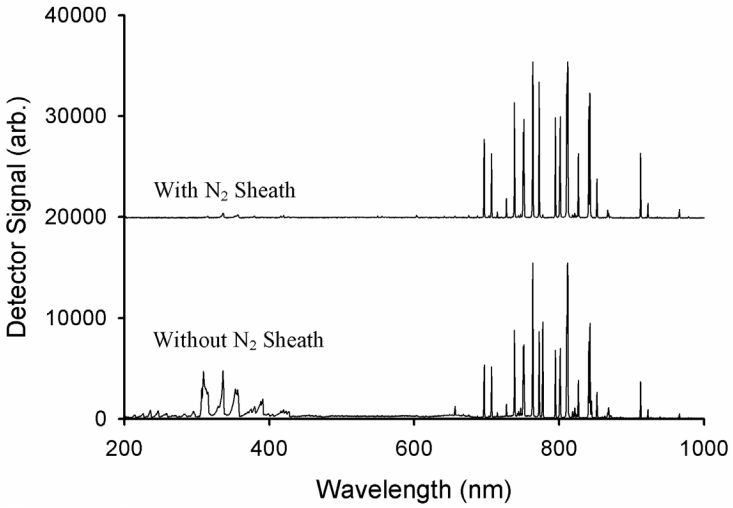

Figure 4.5. Spectrum of the argon plasma with and without nitrogen sheath gas. The sheath gas eliminates emission from species in ambient air (e.g. OH emission near 300 nm), leaving only the plasma spectrum.

Plasma temperature was determined from this spectrum using the Boltzmann plot method. This method is based on the Boltzmann equation:

$$I = g_k A_{ki} e^{-(\frac{E_k}{k_B T})} \quad (1)$$

where I is the measured relative peak intensity, g_k is the degeneracy of the upper level of the transition for the line in question, A_{kj} is the spontaneous transition probability (the Einstein A coefficient), E_k is the energy of the upper level of the transition (in cm^{-1}), k_B is the Boltzmann constant, and T is the excitation temperature in Kelvin. Values of g_k and A_{jk} for the various argon lines used in creating this plot were taken from the National Institute of Standards and Technology (NIST) online database of atomic spectra [24]. Data pertaining to the argon lines used for the Boltzmann plot are given in Table 4.1.

Wavelength (nm)	**E_k (cm^{-1})**	**g_k**	**A_{jk}**
696.54	107496.4166	3	6.39×10^6
706.72	107289.7001	5	3.80×10^6
727.29	107496.4166	3	1.83×10^6
738.39	107289.7001	5	8.47×10^6
750.38	108722.6194	1	4.45×10^7
763.51	106237.5518	5	2.45×10^7
772.42	106087.2598	3	1.17×10^7
779.86	118906.6110	5	8.70×10^4
794.81	107131.7086	3	1.84×10^7
801.50	105617.2700	5	9.28×10^6
811.91	105462.7596	7	3.31×10^7

Table 4.1. Values used for plasma temperature determination by the Boltzmann plot method. E_k is the energy of the upper state of the transition, g_k is the degeneracy of the upper level of the transition, and A_{jk} is the spontaneous transition probability (the Einstein-A coefficient). Data were taken from the NIST online atomic spectra database [24].

4.3.3 Post-Plasma Particle Analysis

For the majority of tests, the aerosol flow was allowed to flow to the walls of the Faraday cage after passing through the plasma. In some cases, however, the particles exiting the plasma were collected in order to investigate the effect of the plasma on the particles. When particle collection was necessary, a large Pyrex funnel was positioned six inches above the plasma tail and connected by conductive tubing to the inlet of the SMPS. In this case, size selection of particles was not possible since only one SMPS system was available, and so only changes to the overall size distribution and number concentration could be observed in this manner. The effect of the plasma on individual sizes of particles was therefore not considered.

4.4 Results and Discussion

4.4.1 Plasma parameters

The effects of several parameters on the plasma temperature were investigated. The first was the effect of applied microwave power. Figure 4.6 shows that there was no strong dependence of temperature on applied power for applied powers in the range of 80 to 225 W.

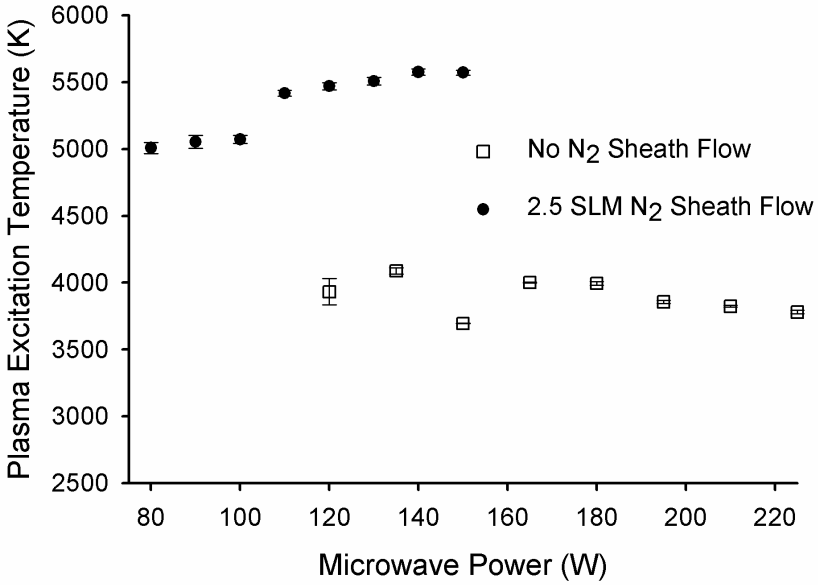

Figure 4.6. Plasma excitation temperature vs. applied microwave power with (A) and without (B) nitrogen sheath flow (2.5 SLM).

A search in the literature found that other researchers have noticed similar behavior for microwave induced plasmas in the past [25-27]. At all microwave powers, the plasma temperature was higher when a nitrogen sheath flow was used than when no sheath was present.

As opposed to the microwave power, the argon flow rate had a strong influence on the temperature. Figure 4.7 shows the relationship of the argon flow to the plasma's excitation temperature with argon flows ranging from 300 sccm to 1 SLM. The temperature increases at higher flows. Replacing air with an outside sheath flow of nitrogen further increases the temperature.

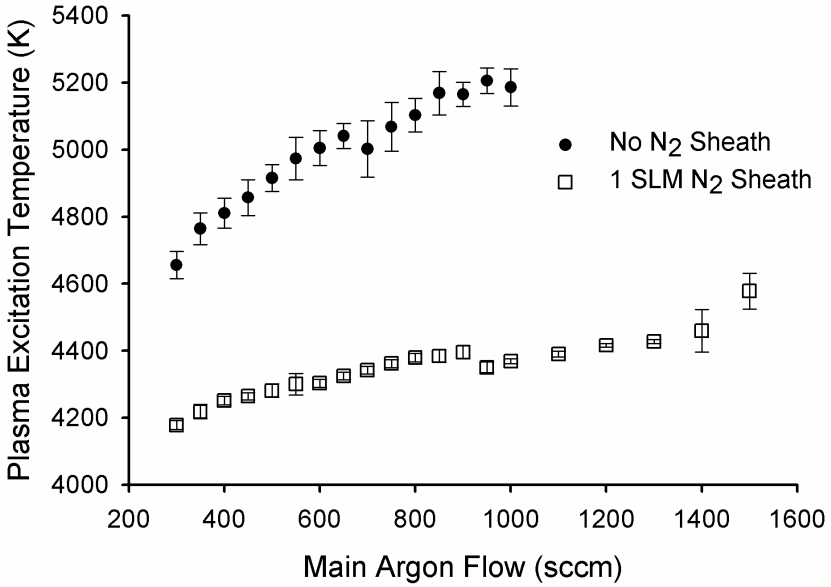

Figure 4.7. Influence of main Argon flow (from the 1/4" tube) on the plasma's excitation temperature. The effect of the sheath flow on the plasma's temperature is also demonstrated.

The flow through the central (aerosol inlet) tube also had a visible effect on the plasma temperature. When a moderate (100 sccm) flow of argon was sent through the central tube in the torch in an absence of aerosol particles, the plasma excitation temperature decreased by a small amount (between 100 and 400 K, depending on argon flowrate), as seen in Figure 4.8. This behavior was most likely due to the spatial instability of the plasma. The increased sizes of the error bars in Figure 4.8 provide support for this hypothesis; a more turbulent plasma gives larger error bars when temperature measurements are taken, since the plasma moves from side to side unpredictably and different areas are imaged by the detector as a consequence. A visual inspection of the plasma at the time also lent support to this theory, as the plasma was observed moving from side to side while the 1/8” tube contained an argon flow. When the argon flow rate was

decreased below 50 sccm the plasma became more stable and the emission was steadier.

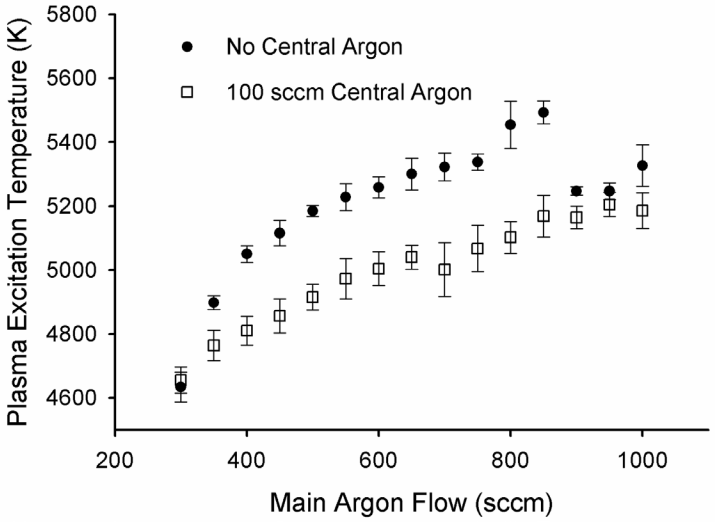

Figure 4.8. Effect of argon added to the central (1/8") tube on the plasma's temperature and stability. The larger error bars on the data set corresponding to the central argon flow (open circles) are indicators of the plasma's spatial instability. Error bars represent one σ.

Though a supplemental flow of argon though the innermost tube led to a decrease in the excitation temperature, the excitation temperature was lowered to a greater extent (up to 1000 K for certain argon flowrates) by a similar flow of dry air, even when no particles were present. This is due not only to turbulence (as seen with the supplemental argon flow), but also to the higher ionization potential of dry air compared to argon. Indeed, the volume of the plasma decreased when dry air was present as confirmed by visual observation. Thus, there is an advantage to carrying aerosol particles through the torch in a combined flow of argon and dry air instead of only air.

A visual observation of the plasma flame in a flow of pure argon led to the conclusion that the plasma was optically dense. This observation was experimentally confirmed by passing various wavelengths of visible radiation through the plasma. The plasma was found to absorb between 30 and 80% of incident radiation, depending on the wavelength. This was deemed unacceptable for our purposes, since it was likely that particles excited in the center of the plasma may not produce an emission signal strong enough to penetrate the plasma and be observed by the detector. We decided to add a nitrogen sheath flow to the plasma, working on the theory that the optical density was caused not by argon, but by other species from the surrounding air being caught up in the argon flow and incorporated into the plasma. The addition of a 1 SLM nitrogen sheath flow reduced (but did not eliminate) the plasma's optical density in the visible region and also had the desirable effect of increasing the plasma's excitation temperature. This effect can be seen in Figure 4.6 (for different microwave powers) and Figures 4.7 and 4.8 (for different flows of argon through the torch at a single microwave power).

4.4.2 Atomic Emission Spectra of Metals

As a preliminary test of the ability of the torch to excite metal atoms, a 0.1 M sodium chloride solution was aerosolized and sent into the plasma. Minimal dilution of the aerosol was employed; the aerosol particle flow was diluted in a 1-liter flask and mixed with 100 sccm of argon before being sent to the torch. The resulting atomic emission spectrum is seen in Figure 4.9.

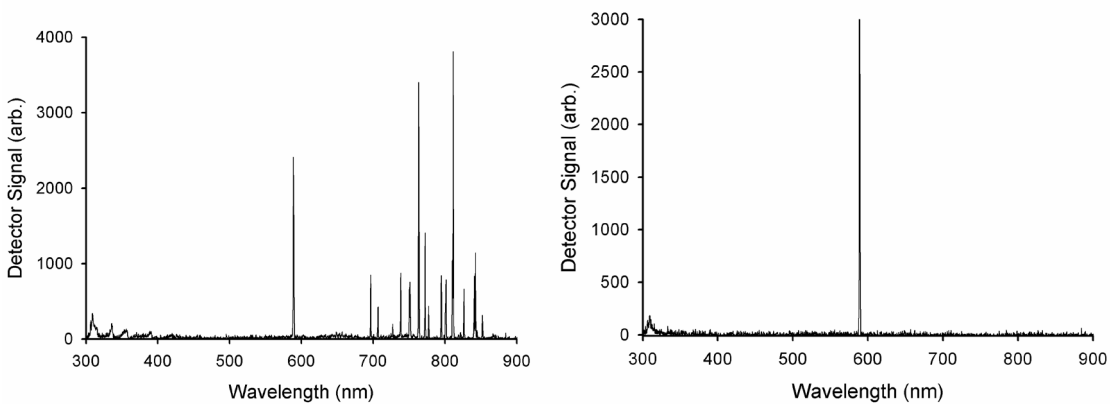

Figure 4.9. Left panel: the spectrum of an argon plasma into which a 0.1 M NaCl solution has been nebulized. The peak at 589 nm is due to sodium emission. Peaks at lower wavelength re-appear due to the air in the aerosol flow. Right panel: the same plasma imaged at a higher position in the plasma; the plasma background is no longer visible.

The spectrum in the left panel of Figure 4.9 was taken at the height in the plasma at which temperature measurements were taken. It is shown for illustrative purposes, to demonstrate that the emission from the plasma does not overlap with the emission lines of sodium. When an area of the plasma 2 mm above this region is imaged, the plasma features can no longer be seen, and only the emission from the sodium atoms is visible, as seen in the right panel of Figure 4.9. This was the height that was monitored during single particle studies.

For the MPT to be useful as an atmospheric sampling device for single particles, it will be important that it be able to simultaneously observe multiple elements in a single particle. The chemical composition of a given aerosol particle is dependent on its source and its size [30], and being able to monitor each element simultaneously will be important in source appropriation. This would require a multi-wavelength detector such as a CCD array, but such

detectors were not available for this instrument. As an initial step, monitoring of a solution with several elements present was attempted using a high concentration of aerosol particles so that continuous emission could be monitored. A preliminary spectrum of this type is shown in Figure 4.10, for the example of a solution containing 0.02 M calcium, sodium, potassium and magnesium.

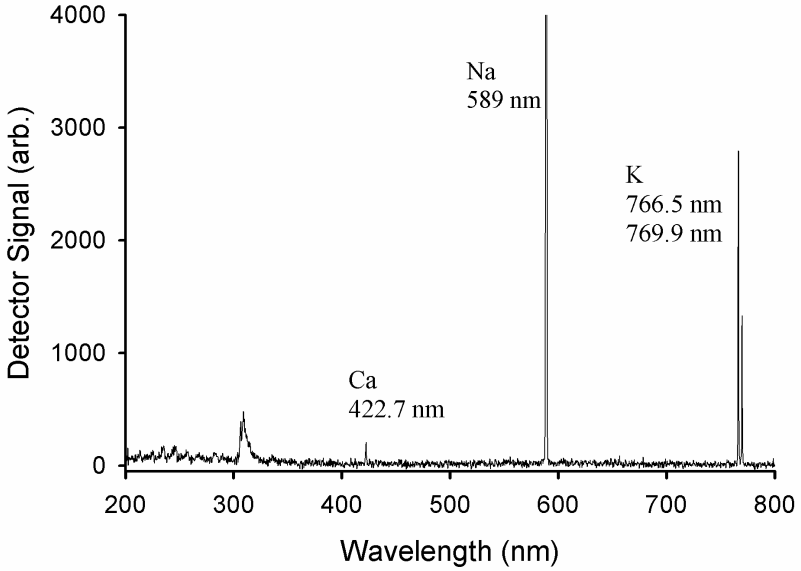

Figure 4.10. Spectrum of emission from aerosols of a solution of 0.02 M Na, Mg, Ca and K. Emission wavelengths and their corresponding elements are given in Table 2. Magnesium emission was not observed because it is hidden under a peak of OH emission from ambient water.

The peaks from calcium emission (at 422.7 nm), potassium emission (766.5 and 769.9 nm), and sodium emission (588.9 and 589.5 nm) are all visible and distinguishable from the background; magnesium emission (309.3 nm) was not definitively observed due to the presence of OH emission around the same wavelength. It is clear from Figure 4.10 that sodium and potassium are more readily excited by the plasma than are magnesium and calcium.

Element	Emission Wavelength (nm)	Upper level energy (cm^{-1})
Mg	309.3	54192.33
Ca	422.7	23652.33
Na	588.9	16973.37
Na	589.5	16956.17
K	766.5	13042.88
K	769.9	12985.17

Table 4.2. Upper transition level energies for the emission lines observed in Figure 4.10.

Table 4.2 shows why this is the case: the upper energy levels of the elements with large peaks (sodium and potassium) are far lower than those of the elements whose signals are small. If the excitation temperature of the torch could be increased, the peaks for calcium and magnesium would increase in magnitude and the signal-to-noise ratios would increase. Research in this area was unsuccessful, however.

4.4.3 Detection of Emission from Single Particles

When a sufficiently low concentration of particles (usually monodisperse) was sent from the DMA to the torch plasma, emission from individual particles could be observed. This type of signal was detected as a sudden spike in the signal at a given wavelength. Multiple particle sizes were selected using the DMA and each size was sent to the torch plasma individually. An example of the signal from a single 350 nm sodium chloride particle passing through the plasma is shown in Figure 4.11.

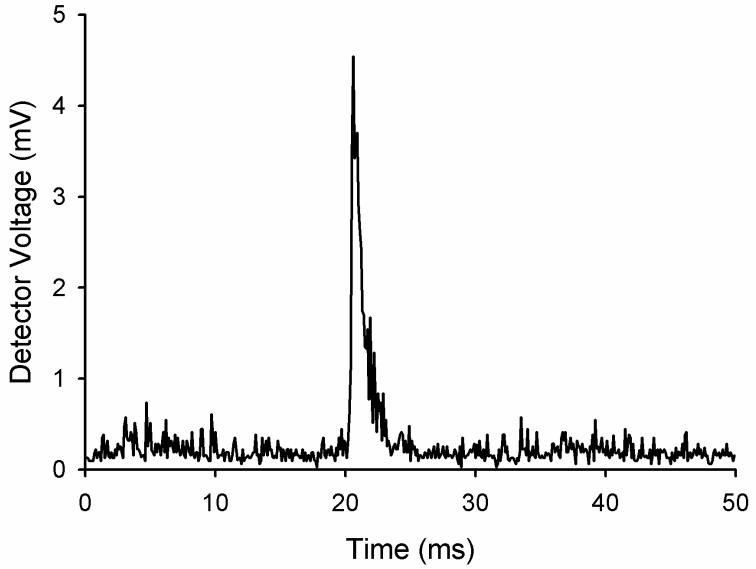

Figure 4.11. Emission peak from a single, 350 nm sodium chloride particle.

The signals from each particle size were saved and analyzed, and the average signal was plotted versus the corresponding particle diameter or versus the mass of sodium in the particle.

The lack of a well-defined correlation between particle diameter and signal intensity is surprising. As the diameter of the particles increases, the intensity of the average signal is predicted to increase as well, since more sodium is present in a larger particle. In theory, the dependence should be proportional to the cube of the particle's diameter, since the number of atoms of the metal in the particle increases with the cube of the radius. A similar trend is predicted when the mass of sodium in the particles is plotted against the average signal intensity, but with a linear dependence.

In fact, the signal did increase with particle size, but not with the expected dependences on either particle diameter or mass of sodium in the particle. The

mass of sodium present in a given particle was calculated based on the assumption of spherical, dry particles. This assumption is valid because the relative humidity (RH) in the drying chamber is typically about 40%. In a study on the efflorescence and deliquescence points of nanoscale sodium chloride aerosols, Biskos et. al. [29] found that for particles larger than 40 nm in diameter, the efflorescence point was 45% RH. This means that at a relative humidity below 45%, the particles in our chamber will have lost the water on their surfaces as long as they have diameters larger than 40 nm. Since particles smaller than 100 nm in diameter were not studied in our experiments, we are confident that all particles leaving our DMA and passing on to the torch were dry.

The instrument response to increasing particle concentration was also investigated. The concentration of dry sodium chloride particles in the dilution chamber was increased over a range from < 100 particles/cm^3 (filtered air) to 2500 particles/cm^3 and the number of peaks detected per minute was monitored for ten minute time periods. A dry air flow of 10 sccm was used to carry the particles through the plasma. Figure 4.12 shows the instrument response to changing particle concentration. Increasing the concentration resulted in an increase in the number of signals observed; however, there was far from a 1:1 relationship between particles in the plasma and observed peaks.

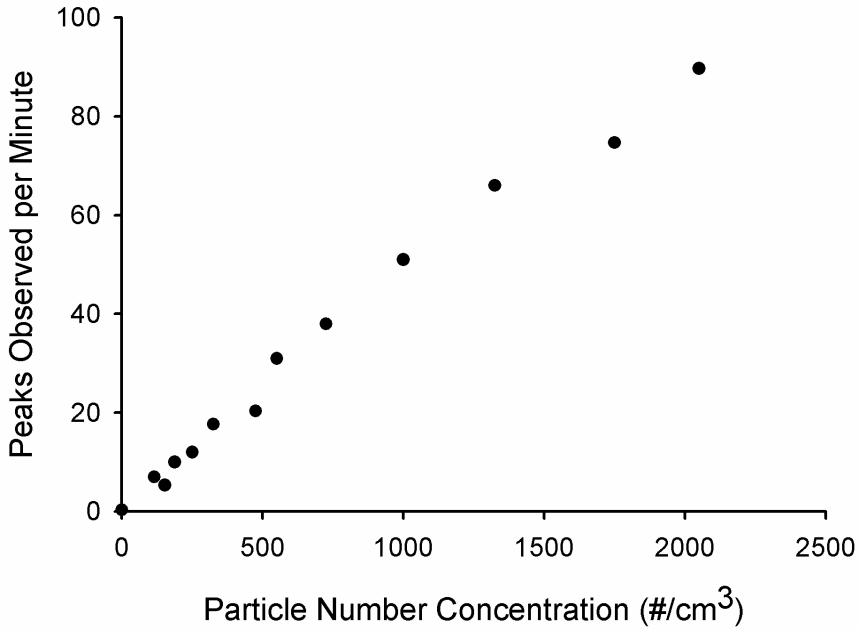

Figure 4.12. The dependence of peaks counted per unit time on the total particle concentration of the air being sent into the plasma. All sizes of particles (from a distribution like that shown in Figure 4.4) were sent into the torch.

Because 10 cm^3 of particle filled air passed through the plasma every minute and the plasma has an approximate volume of 1 cm^3, the total number of particles that pass through the plasma in one minute should be ten times the number concentration (in $\#/cm^3$) in the dilution chamber. Clearly, then, only a small fraction (4.4 %, based on a linear least-squares fit of the data) of the particles that pass through the plasma are actually detected.

The reason for such poor detection efficiency is unclear, but the fact that all particles are destroyed by the plasma (see below) suggests that the plasma is hot enough to vaporize aerosol particles but not hot enough to electronically excite all the atoms from those particles. Another (more likely) possibility is that

the sheath flow did not reduce the optical density of the plasma enough, and particles that are excited too close to the center of the plasma (or on the opposite side of the plasma from the detector) are not being detected. We observed that as the size of the particles passing through the plasma increases, the intensity of the single particle signals collected by the computer program also increases. However, we have so far not observed the previously discussed relationships between the various parameters (the linear dependence of signal on sodium mass and the cubic dependence of signal on particle diameter). Furthermore, the efficiency with which single particle bursts are detected appears to plummet when the particle size decreases, indicating an unresolved issue with optical density or some other plasma parameter.

4.4.4 Characteristics of Particles Collected After the Torch

In order to investigate the effect that the torch plasma had on particles passing through it, the particle flow exiting the torch was collected and sent to the SMPS. The resulting particle size distribution, along with the distribution that had been sent into the torch, is shown in Figure 4.13. The particle size distribution is completely altered by the plasma, since the larger particles are all destroyed. As the components of the particles cool down while leaving the plasma, they re-form into a fairly monodisperse set of smaller particles. An alternative explanation is that each particle is reduced to a certain characteristic size by the plasma, but that the cycle of destruction and condensation does not actually occur. However,

the total number of particles collected before and after the plasma is not the same, as would be expected if the particles were simply reduced in size.

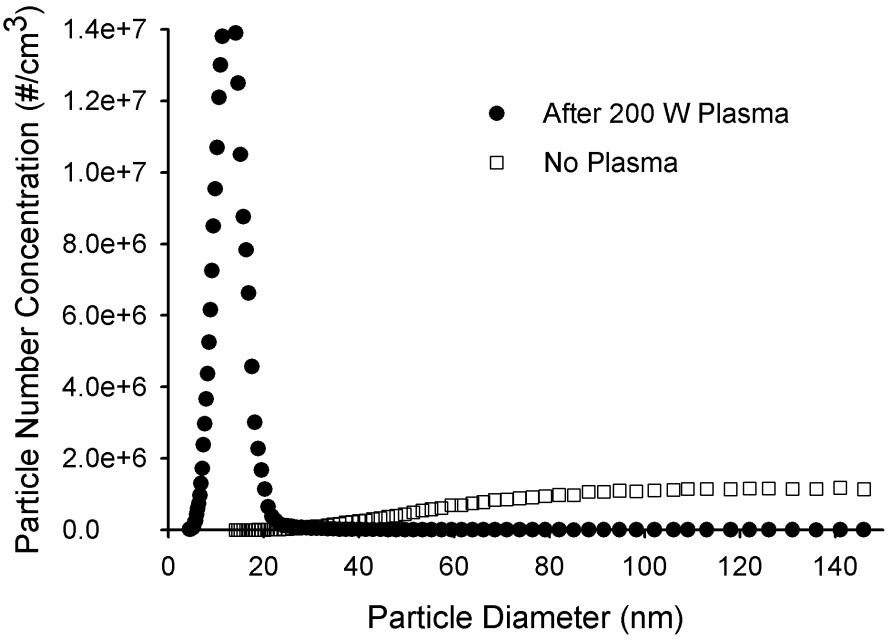

Figure 4.13. Particle size distribution measured at the top of the torch with (squares) and without (circles) the plasma ignited. Total particle count increased by an order of magnitude when the torch plasma was present.

Before the torch, the total concentration of particles (of all sizes) was on the order of 10^4 per cubic centimeter. This concentration increased by nearly an order of magnitude once the particles had been sent through the plasma and to the SMPS. This gives strong support to the theory of destruction of the original (larger) particles followed by re-formation of many smaller particles. Figure 4.13 raises the intriguing possibility that our atmospheric pressure MPT might find use in the production of nanostructures of various materials. Some preliminary work has been done in this area, notably with the synthesis of carbon nanotubes [30],

aluminum nanoparticles [31], and magnesium oxide nanopowder [32]. The latter work involved synthesizing the magnesium oxide via a reaction in the plasma itself, by introducing magnesium atoms into an oxygen plasma. The resulting nanoparticles were found to be monodisperse and of fairly regular size. This has interesting implications for materials chemistry, and may be an additional area into which our research could expand.

4.5 Conclusions

Our research has explored the possibility of using an atmospheric pressure plasma for sensitive, selective detection of single atmospheric particles. A microwave plasma torch was constructed, and various experimental parameters were optimized. Initially the optical density of the plasma was a problem, and this obstacle was only partially overcome by the addition of a nitrogen sheath flow to the torch. This sheath flow isolated the plasma to some extent from interfering species in the air around the torch, and also improved the stability of the plasma by confining it to a narrow space in the center of the instrument. Still, the optical density of the plasma meant that only sodium atoms that emitted light on the outside of the plasma on the same side as the detector had a chance of being observed.

Particles were sent to the torch, either in a flow of dry air or mixed with a small amount of argon. In some cases the entire population of particles produced by the nebulizer was sent to the plasma; other times, particles were

dried in a dilution chamber and size selected using a differential mobility analyzer. Emission from these particles was detected by a monochromator and photomultiplier, signals were saved and analyzed using custom computer programs, and the emission from single particles passing through the plasma was observed. By grouping these emission signals with the size of particle that produced them, a trend was shown of increasing emission intensity with increasing particle size. In addition, the number of observed peaks was seen to increase linearly with increasing number of particles in the plasma, although the absolute detection efficiency was less than 5%. The fact that the detection efficiency was so low strongly implies that an atmospheric pressure microwave plasma, at least as created by a MPT of the above discussed design, is not suitable for real-time detection of atmospheric aerosol particles because of the problems with the optical density of the plasma. However, the studies on the effect of the plasma on the size and population of particles imply that this torch design might find some usefulness in materials science, specifically the generation of nanostructures from a variety of starting materials

.

4.6 References

1. McClellan, R.O., *Health effects of exposure to diesel exhaust particles.* Annu. Rev. Pharmacol. Toxicol., 1987. **27**: p. 279-300.
2. Rosenkranz, H.S., *Mutagenic nitroarenes, diesel emissions, particulate-induced mutations and cancer: an essay on cancer-causation by a moving target.* Mutat. Res., 1996. **367**(2): p. 65-72.
3. Gauderman, W.J., et al., *Association between air pollution and lung function growth in southern California children: results from a second cohort.* Am. J. Respir. Crit. Care Med., 2000. **166**(1): p. 76-84.
4. Pope, C.A., III, et al., *Lung cancer, cardiopulmonary mortality, and long-term exposure to fine particulate air pollution.* J. Amer. Med. Assoc., 2002. **287**(9): p. 1132-1141.
5. Euler, G.L., D.E. Abbey, A.R. Magie, J.E. Hodgkin, *Chronic obstructive pulmonary disease symptom effects of long-term cumulative exposure to ambient levels of total suspended particulates and sulfure dioxide in California Seventh-Day Adventist residents.* Archives of Environmental Health, 1987. **42**(4): p. 213-222.
6. Dockery, D.W., C.A. Pope, X. Xu, J.D. Spengler, J.H. Ware, M.E. Fay, B.G. Ferris, F.E. Speizer, *An Association between Air Pollution and Mortality in Six US Cities.* The New England Journal of Medicine, 1993. **329**: p. 1753-1759.
7. Pope, C.I., *Review: Epidemiological Basis for Particulate Air Pollution Health Standards.* Aerosol Science and Technology, 2000. **32**(1): p. 4-14.
8. Dye, J.A., et al., *Acute pulmonary toxicity of particulate matter filter extracts in rats: coherence with epidemiologic studies in Utah Valley residents.* Environmental Health Perspectives Supplements, 2001. **109**(3): p. 395-403.
9. Noble, C.A. and K.A. Prather, *Real-time single particle mass spectrometry: A historical review of a quarter century of the chemical analysis of aerosols.* Mass Spectrometry Reviews, 2000. **19**(4): p. 248-274.
10. Sipin, M.F., S.A. Guazzotti, and K.A. Prather, *Recent Advances and Some Remaining Challenges in Analytical Chemistry of the Atmosphere.* Analytical Chemistry, 2003. **75**(12): p. 2929-2940.
11. Middlebrook, A.M., et al., *A comparison of particle mass spectrometers during the 1999 Atlanta Supersite Project.* Journal of Geophysical Research, 2003. **108**(D7): p. SOS 12/1-SOS 12/13.
12. Tendero, C., C. Tixier, P. Tristant, J. Desmaison, P. Leprince, *Atmospheric pressure plasmas: A review.* Spectrochimica Acta Part B, 2006. **61**: p. 2-30.
13. Yang, W., et al., *Microwave plasma torch analytical atomic spectrometry.* Microchemical Journal, 2000. **66**: p. 147-170.
14. Huang, M., H. Kojima, T. Shirasaki, A. Hirabayashi, H. Koizumi, *Study on solvent-loading effect on inductively coupled plasma and microwave-induced plasma sources with a microliter nebulizer.* Analytica Chimica Acta, 2000. **413**: p. 217-222.
15. Jin, Q., et al., *A microwave plasma torch assembly for atomic emission spectrometry.* Spectrochimica Acta, Part B: Atomic Spectroscopy, 1991. **46B**(3): p. 417-30.
16. Clark, C.D., et. al., *Real-time measurement of sodium in single aerosol particles by flame emission: laboratory characterization.* Journal of Aerosol Science, 2001. **32**(1): p. 765-778.
17. Campuzano-Jost, P., C.D. Clark, H. Maring, D.S. Covert, S. Howell, V. Kapustin, K.A. Clarke, E.S. Saltzman, A.J. Hynes, *Near-Real-Time Measurement of Sea-Salt Aerosol during the SEAS Campaign: Comparison of Emission-Based Sodium Detection with an Aerosol Volatility Technique.* Journal of Atmospheric and Oceanic Technology, 2003. **20**: p. 1421-1430.

18. Heltai, G., T. Jozsa, K. Percsich, I. Fekete, Z. Tarr, *Application of MIP-AES as element specific detector for speciation analysis.* Fresenius Journal of Analytical Chemistry, 1999. **363**: p. 487-490.
19. Selby, M., G.M. Heiftje, *Taming the surfatron.* Spectrochimica Acta Part B, 1987. **42**: p. 285-298.
20. Duan, Y., Y. Su, and Z. Jin, *A Field-Portable Plasma Source Monitor for Real-Time Air Particulate Monitoring.* Analytical Chemistry, 2000. **72**(7): p. 1672-1679.
21. Stonies, R., S. Schermer, E. Voges, J.A.C. Broekaert, *A new small microwave plasma torch.* Plasma Sources Science and Technology, 2004. **13**: p. 604-611.
22. Bilgic, A.M., et al., *Design and modeling of a modified 2.45 GHz coaxial plasma torch for atomic spectrometry.* Spectrochimica Acta, 1998. **53B**(5): p. 773-777.
23. Timmermans, E.A.H. and J.J.A.M. Van der Mullen, *Microwave induced plasma torches for on-line combustion gas analysis.* Spectroscopy Europe, 2003. **15**(5): p. 14,16,18,20-21.
24. *NIST Atomic Spectra Database*. 2005, National Institute of Standards and Technology.
25. Uhm, H.S., Y.C. Hong, D.H. Shin, *A microwave plasma torch and its applications.* Plasma Sources Science and Technology, 2006. **15**: p. 26-34.
26. Chaker, M., M. Moisan, Z. Zakrzewski, *Microwave and RF Surface Wave Sustained Discharges as Plasma Sources for Plasma Chemistry and Plasma Processing.* Plasma Chemistry and Plasma Processing, 1986. **6**(1): p. 79-96.
27. Schermer, S., N.H. Bings, A.M. Bilgic, R. Stonies, E. Voges, J.A.C. Broekaert, *An improved microstrip plasma for optical emission spectrometry of gaseous species.* Spectrochimica Acta Part B, 2003. **58**: p. 1585-1596.
28. Finlayson-Pitts, B.J., J.N. Pitts Jr., *Chemistry of the Upper and Lower Atmosphere*. 1 ed. 2000, San Diego: Academic Press. 380.
29. Biskos, G., A. Malinowski, L. Russell, P. Buseck, S. Martin, *Nanosize Effect on the Deliquescence and the Efflorescence of Sodium Chloride Particles.* Aerosol Science and Technology, 2006. **40**(2): p. 97-106.
30. Hong, Y.C., H.S. Uhm, *Production of carbon nanotubes by microwave plasma torch at atmospheric pressure.* Physics of Plasmas, 2005. **12**.
31. Weigle, J.C., C.C. Luhrs, C.K. Chen, W.L. Perry, J.T. Mang, M.B. Nemer, G.P. Lopez, J. Phillips, *Generation of Aluminum Nanoparticles Using an Atmospheric Pressure Plasma Torch.* J. Phys. Chem. B, 2004. **108**: p. 18601-18607.
32. Hong, Y.C., H.S. Uhm, *Synthesis of MgO nanopowder in atmospheric microwave plasma torch.* Chemical Physics Letters, 2006. **422**: p. 174-178.

Chapter 5

Summary and Future Directions

5.1 Summary of Results

The behavior of monoterpene SOA with respect to tropospheric radiation is an important field of study because of the potential impacts on the energy balance of the Earth's atmosphere. Currently, a net negative radiative forcing is assigned to aerosol particles [1], meaning that they redirect more radiation out of the troposphere than they keep in. More specifically and more applicably to the results discussed in Chapter 3, this means that their extinction coefficient with respect to scattering and reflection of radiation is thought to be large compared to their extinction coefficient with respect to absorption.

One important problem with this is the lack of understanding of the absorption profiles of real atmospheric aerosol particles [1]. Most models assume that the only aerosol absorbers of radiation are those particles that contain black carbon; all other particles are treated as scatterers. In Chapter 3 of this thesis, I have described a method of measuring the absorption spectra of ensembles of aerosol particles, the results of which cast doubt on this assumption. This procedure allows us to measure spectra of the particles directly, without worrying about solvent effects. The results of using this

technique, presented in Section 3.2, show that SOA formed from the ozonolysis of monoterpenes have absorption profiles that overlap significantly with the tropospheric actinic window (radiation with λ > 295 nm). We have calculated the lifetime of these SOA with respect to photolysis, and found that it is often an order of magnitude shorter than the most important competing aging process, attack by OH.

The lifetime of the particles with respect to photolysis depends on the kind of reactions that absorbed radiation will be able to initiate. In Chapter 2 we investigated this question by detecting the gas phase products of SOA photolysis in order to draw conclusions about the mechanisms of monoterpene SOA photolysis.

5.1.1 Chapter 2 – Gas Phase Photolysis Products from Monoterpene SOA

The experiments presented in Chapter 2 deal with the observation of the gas phase products of SOA photolysis. Particles formed during the ozonolysis of limonene were collected on a filter and photolyzed inside an infrared cavity ring down spectrometer. This high-resolution spectroscopic technique was used to monitor the production of gaseous carbon monoxide from the samples as they were exposed to UV radiation at a variety of wavelengths. While IR-CRDS is a sensitive technique, it has the limitation of only being able to detect molecules with one to two carbon atoms. To monitor the rest of the gas phase products of photolysis, we collaborated with the Rowland-Blake group, who specialize in trace gas detection in atmospheric samples. Photolysis products were

cryogenically trapped and analyzed in a gas chromatography system to give us a more complete picture of the product distribution from the photochemical reactions.

Based on this distribution and on the known composition of monoterpene SOA, we proposed that the Norrish type I and II photolysis of carbonyl-containing molecules is likely to be an important mechanism of photochemical aging for monoterpene aerosols in the troposphere. The aging proceeds via one of the well-defined Norrish mechanisms, whereby a carbonyl-containing molecule is photodissociated, resulting in the release of small molecules to the gas phase, and in the modification of the molecules left behind [2-6]. Ketone groups are most susceptible to this sort of photoprocessing, and larger ketones will have higher quantum yields [7]. The presence of oligomers in the SOA makes it likely that the quantum yield will be large enough to make photolysis an efficient aging mechanism for monoterpene SOA in the troposphere.

Photochemical aging of monoterpene SOA will result in a small flux of low molecular weight oxygenated species back into the gas phase, and will also lead to the modification of the particles themselves. Based on established atmospheric chemistry, it is likely that photochemically aged SOA will contain more oxygenated species and will be more highly polymerized than the 'fresh' aerosol. This result has implications for particle toxicity and for the ability of the aged particles to act as cloud condensation nuclei.

It has long been established that organic aerosol particles are aged chemically in the atmosphere, via reactions with OH radicals, ozone and other

oxidants [8-10]. We have now demonstrated significant aging in the absence of any such oxidants, initiated by only actinic UV radiation. This means that, whether via chemical or photochemical processes, particles are likely to be significantly altered even after a day in the troposphere if they contain functional groups (such as carbonyls) that are susceptible to the kind of photochemistry discussed in Chapter 2.

5.1.2 Chapter 3 – Aging of Particle Phase Components of Monoterpene SOA

In Chapter 3, I have presented results from experiments on particle aging in the absence of UV radiation. These results imply that particles can be aged by non-photochemical processes, meaning that even during times of very low solar zenith angles, particles will be modified during their time in the troposphere. The changes that we have observed in monoterpene SOA samples lead to a substantial modification of the particles' absorption profile, causing an increase in the total extinction coefficient and an increased absorption profile in the visible region of the spectrum. This has potentially profound impacts for the climate forcing of organic aerosol particles; indeed, it has already been suggested by at least one author that aerosols might have positive forcings based on a larger-than-expected absorption profile in the visible [11].

The mechanism of the changes that alter the absorption profile of monoterpene SOA in the absence of light is unknown at this time. We have speculated that acid catalyzed reactions analogous to aldol condensation reactions may be occurring, but the matter is far from settled. Mass spectrometry

experiments aimed at more fully understanding the changes taking place in the particles are ongoing.

5.1.3 Chapter 4 – Single Particle Counting with Microwave Plasma Torch Atomic Emission Spectroscopy

Chapter 4 recounts experiments that were performed on a different track from the experiments discussed in Chapters 2 and 3. An atmospheric pressure plasma source, the Microwave Plasma Torch, was constructed with the goal of sensitively detecting single metal-containing aerosol particles in ambient air. The advantage of using an atmospheric pressure plasma for particle detection is that the wavelength of emission from the torch is dependent on the chemical composition of the plasma. The microwave torch plasma is robust with respect to water loading and other interferences compared to other plasma sources (such as Inductively Coupled Plasmas), and therefore it was though that it would make a useful field instrument for particle counting applications.

A torch was constructed based on information in the literature and modified according to our needs. A detection system was set up and software was written to control signal acquisition. Initial experiments focused on detecting large numbers of particles passing through the plasma based on the continuous emission of light at a wavelength corresponding to the metal atoms of interest (for example, to detect aqueous NaCl particles, a monochromator was used to direct only 589 nm emission onto a photomultiplier tube). Samples of mixed composition were also used to establish the ability of the torch system to excite

and detect emission from multiple elements at once. The response of the torch to small concentrations (< 1000 cm^{-3}) of aqueous NaCl particles was also investigated and found to be linear.

Unfortunately, single particle detection proved beyond the limits of the system. Atmospheric pressure plasmas suffer from the limitation of optical density, due to species from the air becoming entrained in the plasma. A sheath flow of nitrogen around the outside of the plasma can mitigate, but not eliminate, this effect. The plasma's optical density means that only atoms that relax and emit light at the very outside of the plasma flame closest to the detector will be detected; emission from all other atoms will be absorbed or scattered by the plasma itself. For this reason the project was abandoned before it resulted in any publications or significant conclusions.

5.2 Future Directions

The most promising project for future research is the investigation of color change mechanisms in monoterpene SOA. As mentioned previously, much of the work presented in Chapter 3 is preliminary, and much more work is needed to fully understand the reactions playing out in the particles as they age. Mass spectrometry of particles before and after aging will be important to this research. Also, investigating the photoactivity of the aged particles with respect to the Norrish reactions will be interesting. The particles absorb much more tropospheric radiation after they age, but yet to be seen is whether this radiation is capable of initiating photochemistry in the aged particles. Initial investigations

using IR-CRDS suggested that photochemistry would not be important for the aged particles, but much more thorough investigation is warranted.

The observation of a wet appearance to the particles after aging also brings up intriguing possibilities. The cloud condensation nuclei properties of monoterpene SOA have been studied [12, 13], with the conclusions being that these particles have high CCN activity. It is possible that the aging processes that cause the color change will also alter the CCN activity of the particles, since they become visibly wet in our lab, which stays between 30 and 50% relative humidity. The wet appearance could also be due to condensation reactions occurring inside the particles.

Finally, there is more work to be done in expanding the scope of the IR-CRDS experiments. The action spectra presented in this work represent only those particles prepared at high reagent concentrations with ozone as the oxidant, in the absence of water vapor, and photolyzed under helium gas (that is, in the absence of oxygen or other atmospheric species). These experiments were useful for establishing that the particles could be aged photochemically and that the mechanism by which they age was photodegradation of carbonyl-containing molecules. However, more atmospherically-relevant conditions (especially the presence of oxygen during photolysis) will most likely change the products of photolysis and may change the extent of aging that happens. Other oxidants (such as NO_3) may produce particles that have different susceptibilities to tropospheric radiation and produce a different distribution of small molecules during photolysis.

5.3 References

1. Forster, P., et al., *Changes in Atmospheric Constituents and in Radiative Forcing.* Climate Change 2007: The Physical Science Basis. Contribution of Working Group I to the Fourth Assessment Report of the Intergovernmental Panel on Climate Change., ed. S. Solomon, et al. 2007, Cambridge, United Kingdom: Cambridge University Press.
2. Bamford, C.H. and R.G.W. Norrish, *359. Primary photochemical reactions. Part VII. Photochemical decomposition of isovaleraldehyde and di-n-propyl ketone.* J. Chem. Soc., 1935. **DOI: 10.1039/JR9350001504**: p. 1504-1511.
3. Davis, W. and W.A. Noyes, *Photochemical Studies. XXXVIII. A Further Study of the Photochemistry of Methyl n-Butyl Ketone.* J. Am. Chem. Soc., 1947. **69**(9): p. 2153-2158.
4. McMillan, G.R., J.G. Calvert, and J.N. Pitts, *Detection and Lifetime of Enol-Acetone in the Photolysis of 2-Pentanone Vapor.* J. Am. Chem. Soc., 1964. **86**(18): p. 3602-3605.
5. Rice, F.O. and E. Teller, *The Role of Free Radicals in Elementary Organic Reactions.* The Journal of Chemical Physics, 1938. **6**(8): p. 489-496.
6. Srinivasan, R., *The Photochemical Type II Process in 2-Hexanone-5,5-d2 and 2-Hexanone.* J. Am. Chem. Soc., 1959. **81**(19): p. 5061-5065.
7. Hartley, G.H. and J.E. Guillet, *Photochemistry of Ketone Polymers. II. Studies of Model Compounds.* Macromolecules, 1968. **1**(5): p. 413-417.
8. Broekhuizen, K.E., et al., *Formation of cloud condensation nuclei by oxidative processing: Unsaturated fatty acids.* J. Geophys. Res., 2004. **109**(D24206): p. doi: 10.1029/2004JD005298.
9. Ellison, G.B., A.F. Tuck, and V. Vaida, *Atmospheric processing of organic aerosols.* Journal of Geophysical Research, 1999. **104**(D9): p. 11633-11641.
10. Worsnop, D.R., et al., *A chemical kinetic model for reactive transformations of aerosol particles.* Geophysical Research Letters, 2002. **29**(20): p. doi: 10.1029/2002GL105542.
11. Ramanathan, V., et al., *Warming trends in Asia amplified by brown cloud solar absorption.* Nature, 2007. **448**(7153): p. 575-578.
12. Huff Hartz, K.E., et al., *Cloud condensation nuclei activation of monoterpene and sesquiterpene secondary organic aerosol.* Journal of Geophysical Research, 2005. **110**: p. D14208.
13. Prenni, A.J., et al., *Cloud droplet activation of secondary organic aerosol.* Journal of Geophysical Research, 2007. **112**: p. D10223.